Reducing climate model biases by exploring parameter space with large ensembles of climate model simulations and statistical emulation

Sihan Li[1,2], David E. Rupp[3], Linnia Hawkins[3,6], Philip W. Mote[3,6], Doug McNeall[4], Sarah N. Sparrow[2], David C. H. Wallom[2], Richard A. Betts[4,5], Justin J. Wettstein[6,7,8]

[1]Environmental Change Institute, School of Geography and the Environment, University of Oxford, Oxford, United Kingdom

[2]Oxford e-Research Centre, University of Oxford, Oxford, United Kingdom

[3]Oregon Climate Change Research Institute, College of Earth, Ocean, and Atmospheric Science, Oregon State University, Corvallis, Oregon

[4]Met Office Hadley Centre, FitzRoy Road, Exeter, United Kingdom

[5]College of Life and Environmental Sciences, University of Exeter, Exeter, UK

[6]College of Earth, Ocean, and Atmospheric Science, Oregon State University, Corvallis, Oregon

[7]Geophysical Institute, University of Bergen, Bergen, Norway

[8]Bjerknes Centre for Climate Change Research, Bergen, Norway

Correspondence to: Sihan Li (sihan.li@ouce.ox.ac.uk)

Abstract

Understanding the unfolding challenges of climate change relies on climate models, many of which have large summer warm and dry biases over Northern Hemisphere continental mid-latitudes. This work, using the example of the model used in the updated version of the weather@home distributed climate model framework, shows the potential for improving climate model simulations through a multi-phased parameter refinement approach, particularly over northwestern United States (NWUS). Each phase consists of 1) creating a perturbed parameter ensemble with the coupled global - regional atmospheric model, 2) building statistical emulators that estimate climate metrics as functions of parameter values, 3) and using the emulators to further refine the parameter space. The refinement process includes sensitivity analyses to identify the most influential parameters for various model output metrics; results are then used to cull parameters with little influence. Three phases of this iterative process are carried out before the results are considered to be satisfactory; that is, a handful of parameter sets are identified that meet acceptable bias reduction criteria. Results not only indicate that 74% of the NWUS regional warm biases can be reduced by refining global atmospheric parameters that control convection and hydrometeor transport, and land surface parameters that affect plant photosynthesis, transpiration and evaporation, but also suggest that this iterative approach to perturbed parameters has an important role to play in the evolution of physical parameterizations.

Introduction

Boreal summer (June-July-August, JJA) warm and dry biases over North Hemisphere (NH) continental midlatitudes are common in many global and regional climate models (e.g., Boberg and Christensen, 2012; Mearns et al., 2012; Mueller and Seneviratne, 2014; Kotlarski et al., 2014; Cheruy et al., 2014; Merrifield and Xie, 2016), including very high resolution convection-permitting models (e.g. Liu et al., 2017). These biases can have non-negligible impacts on climate change studies, particularly where relationships are non-linear, such as is the case of surface latent heat flux as a function of water storage (e.g. Rupp et al., 2017). Biases in present-day climate model simulations reduce the reliability of the future climate projections from those models. As shown by Boberg and Christensen (2012), after applying a bias correction conditioned on temperature to account for model deficiencies, the Mediterranean summer temperature projections were reduced by up to 1°C. Cheruy et al. (2014) demonstrated that of the climate models contributing to the Coupled Model Intercomparison Project Phase5 (CMIP5), the models that simulate a higher-than-average warming overestimated the present climate net shortwave radiation which increased more than multi-model average in the future; those models also showed a higher-than-average reduction of evaporative faction in areas with soil moisture-limited evaporation regimes. Both studies suggested that models with a larger warm bias in surface temperature tend to overestimate the projected warming. The implication of the warm bias goes beyond climate model simulations, as many impact modeling (e.g. hydrological, fire, crop modeling) studies (e.g. Brown et al., 2004; Fowler et al., 2007; Hawkins et al., 2013; Rosenzweig et al., 2014) use climate model simulation results as driving data. Recently, there have been coordinated research efforts (Morcrette et al., 2018; van Weverberg et al.,

2018; Ma et al., 2018; Zhang et al., 2018) to better understand the causes of the near-surface atmospheric temperature biases through process level understanding and to identify the model deficiencies that generate the bias. These studies suggest that biases in the net shortwave and downward longwave fluxes as well as surface evaporative fraction are contributors to surface temperature bias.

In the aforementioned climate models, many small-scale atmospheric processes have significant impacts on large-scale climate states. Processes such as precipitation formation, radiative balance, and convection, occur at scales smaller than the spatial resolution explicitly resolved by climate models, though very high resolution regional climate models are able to resolve or partially resolve some of these processes (e.g., convection). These processes must be represented by parameterizations that include parameters whose uncertainty are often high because: 1) there are insufficient observations with which to constrain the parameters, 2) a single parameter is inadequate to represent the different ways a process behaves across the globe, and/or 3) there is incomplete understanding of the physical process (Hourdin et al., 2013). Many studies have demonstrated the importance of considering parameterization uncertainty in the simulation of present and future climates by perturbing single and multiple model parameters within plausible parameter ranges usually established by expert judgment (e.g., Murphy et al., 2004; Stainforth et al., 2005; Sanderson et al., 2008a, b, 2010, 2011; Collins et al., 2011; Bellprat et al., 2012a,b, 2016). These studies have argued for careful tuning of models not only to reduce model parameter uncertainties by selecting parameter values that result in a better match between model simulation results with observations, but also to better understand relationships among

physical processes within the climate system via systematic experiments that alter individual parameter values or combinations thereof, in order to assess model responses to perturbing parameters.

Older generation Hadley Centre coupled models (HadCM2 and HadCM3), and atmospherere-only global (HadAM) and regional (HadRM) models have been used in numerous attribution studies (e.g., Tett et al., 1996; Stott et al., 2004; Otto et al., 2012; Rupp et al., 2017a; van Oldenborgh et al., 2016; Schaller et al., 2016; van Oldenborgh et al., 2017; Uhe et al., 2018), and the same models have been used for future projections (e.g., Rupp and Li, 2017; Rupp et al., 2017b; Guillod et al., 2018). These model families exhibit warm and dry biases during JJA over continental midlatitudes, biases that have persisted over model generations and enhancements (e.g., Massey et al., 2015; Li et al., 2015; Guillod et al., 2017). The more recent generations of Hadley Centre models – HadGEMx (HadGEM1, Johns et al, 2016; HadGEM2, Collins et al., 2008) also have the same biases to some extent.

Many of the aforementioned studies using HadAM and HadRM generated simulations through a distributed computing system known as climateprediction.net (CPDN, Allen et al., 1999), within which a system called weather@home is used to dynamically downscale global simulations using regional climate models (Massey et al., 2015; Mote et al., 2016; Guillod et al., 2017). As with the previous version of weather@home, the current operational version of weather@home (version 2: weather@home2) uses the coupled HadAM3P/HadRM3P with the atmosphere component based on HadCM3 (Gordon et al.,

114 2000), but updates the land surface scheme from the Met Office Surface Exchange Scheme
115 version 1 (MOSES1, Cox et al., 1999) to version 2(MOSES2, Essery et al., 2003).
116
117 Although the current model version in weather@home2 produces some global-scale
118 improvements in the global model's simulation of the seasonal mean climate, warm biases
119 in JJA increase over North America north of roughly 40° compared with the previous
120 version in weather@home1 (Fig. 2 in Guillod et al., 2017). The warm and dry JJA biases
121 appear clearly in the regional model simulations over the northwestern US region (NWUS,
122 defined here as all the continental US land points west of 110° and between 40°N-49°N -
123 the grey bounding box in Fig.S1). These biases may be related to, among other things, an
124 imperfect parameterization of certain cloud processes, leading to excess downward solar
125 radiation at the surface, which in turn triggers warm and dry summer conditions that are
126 further amplified by biases in the surface energy and water balance in the land surface
127 model (Sippel et al., 2016; Guillod et al., 2017). The fact that recent model enhancements
128 did not reduce biases over most of the northwest US motivates the present study, which
129 aims at reducing these warm/dry biases by way of adjusting parameter values, herein
130 referred to as 'parameter refinement'.
131
132 Improving a model by parameter refinement can be an iterative process of modifying
133 parameter values, running a climate simulation, comparing model output to observations,
134 and refining the parameter values again (Mauritsen et al., 2012; Schirber et al., 2013). This
135 iterative process can be both computationally expensive and labor-intensive. Any
136 parameter refinement process performed with the intent of improving the model also

involves unavoidably arbitrary decisions - though guided by expert judgement - about which parameter(s) to adjust, which metric(s) to evaluate (i.e., which feature(s) of the climate system to simulate at some level of accuracy), and which observational dataset(s) to use as the basis for the evaluation metric(s). Nonetheless, model tuning through parameter refinement is invariably needed to better match model simulations with observations (Schirber et al., 2013).

One systematic, yet computationally demanding, approach to model tuning is through perturbed parameter experiments (Allen et al., 1999; Murphy et al., 2004). These experiments use a perturbed parameter ensemble (PPE) of simulations from a single model where a handful of uncertain model parameters are varied systematically or randomly. Each set of perturbed parameter (PP) values is considered to be a different model variant - a PP set refers to a combination of parameter values from herein on. PPEs can be treated as a sparse sample of behaviours from a vast, high-dimensional parameter space (Williamson et al., 2013). A PPE directly informs us about model behaviour at those points in parameter space where the model is run (the PP sets), and helps us infer model behavior in nearby parameter space where the model has not been run. Besides parameter refinement, PPEs have also been used in many studies to estimate probability distribution functions (PDFs) of equilibrium climate sensitivity (e.g., Murphy et al., 2004) and transient regional climate change (e.g., Sexton et al., 2012a,b), permitting probabilistic projection of climate change (Murphy et al., 2007, 2009; Harris et al., 2013). PPEs are becoming common as a means to assess the range of uncertainty in climate model projections (Murphy et al., 2004; Stainforth et al., 2005; Collin et al., 2006; Sanderson, 2011; Sexton et al., 2012a,b2019;

160 Shiogama et al., 2012; Karmalkar et al., 2019).

161

162 Studies of climate model tuning using PPEs generally fall into three categories. The first
163 category makes only direct use of the ensemble itself (e.g., Murphy et al., 2004; Rowlands
164 et al., 2012) by screening out ensemble members that are deemed too far from the observed
165 target metrics. This is often referred to as ensemble filtering. However, this approach can
166 overlook certain critical parts of the parameter space not sampled by the PPE. One
167 promising improvement of this approach is to estimate the response of metric(s) in a
168 geophysical (e.g., atmospheric) model to parameter perturbations using a computationally
169 efficient statistical model (i.e. emulator) that is trained from the PPE results. The emulator's
170 skill is evaluated based on its metric prediction accuracy using independent simulations of
171 the model and, if deemed sufficiently skilful, can be used to estimate the model's output
172 metrics as a function of the model parameters in the parameter space not sampled by the
173 PPE.

174

175 The second category uses a PPE to train a statistical emulator, or establish some cost
176 function, which is then used to automatically search for optimal parameter values that
177 produce simulations closest to observations (e.g., Bellprat et al., 2012a, 2016; Zhang et al.,
178 2015; Tett et al., 2017). Different approaches have been used in optimization, ranging from
179 ensemble Kalman filters (Annan et al., 2005; Annan and Hargreaves, 2007 and the
180 references therein), stochastic Bayesian approach (e.g. Jackson et al., 2004), Markov chain
181 Monte Carlo integrations (Jackson et al., 2008; Järvinen et al., 2010), as well as
182 optimization over multiple objectives (Neelin et al., 2010). These studies advocated for this

183 approach particularly because of the efficiency and automation of available searching
184 algorithms. However, as with any model evaluation effort, the use of a cost function with
185 multiple target metrics means that optima for different metrics may occur at different
186 parameter values. This approach (automatically searching for optimal parameters) also runs
187 the risk of being trapped into local minima in the associated cost function; thus, searching
188 results are heavily dependent on the initial parameter values. Admittedly, the idea of
189 automatic searching to obtain optimal combinations of model parameters is appealing, but
190 in reality there is still a high level of subjectivity, e.g. selecting which model performance
191 metrics and observation(s) to use in evaluating the model, and the methods of optimization
192 and searching algorithm.
193
194 Unlike the second category, which searches for the optimal parameter values that result in
195 the closest match to observations, the third category, named 'history matching' (McNeall
196 et al., 2013, 2016; Williamson et al., 2013, 2015, 2017), seeks to rule out parameter choices
197 that do not adequately reproduce observations. History matching uses PPEs to train
198 statistical emulators that predict key metrics from the model output, and then uses the
199 emulators to rule out parameter space that is implausible. Williamson et al. (2017)
200 demonstrated that this method is more powerful when iterative steps are taken to rule out
201 implausible parameter space, where each step helps refine the parameter space containing
202 potentially better performing model variants. A drawback is that iterative history matching
203 requires more model runs in the not-ruled-out-yet parameter space for later iterations. It is
204 worth pointing out that the second and the third categories may not be different from each
205 other if a sufficient number of model simulations are used to train a statistical emulator

206 over the full parameter space. With a good emulator, it is possible to rule out parameter
207 space and optimize parameter values, in which case categories two and three are post-
208 processing steps. The method we adopted in this study fits into the third category,
209 borrowing the idea of 'iterative refocusing' where parameter values are refined through
210 phases of experiments. Our methodology differs from history matching in that we do not
211 employ a formal statistical framework based on the definition of implausibility.
212
213 All three approaches begin with an initial PPE, which can be computationally expensive
214 even with a modest number of free parameters. To cope with the computational demand,
215 many previous studies have generated PPEs from a global climate model (GCM) using
216 CPDN. The studies span a range of topics, from the earlier studies focusing on climate
217 sensitivity (e.g., Murphy et al., 2004; Stainforth et al., 2005; Sanderson et al., 2008a,b,
218 2010, 2011), to later ones attempting to generate plausible representations of the climate
219 without flux adjustments (e.g. Irvine et al., 2013; Yamazaki et al., 2013) and using history
220 matching to reduce parameter space uncertainty (Williamson et al., 2013). More recently,
221 Mulholland et al. (2016) demonstrated the potential of using PPEs to improve the skill of
222 initialized climate model forecasts of 1 month lead time, and Sparrow et al. (2018) showed
223 that large PPE can be used to identify subgrid scale parameter settings that are capable of
224 best simulating the ocean state over the recent past (1980-2010). However, very little
225 (Bellprat et al., 2012b; 2016) has been published on using PPEs for parameter refinement
226 with the aim of improving regional climate models (RCMs).
227

228 The goals of this study were to: 1) identify model parameters that most strongly control the
229 annual cycle of near-surface temperature and precipitation over the NWUS in
230 weather@home2, and 2) select model parameterizations that reduce the warm/dry summer
231 biases without introducing or unduly increasing other biases. We acknowledge that
232 changing a model in any way inevitably involves making sequences of choices that
233 influence the behaviour of the model. Some of the model behavioural changes are targeted
234 and desirable, but parameter refinement may have unintended negative consequences.
235 There is a general concern that 'improved' performance arises because of compensation
236 among model errors, and an 'accurate' climate simulation may very well be achieved by
237 compensating errors in different processes, rather than by best simulating every physical
238 process. This concern motivated us to select multiple parameter sets from the tuning
239 exercise rather than seek an "optimal" set. Though having multiple parameter sets does not
240 eliminate the problem, to the degree that each parameter set compensates for errors
241 uniquely, obtaining a similar model response to some change in forcing across parameter
242 sets may provide more confidence in that response. An alternative approach would be to
243 interpolate between the sampled points in the parameter space, and estimate a posterior
244 parameter probability density function (PDF), which could then be used to produce a PDF
245 of model outputs of interests (e.g., Murphy et al., 2004; Sexton et al., 2012a,b). We chose
246 to select multiple parameter sets instead of using parameter PDFs because the intended use
247 is to make projections with a small ensemble of parameter sets with reduced biases in
248 summer temperature and precipitation.
249

It is worth noting that this study looks mainly at atmospheric parameters because we intended to focus this study on larger-scale atmospherics dynamics that influence the boundary conditions of the regional model, especially how much moisture and heat is advected to the regional model, while local land surface/atmosphere interactions are being examined in a subsequent study that perturbs a suite of atmospheric and land surface parameters in the regional model.

2. Methodology

Throughout this paper we use 'simulated' to refer to outputs from climate models, and 'emulated' results to refer to estimated/predicted outputs from statistical emulators.

2.1. Overview of the parameter refinement process

This study carried out an iterative parameter refinement exercise, or an 'iterative refocusing' procedure to use a term coined in Williamson et al. (2017). The multi-dimensional parameter space is reduced in phases, where each phase includes the following steps:

1) Using space-filling Latin hypercube sampling (McKay et al., 1979) to randomly sample the initially defined parameter space (defined by the bounds of the 17 parameters listed in Table1) to generate sets of parameter combinations;

2) generate a PPE with the parameters sets from step (1) through weather@home;

3) train statistical emulators for multiple climate metrics using the PPE from step (2);

4) reduce the parameter space (i.e., narrow the ranges of acceptable values for parameters) such that the space excludes ensemble parameter sets that are 'too far away' from target

metrics;

5) randomly sample the reduced parameter space to design a new set of parameter combinations;

6) use the trained emulators to filter the sample from step (5), and reject a parameter set if the emulator prediction is too far away from a target value;

7) repeat steps (2) through (6) until the desired outcome is achieved.

Detailed descriptions of the parameter refinement process throughout three phases is presented in Appendix A, including decisions on what key climate metrics to use in each phase, and the stopping point of this iterative exercise - after three phases.

Here we briefly summarize the objective of each phase. The objective of Phase 1 was to eliminate regions of parameter space that led to top-of-atmosphere (TOA) radiative fluxes that are too far out of balance. The objective of Phase 2 was to reduce biases in the simulated regional climate of NWUS, while not straying too far away from TOA radiative (near-) balance. Lastly, the objective of Phase 3 was to further refine parameter space, specifically to reduce the JJA warm and dry bias over the NWUS.

The principle climate metrics used to access the effect of parameter perturbation are: Phase 1) TOA radiative fluxes, where we considered outgoing (reflected) shortwave radiation (SW) and outgoing longwave radiation (LW) separately; Phase 2) NWUS regional surface metrics - the mean magnitude of the annual cycle of temperature (MAC-T), and mean temperature (T) and precipitation (Pr) in December-January-February (DJF) and (JJA), while still being mindful of SW and LW; and Phase 3) same as Phase 2, except for selecting

296 model parameterizations that reduce the JJA warm and dry biases over the NWUS.

297

298 **2.2. Climate simulations with weather@home**

299 The climate simulations used in this study were generated through the weather@home
300 climate modelling system (Massey et al., 2015; Mote et al., 2016) with updates (Guillod et
301 al., 2017) that includes MOSES2. MOSES2 simulates the fluxes of CO_2, water, heat, and
302 momentum at the interface of the land and atmospheric boundary layer, and is capable of
303 representing a number of sub-grid tiles within each grid box, allowing a degree of sub-grid
304 heterogeneity in surface characteristics to be modeled (Williams et al., 2012).

305

306 The western North America application of weather@home (weather@home-WNA)
307 consists of HadRM3P (0.22° × 0.22°) nested within HadAM3P (1.875° longitude ×1.25°
308 latitude). Weather@home-WNA prior to recent enhancements was evaluated for how well
309 it reproduced various aspects of the recent historical climate of the western US by Li et al.
310 (2015), Mote et al. (2016), Rupp and Li (2016), and Rupp et al. (2017). Notable warm/dry
311 biases in JJA were present over the NWUS and these biases persist with MOSES2 (Fig.
312 S1), with a temperature bias of 3.9 °C and a precipitation biases of -8.5 mm/month (-32%)
313 in JJA over Washington, Oregon, Idaho and western Montana, as compared with the
314 PRISM gridded observational dataset (Daly et al., 2008). Note these were biases using
315 default, i.e. standard physics (SP), model parameter values.

316

317 Each simulation in the PPE spanned 2 years, with the first year serving as spin-up and only
318 the second year used in the analysis. Simulations began on 1 December of each year for

319 the years 1995 to 2005, except for Phase 1 (see description of Phases in Appendix A).
320 Climate metrics were averaged over December 1996 to November 2007 (except Phase 1).
321 This time period was chosen because it contained a wide range of SST anomaly patterns -
322 including the very strong 1997-98 El Niño – which helps reduce the influence that any
323 particular SST anomaly pattern may have on the sensitivities of chosen climate metrics to
324 parameters.
325
326 **2.3. Perturbed parameters**
327 In our PPE, we initially selected 17 model parameters to perturb simultaneously, 16 in the
328 atmospheric model, and one in the land surface model (Table 1). The parameters reside in
329 the global model as well as the regional model, and are set to the same values in HadAM3P
330 and HadRM3P in the experiments performed for this study, thus any reduction of regional
331 biases are considered to have been achieved through the improvement of boundary fluxes
332 from the GCM to the RCM, and improvement of the RCM itself. The atmospheric
333 parameters are a subset of those perturbed in Murphy et al. (2004) and Yamazaki et al.
334 (2013); both studies also perturbed ocean parameters, and Yamazaki et al. (2013) perturbed
335 forcing parameters (e.g., scaling factor for emission from volcanic emissions) as well. Our
336 selection of parameters was constrained to those available to be perturbed using
337 weather@home at the time. Ranges for most parameter perturbations were 1/3 to 3 times
338 the default value, but for certain parameters (e.g., empirically adjusted cloud fraction,
339 EACF), only values greater than the default value were used (Table 1). We intentionally
340 began with ranges generally wider than those used in previous studies (Murphy et al. 2004;

341 Yamazaki et al. 2013) because we intended to refine the ranges through multiple phases of
342 PPEs.
343
344 Though a principal objective was to evaluate sensitivity of the regional climate to
345 atmospheric parameters, sensitivities may be a function of land-atmosphere exchanges
346 (Sippel et al., 2016; Guillod et al., 2017). While many parameters influence land-
347 atmosphere energy and water exchanges in MOSES2, one (V_CRIT_ALPHA) has been
348 shown to be particularly important (Booth et al., 2012) so was included in our tuning
349 exercise. V_CRIT_ALPHA defines the soil water content below which transpiration
350 begins being limited by soil water availability and not solely the evaporative demand.
351
352 **2.4 Observational data**
353 The regional biases in MAC-T, JJA-T, JJA-Pr, DJF-T and DJF-Pr - were all calculated
354 with respect to the 4-km resolution monthly PRISM dataset, after regridding the PRISM
355 data to the HadRM3P grid. To consider observational uncertainty, we also compared JJA-
356 T biases using four other observational datasets: 1) NCEP/NCAR Reanalysis 1 (NCEP,
357 Kalnay et al., 1996), 2) the Climate Forecast System Reanalysis and Reforecast (CFSR,
358 Saha et al., 2010), 3) the Modern-Era Retrospective Analysis for Research and
359 Applications Version2 (MERRA2, Gelaro et al., 2017), and 4) Climatic Research Unit
360 temperature dataset v4.00 (CRU, Harris et al., 2014). The four datasets are not shown here
361 for the regional analysis because the maximum regionally averaged difference (0.71 °C)
362 among the datasets is less than 1/5 of the regionally averaged JJA-T bias. Throughout this
363 paper, biases of the regional model outputs are calculated with respect to PRISM.

364

365 The biases in global temperature were calculated with respect to CRU, MERRA2, CSFR,
366 NCEP, and the Climate Prediction Centre global land surface temperature data; the latter
367 is a combination of the station observations collected from Global Historical Climatology
368 Network version 2 and the Climate Anomaly Monitoring System (GHCN-CAMS, Fan and
369 van den Dool, 2008). The biases in global precipitation were calculated with respect to
370 CRU, MERRA2, CFSR, Global Precipitation Climatology Project monthly precipitation
371 (GPCP, Adler et al., 2003), Global Precipitation Climatology Centre monthly precipitation
372 (GPCC, Schneider et al., 2013), ERA-Interim reanalysis dataset (ERAI, Dee et al., 2011),
373 Japanese 55-year Reanalysis (JRA-55, Onogi et al., 2007), NOAA-CIRES 20th Century
374 Reanalysis version 2c (20CRv2c, Compo et al.. 2011), the CPC Merged Analysis of
375 Precipitation (CMAP; Xie and Arkin, 1996), and the Version 7 TRMM Multi-Satellite
376 Precipitation Analysis -3B42 research version (TRMM; Huffman et al., 2014). All the
377 datasets were regridded to the HadAM3P grid before biases were calculated.

378

379 For all the observational datasets, data from December 1996 to November 2007 (the same
380 time period the model simulations cover as shown in Table2) was used to calculate model
381 biases, except TRMM, which is only available starting from 1998.

382

383 2.5 Emulators

384 In Phase 1, a 2-layer feed-forward Artificial Neural Network (ANN, Knutti et al., 2003;
385 Sanderson et al., 2008; Mulholland et al., 2016) was used. Although other machine-
386 learning algorithms could be suitable (Rougier et al., 2009; Neelin et al., 2010; Bellprat et

387 al., 2011, 2012, 2016), we chose ANN because it permits multiple simultaneous emulator
388 targets (i.e., TOA SW and LW at the same time). Although ANN has the advantage of
389 using multiple metrics as targets simultaneously, the underlying emulator structure remains
390 obscure. From Phase 2, for the sake of simplicity and transparency, we used kriging -
391 which is similar to a Gaussian process regression emulator - following McNeall et al.
392 (2016) as coded in the package DiceKriging (Roustant et al., 2012) in the statistical
393 programming environment R. We used universal kriging, with no 'nugget' term, meaning
394 that the uncertainty on model outputs shrinks to zero at the parameter input points that have
395 already been simulated by the climate model (Roustant et al., 2012). Please refer to
396 Appendix A for further details.
397
398 **2.6 Sensitivity Analysis**
399 The response of the climate model to perturbations in the multidimensional parameter
400 space can be non-linear. In order to isolate the influence of each parameter on key climate
401 metrics and eliminate parameters that do not have a strong control on those metrics, we
402 performed two types of sensitivity analysis. One determines the sensitivity of a single
403 parameter by perturbing one parameter with all other parameters fixed, i.e. one-at-a-time
404 (OAAT) sensitivity analysis. Following Carslaw et al. (2013) and McNeall et al. (2016),
405 we also used a global sensitivity analysis using Fourier Amplitude sensitivity test (FAST)
406 for qualitative sensitivity analysis to validate the results of OAAT and to estimate
407 interactions among parameters. FAST allows the computation of the total contribution of
408 each input parameter to the output's variance, where total includes the factor's main effect,
409 as well as the interaction terms involving that input parameter. In the FAST method, the

fraction of the total variance due to the interactions is not resolved as the sum of individual interactions, but is computed from the parameter contribution to the residual variance , i.e., variance not accounted for by the main effects. The computational aspects and advantages of FAST are described in Satelli et al. (1999). Emulators are used for the sensitivity analysis.

3. Results and Discussion

Top-of-atmosphere (TOA) radiative balance is an emergent property in GCMs (Irvine et al., 2013), and the fact that the models of the IPCC Assessment Report 4 did not need flux-adjustment was seen as an improvement over earlier models (Solomon et al., 2007). Although climate models approximately balance the net absorption of solar radiation with the outward emission of longwave radiation (OLR) at the TOA, the details of how solar absorption and terrestrial emission are distributed in space and time depend on global atmospheric and oceanic circulation, clouds, ice, and other aspects of model behaviour. The surface expression of those global processes is also important given that a primary and practical purpose of climate modelling is to understand how (surface) climate will change. We describe the responses of both global TOA and regional surface climate to parameter refinement.

3.1. TOA radiative fluxes

In Fig. 1, we show the TOA energy flux components from the PPEs from each of the three phases. The ranges of acceptability for SW and LW (as denoted by the ellipse in Fig. 1) were defined by taking the observational uncertainty ranges given in Stephens et al. (2012),

433 but tripling them (deliberately setting a lenient elimination criteria), and then expanding
434 both the negative and positive thresholds by an additional 1 W m-2 to account for internal
435 variability as estimated from SP (Fig. S5). Please refer to Appendix A for further details.
436 In Phase 1, many parameter sets (72%) resulted in TOA energy fluxes that vastly exceeded
437 our ranges of acceptability (as defined in Appendix A). In Phase 2, most of the parameter
438 sets resulted in TOA energy fluxes that fell within the ranges of acceptability; the 20% that
439 did not reveal the error in our predictions using the emulator since the parameter sets were
440 chosen to specifically achieve TOA fluxes within the region of acceptability. In Phase 3,
441 nearly all (97%) the parameter sets yielded acceptable results. It is worth mentioning again
442 that in Phase 3, selection of parameter sets was based only secondarily on TOA fluxes and
443 primarily on regional climate metrics (see detailed description of Phase 3 in Appendix A).
444 Fig. B1 and B2 (in Appendix B) show predictions from emulators against model-simulated
445 values for model output metrics as validations of the emulators. The linear relationships
446 between the emulated and simulated results are very strong (regression coefficient
447 regcoef>0.9 for both LW and SW), while the emulated results can predict the simulated
448 results relative well, with coefficient of determination R2 > 0.9 for both LW and SW.
449 Please refer to Appendix B for further details on emulator validations.
450
451 Rowlands et al. (2012) discarded any ensemble member that required a global annual mean
452 flux adjustment of absolute magnitude greater than 5 W m-2 (see red lines in Fig. 1) and
453 Yamazki et al. (2013) defined a confidence region of (SW, LW) that corresponded to a
454 TOA imbalance of less than 5 W m^{-2} as one that did 'not drift significantly' from a realistic
455 TOA state. Although the ranges of acceptability (Fig.1) permits net TOA imbalance

456 greater than 5 W m^{-2}, more than half (55.8%) of the Phase 3 parameter sets generated a
457 TOA imbalance less than 5 W m^{-2}, and the smallest TOA imbalance was less than 0.1 W
458 m^{-2}.
459
460 The entrainment coefficient (ENTCOEF) and the ice fall speed (VF1) were the dominant
461 controls on the TOA outgoing SW and LW fluxes, respectively (see SW and LW response
462 to these two parameters shown in the bottom two rows of Fig. S2). Why these parameters
463 are important becomes clear from understanding their respective roles in the climate model,
464 especially with respect to convection and hydrometeor transport.
465
466 The atmospheric model simulates a statistical ensemble of air plumes inside each
467 convectively unstable grid cell. On each model layer, a proportion of rising air is allowed
468 to mix with surrounding air and vice-versa, representing the process of turbulent
469 entrainment of air into convection and detrainment of air out of the convective plumes
470 (Gregory and Rowntree, 1990). The rate at which these processes occur in the model is
471 proportional to ENTCOEF, which is a parameter in the model convection component
472 (Table1). The implication of perturbing ENTCOEF has been investigated by (Sanderson et
473 al, 2008b) using single perturbation experiments, and they showed that a low ENTCOEF
474 leads to a drier middle troposphere and moister upper troposphere. Conversely, increasing
475 ENTCOEF results in increased low level moisture (more low level clouds) and decreased
476 high level moisture (less high level clouds). Because the albedo effects of low clouds
477 dominate their effects on emitted thermal radiation (Hartmann et al., 1992; Stephens,
478 2005), increasing ENTCOEF increases the outgoing SW fluxes.

VF1 is the speed at which ice particles may fall in clouds. A larger ice fall speed is associated with larger particle sizes and increased precipitation. Wu (2002) studied ice fall speed parameterization in radiative convective equilibrium models, and found that a smaller ice fall speed leads to a warmer, moister atmosphere, more cloudiness, weak convection and less precipitation, which could lead to decreased outgoing LW TOA flux due to absorption in the cloud itself and/or in the moist air. Higher ice fall speeds produce the opposite - a cooler, clearer, less cloudiness, strong convection and more precipitation, which increases the outgoing LW flux.

3.2. Regional climate improvements

A primary and practical purpose of climate modelling is to understand how (surface) climate will change, but model biases can have non-negligible impacts on projections. In Phase 2 and 3 we evaluate the response of regional surface climate to parameter perturbations, and refine the parameter space to reduce biases in regional temperature and precipitation.

In Phase 2, we identified ENTCOEF and VF1 as distinct from the other 15 parameters with respect to their influence on the overall suite of climate metrics to a first order approximation (Fig. S3). Recall the regional surface metrics considered were MAC-T, JJA-T, JJA-Pr, DJF-T, and DJF-Pr. Though MAC-T is our principal metric (section2.1), MAC-T co-varies with JJA-T, JJA-Pr, and DJF-T (Fig. S3), so moving in parameter space toward

lower bias in MAC-T reduces biases in JJA-T, JJA-Pr, and DJF-T. MAC-T does not co-vary strongly with DJF-Pr.

Each OAAT relationship in Fig. 2 depends on the initial ranges of the input parameters from the ensemble design, and is computed while holding all other parameters at their ensemble mean values. OAAT results while holding all other parameters at their SP values are similar to those shown in Fig. 2 (results not shown here). Because sensitivity can change as one moves through the parameter space (e.g. CW_LAND and ENTCOEF in Fig. 2), these relationships must be interpreted with care. Within the refined parameter space in Phase 2, ENTCOEF and the parameter that limits photosynthesis (and thereby latent heat flux via transpiration) as a function of soil water (V_CRIT_ALPHA) were the most influential individual parameters and counter each other when both increased (Fig. 2 and Fig. S3). The parameter that controls the cloud droplet to rain threshold over land (CW_LAND) also had strong influence on MAC-T across the lower end of the parameter perturbation range (up to 0.004). The other parameters had little to effectively no influence on MAC-T. The results of OAAT sensitivity analysis for the other output metrics considered in Phase 2 are presented in Fig. S6-S11.

The global sensitivities of the simulated outputs (the ones considered in Phase 2) due to each input, as both a main effect and total effect, including interaction terms, are presented in Fig. 3. ENTCOEF was the most important parameter for all three surface temperature metrics, with a total sensitivity index of ~0.7, 0.5, and 0.4 for MAC-T, JJA-T, and DJF-T respectively , where maximum sensitivity is 1 (see Satelli et al. 1999). For the metrics

524 MAC-T and JJA-T, V_CRIT_ALPHA was the next most important, with a total sensitivity
525 index of ~0.3 for both metrics. For JJA-Pr, the most important parameter was VF1,
526 followed by ENTCOEF; for DJF-Pr, the most important parameter was ENTCOEF, closely
527 followed by the parameter that controls the roughness length for free heat and moisture
528 transport over the sea (Z0FSEA).
529
530 The interaction terms were relatively small, accounting for a few percent of the variance,
531 except for the effect of ENTCOEF on DJF-Pr, where the interaction with other parameters
532 accounts for ~ 1/3 of the variance. In a study constraining carbon cycle parameters by
533 comparing emulator output with forest observations, McNeall et al. (2016) also found the
534 importance of the interaction terms negligible. In contrast, Bellprat et al. (2012b) used
535 quadratic emulator to objectively calibrate a regional climate model, and found non-
536 negligible interaction terms. They showed that excluding the interactions in the emulator
537 increased the error of the emulated temperature and precipitation results by almost 20%.
538 Further work could be done to assess the magnitude and functional form (i.e. linear or
539 nonlinear) of the interaction terms, but is beyond the scope this study.
540
541 Only the parameters with a total sensitivity index larger than ~0.1 for MAC-T, JJA-T, DJF-
542 T, JJA-Pr, or DJF-Pr were retained for perturbation in Phase 3: CW_LAND, VF1,
543 ENTCOEFF, V_CRIT_ALPHA, ASYM_LAMBDA, G0, and Z0FSEA. Although the
544 parameter that controls the rate at which cloud liquid water is converted to precipitation
545 (CT) had a total sensitivity index of ~0.1 for SW, it was excluded from further perturbation

546 because the primary interest in Phase 2 was in regional surface metrics, not TOA radiative
547 fluxes.
548
549 Phase 3 demonstrated the power of our approach for reducing regional mean biases in
550 MAC-T, JJA-T and JJA-Pr. Simulations from Phase 3 resulted in MAC-T biases 1- 3°C
551 lower than SP (Fig.4 middle row). All Phase 3 parameter sets improved the JJA-Pr dry bias
552 with several eliminating the bias entirely. Many parameter sets reduced the bias in JJA-T
553 to less than 1.5°C, a dramatic improvement (~63%) over the 4°C SP bias. However, these
554 improvements come at a small price, namely a larger regional (NWUS) dry bias in DJF-Pr
555 (about -15% compared with PRISM in the worst case). Because our primary goal was to
556 reduce JJA warm and dry biases, any model variant from Phase 3 is preferable to SP. Any
557 subset of parameterizations from phase 3 can now be used in subsequent experiments.
558
559 V_CRIT_ALPHA plays an important role in controlling JJA-T and MAC-T (as shown in
560 Fig. 2 and Fig. S6) due to its role in the surface hydrological budget. V_CRIT_ALPHA
561 defines the critical point as a fraction of the difference between the wilting soil water
562 content and the saturated soil water content (as described in Appendix C). The critical
563 point is the soil moisture content below which plant photosynthesis becomes limited by
564 soil water availability. When V_CRIT_ALPHA is zero, transpiration starts to be limited as
565 soon as the soil is not completely saturated, whereas when it is one, transpiration continues
566 unlimited until soil moisture reaches wilting point at which point transpiration switches
567 off. Lower values of V_CRIT_ALPHA reduce the critical point allowing plant
568 photosynthesis to continue unabated at lower soil moisture levels, i.e. plants are not water-

569 limited. As plants photosynthesize water is extracted from soil layers and transpired,
570 increasing the local atmospheric humidity and lowering the local temperature through
571 latent cooling. Our results are consistent with previous findings by Seneviratne et al.
572 (2006), who also show reducing the temperature and increasing humidity can feedback
573 onto the regional temperature and precipitation during the summer months.
574
575 The only apparent constraints on ranges of parameter values through three phases of
576 parameter refinement were seen for V_CRIT_ALPHA and ENTCOEF. Values of
577 V_CRIT_ALPHA lower than 0.7 were required to keep the bias of MAC-T under 3 °C.
578 For ENTCOEF, the range between 3 and 5 contains the best candidates to reduce regional
579 warm/dry biases. The range of ENTCOEF identified here is consistent with findings of
580 Irvine et al. (2013), which also show that low values of ENTCOEF tend to give warmer
581 conditions. However, results from other previous studies varies. Williamson et al. (2015)
582 found that low values of ENTCOEF are implausible, and that there are more plausible
583 model variants at the upper end of its perturbed range, whereas Sexton et al. (2012a) and
584 Rowlands et al. (2012) consider the range between 2 and 4 to contain the best model
585 variants. The discrepancy in optimal ranges for ENTCOEF are to be expected given that
586 the primary metrics used to evaluate the effect of parameter refinement are different, with
587 ours being JJA warm/dry biases over the NWUS, William et al. (2015) being the behaviour
588 of Antarctic Circumpolar Current, and other previous studies being climate sensitivities.
589 This demonstrates that any parameter refinement process is tailored to a specific objective,
590 and choices regarding metrics (e.g., variables, validation dataset(s), and / or cost functions)
591 may determine which part of parameter space is ultimately accepted.

592

593 **3.3. Effects on global scale climate**

594 To avoid introducing or increasing biases over other parts of the globe by our regionally-
595 focused model improvement effort, we investigated the large-scale effects of the selected
596 10 'good' (least biased in MAC-T) sets of global parameter values. We focused on surface
597 temperature and precipitation because they are key variables of the climate system and are
598 of high interest for impact studies.

599

600 Figure 5 shows the meridional distribution of Northern Hemisphere (NH) mid-latitude
601 temperature (over land) and precipitation in DJF and JJA. Because of the wide range of
602 parameter values in the PPEs of Phase 1 and Phase 2, the spread for these PPEs is quite
603 large, whereas the ensemble spread in Phase 3 is substantially smaller. Compared with the
604 SP ensemble, the new parameter values (final 10 sets) reduced the zonal mean JJA
605 temperature throughout the NH mid-latitudes (30 °N -60 °N), by ~1 °C – 4 °C (depending
606 on the particular combination of parameters), and increased JJA precipitation over the same
607 latitude bands, except for latitudes south of 33 °N and north of 58 °N. In DJF, the effects
608 are not as large nor are the changes consistent in sign across the NH mid-latitude region
609 (though south of ~38 °N all 10 parameter sets give increasing precipitation). The SP
610 simulations have warm and dry biases over NWUS and mid-latitude land in general (as
611 shown in Fig. 4, Fig. 6 and Fig. 7). In JJA all the selected PP model variants show
612 considerably different results compared with the SP-cooler and wetter, i.e. reduced biases
613 and improved model performance. Figure 5 also demonstrates that varying model

614 parameters has a bigger influence than varying initial conditions, as seen from the wider
615 spread of PP results compared with the spread of SP initial condition perturbation results.
616
617 To examine how parameter refinements affect spatial patterns of biases, we compare the
618 seasonal mean biases of temperature (Fig. 6) and precipitation (Fig. 7) under SP and the
619 selected PP settings, against CRU data. The SP simulations have large warm biases in JJA
620 (and to a lesser extent in MAM and SON, Fig. 6 b-d) over the NH mid-latitude land region,
621 that are substantially lower in the PP simulations (Fig. 6 f-h and Fig.6 j-l). In the tropics,
622 the SP simulations have cold biases over northern South America, central Africa and
623 southern Asia in most seasons that are ameliorated in the PP simulations in some cases
624 (e.g. central Africa in DJF and SON) - even though the focus of the PP simulations was
625 improving the climate of the NWUS. The SP simulations also have cold biases over most
626 of the Southern Hemisphere continents in mid-latitudes in most seasons. A large fraction
627 of the JJA temperature biases were reduced in the PP simulations, as shown in Fig. 6c, g
628 and k. These salient features in JJA temperature biases under SP and PP are not particular
629 to the selection of observational dataset (see Fig. S12-S13 for comparison with other
630 datasets). In the other three seasons, however, the spatial patterns of temperature biases are
631 not consistent across observational datasets.
632
633 The reduction of JJA temperature from SP to PP (Fig. 6k) and the resulting reduction in
634 bias are accompanied by reduction in precipitation in the equatorial regions; increased
635 precipitation over northern North America, northern Africa, and Europe (Fig. 7k); and
636 decreased incoming shortwave radiation at the surface and increased evaporation (Fig.

637 S14). Stronger evaporative cooling and reduced surface radiation lead to a cooling of the
638 JJA climate, which roughly agrees with the geographical pattern of reduced mean JJA
639 temperature, consistent with findings in Zhang et al. (2018) that both overestimated surface
640 shortwave radiation and underestimated evaporation contribute to the warm biases in JJA
641 in CMIP5 climate models.
642
643 For precipitation, the largest biases in SP are over Amazonia in DJF and MAM (Fig. 7a
644 and b), and northern South America, equatorial Africa, and south Asia in JJA (Fig. 7c).
645 These summer biases are increased in the PP simulations (Fig. 7k). However, it is difficult
646 to know whether we are improving the model's global precipitation patterns because of the
647 large uncertainty in historical precipitation observational datasets. Still, it is worth
648 comparing the PP simulations with both a variety of observational-based datasets and other
649 GCMs (Fig. 8). The precipitation amounts differ substantially across different
650 observational datasets, as well as across climate models. In the tropics, Phase 3 PP
651 simulated precipitation is mostly lower (except DJF just north of the equator) and has
652 narrower range than the observations or other climate models, but is higher in DJF and JJA
653 (up to 25% higher) than the SP simulation results. Outside the tropics, the precipitation
654 distributions in PP remain similar to those of SP, and differences from observational
655 datasets and other GCMs are less affected by the use of PP. The tropical precipitation
656 improvements in JJA can be taken as a general improvement, though not with high
657 confidence due to the variability across observational datasets. To further highlight the
658 uncertainties in precipitation, global maps of differences in biases between SP and our

659 selected parameter settings, in comparison with other observational-based datasets, are
660 presented in Fig. S15-22.
661
662 The fact that the large JJA warm bias (shared with many other GCMs and RCMs; see e.g.
663 Mearns et al., 2012; Kotlarski et al., 2014) could be reduced substantially through the use
664 of PP is a notable result, especially since the bias persisted through initial tuning efforts
665 and through the recent updates from version 1 to version 2 of weather@home. We
666 demonstrated here that significant improvements in the simulation of JJA temperature can
667 be made through parameter refinements, and that these JJA temperature biases are not
668 necessarily structural issues of the climate model. These improvements in simulating JJA
669 temperature generally did not overall improve JJA precipitation patterns across the globe,
670 and even worsened the bias in some places (e.g. South America).
671
672 **4. Conclusions**
673 Through an iterative parameter refinement approach to improve model performance, we
674 identified a region of climate model parameter space in which HadAM3P outperforms the
675 SP variant in simulating summer climate over the NWUS specifically, and over NH mid-
676 latitude land in general, while approximately maintaining TOA radiative (near-) balance.
677 Improving the northwest US climate comes with tradeoffs, e.g. larger JJA dry bias over
678 Amazonia. However, it is important to note that there are large uncertainties in observed
679 precipitation climatology, especially outside of the North American and European mid-
680 latitudes, so both apparent increases and decreases in biases should be treated with caution,
681 and compared against the range across observational datasets. In the end, we consider the

682 cost of increasing biases in parts of the globe acceptable for the purposes of selecting
683 multiple global model variants to drive the regional model with reduced JJA biases over
684 NWUS. The fact that improvements can be made at all (for a substantial area of the world)
685 through targeted PPE is encouraging.
686
687 Our parameter refinement yielded important improvements in the representation of the
688 summer climate over the NWUS, and it follows that biases in other models may also be
689 reduced by refining certain parameters that, although may not be identical to those in
690 HadAM3/RM3P, influence the same physical processes similarly. We found ENTCOEF
691 and V_CRIT_ALPHA to be the dominant parameters in reducing JJA biases. These
692 parameters control cloud formation and latent heat flux, respectively. Bellprat et al. (2016)
693 found the key parameter responsible for reduction of JJA biases is increased hydraulic
694 conductivity, which increases the water availability at the land surface and leads to
695 increased evaporative cooling, stronger low cloud formation, and associated reduced
696 incoming shortwave radiation. We only perturbed one land surface parameter, but the
697 effects of additional land surface parameters are being explored in a subsequent study.
698 Given that land model parameters such as V_CRIT_ALPHA could reasonably be expected
699 to interact with sensitive atmospheric parameters like ENTCOEF, it is particularly
700 interesting to consider the multivariate sensitivity of a range of parameters that span across
701 component models (e.g., land, ice, atmosphere, ocean). We argue that this frontier of
702 parameter sensitivity exploration should be done in a transparent and systematic manner,
703 and we have demonstrated that statistical emulators can be effectively leveraged to reduce
704 computational expense.

705

706 The fact that V_CRIT_ALPHA (which is a parameter in the land surface scheme MOSES2)
707 was found to be an important parameter on regional MAT-C and JJA-T, has much further
708 implications beyond this study. MOSES2 is the land surface scheme used in HadGEM1
709 and HadGEM2 family, which were used in CMIP4 and CMIP5. Moreover, the Joint UK
710 Land Environment Simulator (JULES) model (which is the land surface scheme of the
711 CMIP6 generation Hadley Centre models HadGEM3 family, https://www.wcrp-
712 climate.org/wgcm-cmip/wgcm-cmip6) is a development of MOSES2. What we have
713 learned about the atmosphere-land surface interactions here is relevant to even the most
714 recent HadGEM model generation and the in-progress CMIP6.

715

716 The reduction of JJA biases that we achieved in our multi-phase parameter refinement is
717 notable. However, despite out efforts, the 'best' performing parameter set still simulates a
718 MAC-T bias of 1.5 °C, and a JJA-T bias of 1 °C, over the NWUS. Future work could be
719 done to determine whether the model can be further improved by tuning additional land-
720 surface scheme parameters, and/or to what extent the remaining biases are due to structural
721 errors of the model for which we cannot (nor even should not) compensate by refining
722 parameter values. However, with the reduction in JJA temperature bias, future projections
723 using the new parameter settings over the SP should be at less risk of overestimating
724 projected warming in summer (as discussed in the introduction).

725

726 It is also worth noting that we restricted our analysis to seasonal and annual mean climate
727 metrics. Given the use of weather@home for attribution studies of many extreme weather

728 events (e.g., Otto et al., 2012; Rupp et al., 2017a) as well as their impacts, such as flooding-
729 related property damages (Schaller et al., 2016) and heat-related mortality (Mitchell et al.,
730 2016), an important next step would be to investigate how the tails of distributions of
731 weather variables respond to parameter perturbations. Furthermore, looking at biases in
732 seasonal mean temperature and precipitation is insufficient to fully assess model
733 performance. As a follow-up step to this study, we recommend a process-based model
734 evaluation and physical explanation of model improvements to further refine the parameter
735 space that provides improvements (e.g., reduce summer biases) through appropriate
736 physical mechanisms. For example, more accurate representation of clouds in the model
737 could lead to better simulated downward solar radiation at the surface, as well as better
738 simulated surface energy and water balance.
739
740 Another important next step would be to apply the selected PPE over the weather@home
741 - European domain, given the non-trivial JJA warm bias identified over Europe by previous
742 studies (Massey et al., 2014; Sippel et al., 2016; Guillod et al., 2017). Bellprat et al. (2016)
743 showed that regional parameters tuned over Europe domain also produced similar
744 promising results over North America domain but the same model parameterization yielded
745 larger overall biases over North America than for Europe. One could test the transferability
746 of parameter values over different regional domains in the weather@home framework,
747 given weather@home currently uses the same GCM to drive several RCMs over different
748 parts of the world, all using the same parameter values.
749

750 The methodology presented in this study could be applied to other models in the evolution
751 of physical parameterizations, and we advocate that parameter refinement process should
752 be more explicit and transparent as done here. Choices and compromises made during the
753 refinement process may significantly affect model results and influence evaluations against
754 observed climate, hence should be taken into account in any interpretation of model results,
755 especially in intercomparison of multimodel analyses to help understanding of model
756 differences.
757
758 **Code availability**
759 HadRM3P is available from the UK Met Office as part of the Providing REgional
760 Climates for Impacts Studies (PRECIS) program. Access to the source code is dependent
761 on attendance at a PRECIS training workshop
762 (http://www.metoffice.gov.uk/research/applied/international-development/precis/obtain).
763 The code to embed the Met Office models within weather@home is proprietary and not
764 within the scope of this publication.
765
766 **Data availability**
767 The model output data for the experiment used in this study will be freely available at the
768 Centre for Environmental Data Analysis (http://www.ceda.ac.uk) in the next few months.
769 Until the point of publication within the CEDA archive, please contact the corresponding
770 author to access the relevant data.
771
772 **Appendix A: Detailed experimental process**

773 The overarching goal is to refine parameter values to reduce warm and dry summer bias in
774 the NWUS. In total four ensembles were generated, one using the SP values and one for
775 each of 3 PPE phases. Details of each ensemble are listed in Table 2.
776
777 Internal variability of the atmospheric circulation can confound the relationship between
778 parameters values and the response being sought (i.e. result in a low signal-to-noise ratio).
779 Averaging over multiple ensemble members with the same parameter values but different
780 atmospheric initial conditions (ICs) can clarify the true sensitivity to parameters by
781 increasing the signal-to-noise ratio. We set up multiple ICs for each parameter set, but the
782 numbers of ICs applied was not consistent throughout the experiment. The IC applied in
783 each phase was determined somewhat subjectively, trying to strike a balance between
784 running a large enough PPE to probe as many processes and interactions between
785 parameters as possible, having multiple ICs so that the results were representative of the
786 parameter perturbations instead of reflecting the influence of any particular IC, while under
787 the practical limitation of data transfer, storage, and analysis. The actual IC ensemble size
788 used in the final analysis was also constrained by the number of successfully completed
789 returns from the distributed computing network.
790
791 The four ensembles are summarized below:
792 **SP:** A preliminary "standard physics" (SP) ensemble with 10 ICs that used only the default
793 model parameters was generated to provide a benchmark to access the effects of parameter
794 perturbations.
795

Phase 1: The objective of this phase was to eliminate regions of parameter space that led to top-of-atmosphere (TOA) radiative fluxes that are strongly out of balance. Exclusion criteria were deliberately lenient, to avoid eliminating regions of the parameter space that could potentially reproduce the observed temperature and precipitation over the western US. We perturbed 17 parameters simultaneously, using space-filling Latin hypercube sampling (McKay et el., 1979) - maximizing the minimum distance between points - to generate 340 sets of parameterizations across the range of parameter values described in Table 1. To generate enough ensemble members for a statistical emulator, Loeppky et al. (2009) suggested that the number of sets of parameter values be 10 times the number of parameters (p). We used more than $10p$ sets of parameter values in this, and subsequent phases of PPE. A total of 2040 simulations (340 sets of parameter values x 6 ICs) were submitted to the volunteer computing network. This phase was considered finalized when simulations with 220 sets of parameter values and 3 IC ensemble members per set were returned from the computing network.

Model results were used to train a statistical emulator which maps the relationship between parameter values and key climate metrics. In this phase, the metrics were outgoing LW and (reflected) SW TOA radiative fluxes. We considered these two metrics separately because the total net radiation could mask deficiencies in both types of radiation through cancellation of errors.

For the emulator, a 2-layer feed-forward Artificial Neural Network (ANN, Knutti et al., 2003; Sanderson et al., 2008; Mulholland et al., 2016) was used. Although other machine-

819 learning algorithms could be suitable (Rougier et al., 2009; Neelin et al., 2010; Bellprat et
820 al., 2012a,b, 2016), we chose ANN because it permits multiple simultaneous emulator
821 targets (i.e., TOA SW and LW at the same time). We used an ellipse (Fig. 1) to define the
822 space of acceptability for SW and LW, starting with the observational uncertainty ranges
823 given in Stephens et al. (2012), but tripling them (deliberately setting a lenient elimination
824 criteria), and then expanding both the negative and positive thresholds by an additional 1
825 W m^{-2} to account for internal variability as estimated from SP (Fig. S5). Sets of parameter
826 values that fall within our range of acceptability were retained, and the ranges of these
827 refined/restricted parameter values defined the remaining parameter space.
828
829 A new set of 1,000 parameter configurations was generated from the remaining parameter
830 space using space-filling Latin hypercube sampling. With this new ensemble we increased
831 the sample density within the refined parameter space. The statistical emulator was used to
832 predict SW and LW for each of these 1,000 new sets of parameters, and 41% fell within
833 our range of acceptability, reflecting the deficiency of the emulator to some extent.
834 Parameter sets that fell within the acceptable range were used in Phase 2.
835
836 **Phase 2:** The objective of this phase was to reduce biases in the simulated climate of the
837 NWUS, where the warm summer biases were the most obvious (Fig. S1), while not straying
838 far from TOA radiative (near-) balance. The climate metrics considered were the mean
839 magnitude of the annual cycle of temperature (MAC-T), and mean temperature (T) and
840 precipitation (Pr) in December-January-February (DJF) and June-July-August (JJA).
841 Although a primary motivation for this study was to investigate and reduce the warm and

842 dry bias in JJA over NWUS, MAC-T was treated as the primary metric in Phase 2 because
843 it is a comprehensive measure of climate feedbacks in response to a large change in forcing,
844 e.g., solar SW (Hall and Qu 2006). MAC-T is also strongly correlated to the other regional
845 metrics (particularly JJA-T) as evident in Fig. S3 – MAC-T against other metrics. We chose
846 a NWUS average MAC-T of +/-3 °C as the bias threshold over which parameter space
847 would be eliminated. Though this threshold is arbitrary, falling below it would mean
848 reducing the MAC-T bias for the NWUS by about 50%.
849
850 We did not treat all metrics as equally important. The order of importance in this second
851 phase was MAC-T > JJA-T, JJA-Pr, DJF-T, and DJF-Pr > SW and LW.
852
853 The 410 sets of new PPE from Phase 1 became the starting point for Phase 2. A total of
854 27,060 simulations (410 sets of parameter values x 6 ICs x 11 years) was submitted to the
855 computing network. This phase was considered finalized when simulations with 170 sets
856 of parameter values and 3 IC ensemble members per set and per year were completed.
857 These 5,610 simulations were used to train a suite of statistical emulators for various
858 climate metrics. An additional 94 sets of parameters with 3 IC ensemble members per set
859 and per year completed after starting Phase 3 and were used to validate the emulators
860 trained within Phase 2 (see Appendix B).
861
862 Separate statistical emulators were trained for MAC-T, JJA-T, JJA-Pr, DJF-T, DJF-Pr, SW,
863 and LW. Although ANN has the advantage of using multiple metrics as targets
864 simultaneously, the underlying emulator structure remains obscure, because an ANN is a

865 network of simple elements called neutrons which are organized in multilayer, and
866 different layers may perform different kinds of transformations on the inputs. For the sake
867 of simplicity and transparency, in Phase 2 we used kriging instead - which is similar to a
868 Gaussian process regression emulator - following McNeall et al. (2016) as coded in the
869 package DiceKriging (Roustant et al., 2012) in the statistical programming environment R.
870 We used universal kriging, with no 'nugget' term, meaning that the uncertainty on model
871 outputs shrinks to zero at the parameter input points that have already been run through our
872 climate model (Roustant et al., 2012). To validate if the emulators were adequate to predict
873 outputs at unseen parameter inputs, we needed to assure that it predicted relatively well
874 across our designed parameter inputs. For each emulator, we performed 'leave-one-out'
875 cross validation. The cross validation results showed no significant deviations in prediction
876 of the outputs (results not shown).
877
878 In addition to reducing parameter space in Phase 2, we also looked for parameters that
879 consistently showed little influence on our metrics of interest, as any reduction in
880 parameters could benefit subsequent experiments by reducing the overall dimensionality.
881 To identify which parameters have the most influence over the metrics of interest, we
882 performed two types of sensitivity analyses as described in Section 2.5. In the end, the 7
883 most influential parameters were retained after parameter reduction in Phase 2; these are
884 the bold-faced parameters in Table 1.
885
886 After eliminating parameter space resulting in MAC-T biases larger than 3°C, and reducing
887 the number of perturbed parameters to 7, we continued the parameter refinement process,

888 and randomly selected 100 parameter sets that emulated MAC-T biases less than 3°C and
889 had large spread in ENTCOEF and VIF1 (within the refined ranges of Phase 2). 100 was
890 subjectively chosen as a cut off number of new PPE sets to run through weather@home in
891 the next phase, mainly due to concern of not knowing how many more phases would be
892 required to reach our goal, while recognizing the practical constraints posed by the large
893 datasets that would potentially be generated in the following phases.
894
895 **Phase 3:** This objective of this phase was to further refine parameter space to reach the
896 target of northwest US regional bias in MAC-T less than 3°C, and then select 10 sets of
897 parameter values that met this criterion. The results in this phase satisfied our target, so we
898 stopped the iterative process here.
899
900 We were aware that our approach of regionally targeted parameter refinements might
901 degrade model performance elsewhere. Upon achieving our regional target, we
902 investigated the effects of our model tuning on global model metrics.
903
904 **Appendix B: Emulated vs. simulated results**
905 We used 94 additional ensemble members returned from Phase 2 (the 94 simulations that
906 completed after building the emulators from the Phase 2 PPE and starting Phase 3) to
907 provide out-of-sample validations of the emulators trained in Phase 2. In Fig. B1, we show
908 predictions from emulators against model-simulated values for all the output metrics. In all
909 cases, the linear relationship between the emulated and simulated is very strong (regression
910 coefficient regcoef>0.9), while the emulated results can predict the simulated results

911 relative well, with coefficient of determination R2 > 0.9 in the best cases (SW, LW and
912 JJA-T). It is not surprising that R2 for DJF-Pr is the smallest, considering precipitation in
913 DJF over NWUS is dominated by larger-scale atmospheric features such as the polar jet
914 stream, the Pacific subtropical high, and storm tracks (e.g.,Mock, 1996; Neelin et al., 2013;
915 Seager et al., 2014; Langenbrunner et al., 2015), and the internal variability of this metric
916 is the highest among those considered.
917
918 In Fig. B2, we present the emulated vs. simulated results in Phase 3 for the 95 PP sets that
919 were returned in Phase3. These 95 PP sets were run through the emulators from Phase 2 to
920 predict the climate metrics, then the emulated results were compared with the simulated
921 results returned from weather@home simulations. In most cases, r and R2 are lower than
922 the Phase 2 results (Fig. B1), except for LW and DJF-T, where R2 increases by a few
923 percent. This decrease in emulator prediction accuracy could be due to the fact that in Phase
924 3, only 7 parameters were perturbed simultaneously while keeping the rest at their default
925 values, so we have eliminated parts of the parameter space, which are no longer available
926 to the emulators.
927
928 The comparisons between simulated and emulated results from Phase 2 to Phase 3 highlight
929 the necessity of doing parameter refinement exercise in phases. Training a statistical
930 emulator once, then using it to search for optimal parameter settings may not always yield
931 optimum results. An emulator may not fully capture the behaviour of the climate model in
932 every aspect, especially when the number of parameters perturbed was changed during the
933 process, such as in our case.

Appendix C: Soil moisture control on plant photosynthesis in MOSES

The critical point θ_{crit} (m^3 of water per m^3 of soil) is the soil moisture content below which plant photosynthesis becomes limited by soil water availability and is calculated by:

$$\theta_{crit} = \theta_{wilt} + V\_CRIT\_ALPHA\ (\theta_{sat}-\theta_{wilt})$$

where θ_{sat} is the saturation point, i.e. the soil moisture content at the point of saturation; and θ_{wilt} is the wilting point, below which leaf stomata close. V_CRIT_ALPHA varies between zero and one, meaning that θ_{crit} varies between θ_{wilt} and θ_{sat} (Cox et al., 1999).

Author contributions

The model simulations were designed by S. Li ,D. E. Rupp, L. Hawkins, with inputs from P. W. Mote, and D. McNeall. All the results were analysed and plotted by S. Li. The paper was written by S. Li, with edits from all co-authors.

Competing interests

The authors declare that they have no conflict of interest.

Acknowledgements

This work was supported by USDA-NIFA grant 2013-67003-20652. We would like to thank our colleagues at the Oxford eResearch Centre for their technical expertise. We would also like to thank the Met Office Hadley Centre PRECIS team for their technical and scientific support for the development and application of weather@home. Finally, we

would like to thank all of the volunteers who have donated their computing time to climateprediction.net and weather@home.

Reference:

Adler, R.F., Huffman, G.J., Chang, A., Ferraro, R., Xie, P.P., Janowiak, J., Rudolf, B., Schneider, U., Curtis, S., Bolvin, D., Gruber, A., Susskind, J., Arkin, P., and Nelkin, E.: The Version 2 Global Precipitation Climatology Project (GPCP) Monthly Precipitation Analysis (1979-Present), J. Hydrometeor., 4,1147-1167, https://doi.org/10.1175/1525-7541(2003)004<1147:TVGPCP>2.0.CO;2, 2003.

Allen, M.: Do-it-yourself climate prediction, Nature, 401, 642, doi:10.1038/44266, 1999.

Annan, J.D. and Hargreaves, J.C.: Efficient estimation and ensemble generation in climate modelling. Philosophical Transactions of the Royal Society A: Mathematical, Physical and Engineering Sciences, 365(1857), pp.2077-2088, 2007.

Annan, J.D., Lunt, D.J., Hargreaves, J.C. and Valdes, P.J.: Parameter estimation in an atmospheric GCM using the Ensemble Kalman Filter. Nonlinear processes in geophysics, 12(3), pp.363-371, 2005.

Bellprat, O., Kotlarski, S., Lüthi, D., and Schär, C.: Exploring perturbed physics ensembles in a regional climate model, Journal of Climate, 25(13), 4582-4599, https://doi.org/10.1175/JCLI-D-11-00275.1, 2002a.

978 Bellprat, O., Kotlarski, S., Lüthi, D., and Schär, C.: Objective calibration of regional
979 climate models, Journal of Geophysical Research: Atmospheres, 117(D23),
980 https://doi.org/10.1029/2012JD018262, 2012b.
981 Bellprat, O., Kotlarski, S., Lüthi, D., De Elía, R., Frigon, A., Laprise, R., and Schär, C.:
982 Objective calibration of regional climate models: application over Europe and North
983 America, Journal of Climate, 29(2), 819-838, https://doi.org/10.1175/JCLI-D-15-0302.1,
984 2016.
985 Boberg, F. and Christensen, J. H.: Overestimation of Mediterranean summer temperature
986 projections due to model deficiencies, Nat. Climate Change, 2, 433–436, doi:10.1038/
987 nclimate1454, 2012.
988 Booth, B. B. B., Jones, C. D., Collins, M., Totterdell, I. J., Cox, P. M., Sitch, S.,
989 Huntingford, C., Betts, R. A., Harris, G. R., and Lloyd, J.: High sensitivity of future global
990 warming to land carbon cycle processes, Environ. Res. Lett., 7, 024002, doi:10.1088/1748-
991 9326/7/2/024002, 2012.
992 Brown, T. J., Hall, B. L., and Westerling, A. L.: The impact of twenty-first century climate
993 change on wildland fire danger in the western United States: an applications perspective,
994 Climatic change, *62*(1-3), 365-388, 2004.
995 Carslaw, K. S., Lee, L. A., Reddington, C. L., Pringle, K. J., Rap, A., Forster, P. M., Mann,
996 G. W. , Spracklen, D. V. , Woodhouse, M. T. , Regayre, L. A., and Pierce, J. R.: Large
997 contribution of natural aerosols to uncertainty in indirect forcing, Nature, 503(7474), 67,
998 2013.
999 Cheruy, F., Dufresne, J. L., Hourdin, F., and Ducharne, A. :Role of clouds and land-
1000 atmosphere coupling in midlatitude continental summer warm biases and climate change

1001 amplification in CMIP5 simulations, Geophys. Res. Lett., 41, 6493–6500,
1002 doi:10.1002/2014GL061145, 2014.
1003 Collins, M., Booth, B.B., Harris, G.R., Murphy, J.M., Sexton, D.M. and Webb, M.J.:
1004 Towards quantifying uncertainty in transient climate change. Climate Dynamics, 27(2-3),
1005 pp.127-147, 2006.
1006 Collins, W.J., Bellouin, N., Doutriaux-Boucher, M., Gedney, N., Hinton, T., Jones, C.D.,
1007 Liddicoat, S., Martin, G., O'Connor, F., Rae, J., Senior, C., Totterdell, I., Woodward, S.,
1008 Reichler, T., and Kim, J.: Evaluation of the HadGEM2 model, Hadley Cent. Tech. Note,
1009 74, 2008.
1010 Collins, M., Booth, B. B., Bhaskaran, B., Harris, G. R., Murphy, J. M., Sexton, D. M., and
1011 Webb, M. J.: Climate model errors, feedbacks and forcings: a comparison of perturbed
1012 physics and multi-model ensembles, Climate Dynamics, 36(9-10), 1737-1766, 2011.
1013 Compo, G.P., Whitaker, J.S., Sardeshmukh, P.D., Matsui, N., Allan, R.J., Yin, X., Gleason,
1014 B.E., Vose, R.S., Rutledge, G., Bessemoulin, P., Brönnimann, S., Brunet, M., Crouthamel,
1015 R.I., Grant, A.N., Groisman, P.Y., Jones, P.D., Kruk, M.C., Kruger, A.C., Marshall, G.J.,
1016 Maugeri, M., Mok, H.Y., Nordli, Ø., Ross, T.F., Trigo, R.M., Wang, X.L., Woodruff, S.D.,
1017 Worley, S.J.: The Twentieth Century Reanalysis Project. Quart. J. Roy. Meteor. Soc., 137,
1018 1-28, https://doi.org/10.1002/qj.776, 2011.
1019 Covey, C., Brandon, S., Bremer, P.T., Domyancis, D., Garaizar, X., Johannesson, G.,
1020 Klein, R., Klein, S.A., Lucas, D.D., Tannahill, J. and Zhang, Y.: A new ensemble of
1021 perturbed-input-parameter simulations by the Community Atmosphere Model. Technical
1022 report, Lawrence Livermore National Laboratory, Livermore, CA, 2011.

1023 Liu, C., Ikeda, K., Rasmussen, R., Barlage, M., Newman, A.J., Prein, A.F., Chen, F., Chen,
1024 L., Clark, M., Dai, A. Dudhia, J., Eidhammer, T., Gochis, D., Gutmann, E., Kurkute, S.,Li,
1025 Y., Thompson, G., and Yates, D.: Continental-scale convection-permitting modeling of the
1026 current and future climate of North America, Clim Dyn (2017) 49, 71-95,
1027 https://doi.org/10.1007/s00382-016-3327-9, 2017.
1028 Cox, P. M.: Description of the TRIFFID dynamic global vegetation model. Hadley Centre
1029 technical note, 24, 1-16, 2001.
1030 Cox, P. M., Betts, R. A., Bunton, C. B., Essery, R. L. H., Rowntree, P. R., and Smith, J. :
1031 The impact of new land surface physics on the GCM simulation of climate and climate
1032 sensitivity, Climate Dynamics, 15(3), 183-203, 1999.
1033 Daly, C., Halbleib, M., Smith, J.I., Gibson, W.P., Doggett, M.K., Taylor, G.H., Curtis, J.
1034 and Pasteris, P.P.: Physiographically sensitive mapping of climatological temperature and
1035 precipitation across the conterminous United States, International Journal of Climatology:
1036 a Journal of the Royal Meteorological Society, 28(15), 2031-2064, 2008.
1037 Dee, D.P., Uppala, S.M., Simmons, A.J., Berrisford, P., Poli, P., Kobayashi, S., Andrae,
1038 U., Balmaseda, M.A., Balsamo, G., Bauer, P., Bechtold, P., Beljaars, A.C.M., van de Berg,
1039 L., Bidlot, J., Bormann, N., Delsol, C., Dragani, R., Fuentes, M., Geer, A.J., Haimberger,
1040 L., Healy, S.B., Hersbach, H., Hólm, E.V., Isaksen, L., Kållberg, P., Köhler, M.,
1041 Matricardi, M., McNally, A.P., Monge-Sanz, B.M., Morcrette, J.J., Park, B.K., Peubey, C.,
1042 de Rosnay, P., Tavolato, C., Thépaut, J.N., Vitart, F. :The ERA-Interim reanalysis:
1043 configuration and performance of the data assimilation system, Quarterly Journal of the
1044 Royal Meteorological Society 137656 553–597, DOI: 10.1002/qj.828, 2011.

1045 Essery, R. L. H., Best, M. J., Betts, R. A., Cox, P. M., and Taylor, C. M.: Explicit
1046 Representation of Subgrid Heterogeneity in a GCM Land Surface Scheme, J.
1047 Hydrometeorol., 4, 530–543, doi:10.1175/1525-
1048 7541(2003)004<0530:EROSHI>2.0.CO;2, 2003.
1049 Fan, Y. and van den Dool, H.: A Global Monthly Land Surface Air Temperature Analysis
1050 for 1948-Present, J. Geophys. Res., 113, doi: 10.1029/2007JD008470, 2008.
1051 Fowler, H. J., Blenkinsop, S., and Tebaldi, C.: Linking climate change modelling to
1052 impacts studies: recent advances in downscaling techniques for hydrological
1053 modelling, International journal of climatology, 27(12), 1547-1578, 2007.
1054 Gelaro, R., McCarty, W., Suárez, M.J., Todling, R., Molod, A., Takacs, L., Randles, C.A.,
1055 Darmenov, A., Bosilovich, M.G., Reichle, R. and Wargan, K.: The modern-era
1056 retrospective analysis for research and applications, version 2 (MERRA-2).,Journal of
1057 Climate, 30(14), 5419-5454., J. Clim., doi: 10.1175/JCLI-D-16-0758.1, 2017.
1058 Gregory, D., and Rowntree, P. R. :A mass flux convection scheme with representation of
1059 cloud ensemble characteristics and stability-dependent closure, Monthly Weather Review,
1060 118(7), 1483-1506, 1990.
1061 Guillod, B. P., Jones, R. G., Bowery, A., Haustein, K., Massey, N. R., Mitchell, D. M.,
1062 Otto, F. E. L., Sparrow, S. N., Uhe, P., Wallom, D. C. H., Wilson, S., and Allen, M. R.:
1063 weather@home 2: validation of an improved global–regional climate modelling system,
1064 Geosci. Model Dev., 10, 1849-1872, DOI:10.5194/gmd-10-1849-2017, 2017.
1065 Guillod, B.P., Jones, R.G., Dadson, S.J., Coxon, G., Bussi, G., Freer, J., Kay, A.L., Massey,
1066 N.R., Sparrow, S.N., Wallom, D.C. and Allen, M.R. :A large set of potential past, present

and future hydro-meteorological time series for the UK. Hydrology and Earth System Sciences, 22(1), 611-634, https://doi.org/10.5194/hess-22-611-2018, 2018.

Hall, A., and Qu, X. (2006). Using the current seasonal cycle to constrain snow albedo feedback in future climate change, Geophysical Research Letters, 33(3), 2006.

Harris, G.R., Kendon, E.J., Betts, R.A. and Brown, S.J.: UK climate projections science report: climate change projections, 2009.

Harris, G.R., Sexton, D.M., Booth, B.B., Collins, M. and Murphy, J.M.: Probabilistic projections of transient climate change. Climate dynamics, 40(11-12), pp.2937-2972, 2013.

Harris, I.P.D.J., Jones, P.D., Osborn, T.J. and Lister, D.H.: Updated high-resolution grids of monthly climatic observations–the CRU TS3. 10 Dataset, International journal of climatology, 34(3), 623-642, doi:10.1002/joc.3711, 2014.

Hartmann, D.L., Ockert-Bell, M.E., and Michelsen, M.L.,:The effect of cloud type on Earth's energy balance: Global analysis, Journal of Climate, 5(11),1281-1304, https://doi.org/10.1175/1520-0442(1992)005<1281:TEOCTO>2.0.CO;2, 1992.

Hawkins, E., Osborne, T. M., Ho, C. K., and Challinor, A. J. : Calibration and bias correction of climate projections for crop modelling: an idealised case study over Europe, Agricultural and Forest Meteorology, 170, 19-31, 2013.

Hourdin, F., Grandpeix, J.-Y., Rio, C., Bony, S., Jam, A., Cheruy, F., Rochetin, N., Fairhead, L., Idelkadi, A., Musat, I., Dufresne, J.L., Lahellec, A., Lefebvre, M.-P., and Roehrig, R.: LMDZ5B: the atmospheric component of the IPSL climate model with revisited parameterizations for clouds and convection, Climate Dynamics, 40, 2193–2222, doi:10.1007/s00382-012-1343-y, http://dx.doi.org/10. 1007/s00382-012-1343-y, 2013.

1089 Huffman, G., Bolvin, D., Braithwaite, D., Hsu, K., Joyce, R., and Xie, P: Integrated Multi-
1090 satellitE Retrievals for GPM (IMERG), version 4.4. NASA's Precipitation Processing
1091 Center, accessed 31 March, 2015, ftp://arthurhou.pps.eosdis.nasa.gov/gpmdata/, 2014.
1092 Irvine, P. J., Gregoire, L. J., Lunt, D. J., and Valdes, P. J.: An efficient method to generate
1093 a perturbed parameter ensemble of a fully coupled AOGCM without flux-adjustment,
1094 Geoscientific Model Development, 6(5), 1447-1462, 2013.
1095 Jackson, C., Sen, M.K. and Stoffa, P.L.: An efficient stochastic Bayesian approach to
1096 optimal parameter and uncertainty estimation for climate model predictions. Journal of
1097 Climate, 17(14), pp.2828-2841, 2004.
1098 Jackson, C.S., Sen, M.K., Huerta, G., Deng, Y. and Bowman, K.P.: Error reduction and
1099 convergence in climate prediction. Journal of Climate, 21(24), pp.6698-6709, 2008.
1100 Järvinen, H., Räisänen, P., Laine, M., Tamminen, J., Ilin, A., Oja, E., Solonen, A. and
1101 Haario, H.: Estimation of ECHAM5 climate model closure parameters with adaptive
1102 MCMC. Atmospheric Chemistry and Physics, 10(20), pp.9993-10002, 2010.
1103 Johns, T.C., Durman, C.F., Banks, H.T., Roberts, M.J., McLaren, A.J., Ridley, J.K., Senior,
1104 C.A., Williams, K.D., Jones, A., Rickard, G.J., Cusack, S., Ingram, W.I., Crucifix, M.,
1105 Sexton, D. M. H., Joshi, M.M., Dong, B.-W., Spencer, H., Hill, R. S. R., Gregory, J.M.,
1106 Keen, A.B., Pardaens, A.K., Lowe, J.A., Bodas-Salcedo, A., Stark, S., and Searl, Y. : The
1107 new Hadley Centre climate model (HadGEM1): Evaluation of coupled simulations, Journal
1108 of Climate, 19(7), 1327-1353, https://doi.org/10.1175/JCLI3712.1, 2006.
1109 Kalnay, E., Kanamitsu, M., Kistler, R., Collins, W., Deaven, D., Gandin, L., Iredell, M.,
1110 Saha, S., White, G., Woollen, J., Zhu, Y., Chelliah, M., Ebisuzaki, W., Higgins, W.,
1111 Janowiak, J., Mo, K. C., Ropelewski, C., Wang, J., Leetmaa, A., Reynolds, R., Jenne, R.,

and Joseph, D.: The NCEP/NCAR 40-Year Reanalysis Project, Bull. Am. Meteorol. Soc., 77, 437–471, 1996.

Karmalkar, A.V., Sexton, D.M., Murphy, J.M., Booth, B.B., Rostron, J.W. and McNeall, D.J.: Finding plausible and diverse variants of a climate model. Part II: development and validation of methodology. Climate Dynamics, pp.1-31, 2019.

Knutti, R., Stocker, T. F., Joos, F., and Plattner, G. K.: Probabilistic climate change projections using neural networks, Climate Dynamics, 21(3-4), 257-272, 2003.

Kotlarski, S., Keuler, K., Christensen, O. B., Colette, A., Déqué, M., Gobiet, A., Goergen, K., Jacob, D., Lüthi, D., van Meijgaard, E., Nikulin, G., Schär, C., Teichmann, C., Vautard, R., Warrach-Sagi, K., and V. Wulfmeyer: Regional climate modeling on European scales: a joint standard evaluation of the EURO-CORDEX RCM ensemble, Geoscientific Model Development, 7(4), 1297-1333, 2004.

Langenbrunner, B., Neelin, J.D., Lintner, B.R., and Anderson, B.T.: Patterns of precipitation change and climatological uncertainty among CMIP5 models, with a focus on the midlatitude Pacific storm track, Journal of Climate, 28(19), 7857-7872, 2015.

Li, S., Mote, P. W., Rupp, D. E., Vickers, D., Mera, R., and Allen, M.R.: Evaluation of a regional climate modeling effort for the western United States using a superensemble from weather@ home, Journal of Climate, 28(19), 7470-7488, 2015.

Loeppky J.L., Sacks J., and Welch W.J.: Choosing the Sample Size of a Computer Experiment: a Practical Guide, Technometrics, 51(4):366–376, 2009.

Ma, H.Y., Klein, S.A., Xie, S., Zhang, C., Tang, S., Tang, Q., Morcrette, C.J., Van Weverberg, K., Petch, J., Ahlgrimm, M., Berg, L.K., Cheruy, F., Cole, J., Forbes, R., Gustafson Jr, W. I., Huang, M., Liu, Y., Merryfield, W., Qian, Y., Roehrig, R., and Wang,

Y.-C.: CAUSES: On the role of surface energy budget errors to the warm surface air temperature error over the Central United States, Journal of Geophysical Research: Atmospheres, 123, 2888–2909, https://doi.org/10.1002/2017JD027194, 2018.

Massey, N., Jones, R., Otto, F. E. L., Aina, T., Wilson, S., Murphy, J. M., Hassell, D., Yamazaki, Y. H., and Allen, M. R.: weather@home—development and validation of a very large ensemble modelling system for probabilistic event attribution, Quarterly Journal of the Royal Meteorological Society, 141, 1528–1545, doi:10.1002/qj.2455, 2015.

Mauritsen, T., Stevens, B., Roeckner, E., Crueger, T., Esch, M., Giorgetta, M., Haak, H., Jungclaus, J., Klocke, D., Matei, D., Mikolajewicz, U., Notz, D., Pincus, R., Schmidt, H., and Tomassini, L.: Tuning the climate of a global model, Journal of Advances in Modeling Earth Systems, 4, M00A01, doi:doi:10.1029/2012MS000154, 2012.

McKay, M. D., Beckman, R. J., and Conover, W. J.: Comparison of three methods for selecting values of input variables in the analysis of output from a computer code, Technometrics, 21(2), 239-245., 1979.

McNeall, D. J., Challenor, P. G., Gattiker, J. R., and Stone, E. J.: The potential of an observational data set for calibration of a computationally expensive computer model, Geosci. Model Dev., 6, 1715–1728, doi: 10.5194, 2013.

McNeall, D., Williams, J., Booth, B., Betts, R., Challenor, P., Wiltshire, A., and Sexton, D.: The impact of structural error on parameter constraint in a climate model, Earth System Dynamics, 7(4), 917-935, 2016.

Mearns, L.O., Arritt, R., Biner, S., Bukovsky, M.S., McGinnis, S., Sain, S., Caya, D., Correia Jr, J., Flory, D., Gutowski, W., Takle, E.S., Jones, R., Leung, R., Moufouma-Okia, W., McDaniel, L., Nues, A.M.B., Qian, Y., Roads-*, J., Sloan., L., and Snyder, M.: The

North American regional climate change assessment program: overview of phase I results, Bulletin of the American Meteorological Society, 93(9), 1337-1362, 2012.

Merrifield, A. L., and Xie, S. P.: Summer US surface air temperature variability: Controlling factors and AMIP simulation biases, Journal of Climate, 29(14), 5123–5139. https://doi.org/10.1175/JCLI-D-15-0705.1, 2016.

Mitchell, D., Heaviside, C., Vardoulakis, S., Huntingford, C., Masato, G., Guillod, B. P., Frumhoff, P., Bowery, A., Wallom, D., and Allen, M.: Attributing human mortality during extreme heat waves to anthropogenic climate change, Environ. Res. Lett., 11, 074006, doi:10.1088/1748-9326/11/7/074006, 2016.

Mock, C. J.: Climatic Controls and Spatial Variations of Precipitation in the Western United States, J. Climate, 9(5), 1111–1125, 1996.

Morcrette, C.J., Van Weverberg, K., Ma, H.Y., Ahlgrimm, M., Bazile, E., Berg, L.K., Cheng, A., Cheruy, F., Cole, J., Forbes, R. and Gustafson Jr, W.I.: Introduction to CAUSES: Description of weather and climate models and their near-surface temperature errors in 5 day hindcasts near the Southern Great Plains, Journal of Geophysical Research: Atmospheres, 123(5), pp.2655-2683. https://doi.org/10.1002/2017JD027199, 2018.

Mote, P.W., Allen, M.R., Jones, R.G., Li, S., Mera, R., Rupp, D.E., Salahuddin, A. and Vickers, D.: Superensemble regional climate modeling for the western United States, Bulletin of the American Meteorological Society (97), 203-215, doi: 10.1175/BAMS-D-14-00090.1, 2016.

Mueller, B., and Seneviratne S. I.: Systematic land climate and evapotranspiration biases in CMIP5 simulations, Geophys. Res. Lett., 41, 128–134, doi:10.1002/2013GL058055, 2014.

1181 Mulholland, D. P., Haines, K., Sparrow, S. N., and Wallom, D.: Climate model forecast
1182 biases assessed with a perturbed physics ensemble, Climate Dynamics, 49(5-6), 1729-
1183 1746, 2017.
1184 Murphy, J. M., Sexton, D. M. H., Barnett, D. N., Jones, G. S., Webb, M. J., Collins, M.,
1185 and Stainforth, D. A.: Quantification of modelling uncertainties in a large ensemble of
1186 climate change simulations, Nature, 430, 768–772, doi:10.1038/nature02771, 2004.
1187 Murphy, J.M., Booth, B.B., Collins, M., Harris, G.R., Sexton, D.M. and Webb, M.J.: A
1188 methodology for probabilistic predictions of regional climate change from perturbed
1189 physics ensembles. Philosophical Transactions of the Royal Society A: Mathematical,
1190 Physical and Engineering Sciences, 365(1857), pp.1993-2028, 2007.
1191 Murphy, J.M., Sexton, D.M., Jenkins, G.J., Booth, B.B., Brown, C.C., Clark, R.T., Collins,
1192 M.,
1193 Neelin, J. D., Bracco, A., Luo, H., McWilliams, J.C., and Meyerson, J. E.: Considerations
1194 for parameter optimization and sensitivity in climate models. Proc. Natl. Acad. Sci. USA,
1195 107(50), 21349–21354, doi:10.1073/pnas.1015473107, 2010.
1196 Neelin, J.D., Langenbrunner, B., Meyerson, J.E., Hall, A. and Berg, N.: California winter
1197 precipitation change under global warming in the Coupled Model Intercomparison Project
1198 phase 5 ensemble, Journal of Climate, 26(17), 6238-6256, 2013.
1199 oceanic quasi-equilibrium states, J. Atmos. Sci., 59, 1885– 1897.
1200 oceanic quasi-equilibrium states, J. Atmos. Sci., 59, 1885– 1897Bellprat, O., Kotlarski, S.,
1201 Lüthi, D., De Elía, R., Frigon, A., Laprise, R., and Schär, C.: Objective Calibration of
1202 Regional Climate Models: Application over Europe and North America, Journal of
1203 Climate, 29, 819–838, doi:10.1175/jcli-d-15-0302.1, 2016.Williamson, D., Goldstein, M.,

1204 Allison, L., Blaker, A., Challenor, P., Jackson, L., and Yamazaki, K.: History matching for
1205 exploring and reducing climate model parameter space using observations and a large
1206 perturbed physics ensemble, Climate Dynamics, 41, 1703–1729, doi:10.1007/s00382-013-
1207 1896-4, http://dx.doi.org/10.1007/s00382-013-1896-4, 2013.
1208 Onogi, K., Tsutsui, J., Koide, H., Sakamoto, M., Kobayashi, S., Hatsushika, H.,
1209 Matsumoto, T., Yamazaki, N., Kamahori, H., Takahashi, K., Kadokura, S., Wada, K., Kato,
1210 K., Oyama, R., Ose, T., Mannoji, N., and Taira, R.: The JRA-25 Reanalysis, J. Met. Soc.
1211 Jap., 85(3), 369-432, doi: 10.2151/jmsj.85.369, 2007.
1212 Otto, F.E.L., Massey, N., van Oldenborgh, G.J., Jones, R.G. and Allen, M.R.:Reconciling
1213 Two Approaches to Attribution of the 2010 Russian Heat Wave, Geophysical Research
1214 Letters, 39(L04702), 2012.
1215 Rosenzweig, C., Elliott, J., Deryng, D., Ruane, A.C., Müller, C., Arneth, A., Boote, K.J.,
1216 Folberth, C., Glotter, M., Khabarov, N., Neumann, K., Piontek, F., Pugh, T.A.M., Schmid,
1217 E., Stehfest, E., Yang, H., and Jones, J.W. :Assessing agricultural risks of climate change
1218 in the 21st century in a global gridded crop model intercomparison, Proceedings of the
1219 National Academy of Sciences, 111(9), 3268-3273, 2014.
1220 Rougier, J.C., Sexton, D.M.H., Murphy, J.M., and Stainforth, D. : Analyzing the climate
1221 sensitivity of the HadSM3 climate model using ensembles from different but related
1222 experiments, J Clim 22(13):3540–3557, https://doi.org/10.1175/2008JCLI2533.1, 2009.
1223 Roustant, O., Ginsbourger, D., and Deville, Y.: DiceKriging, DiceOptim: Two R Packages
1224 for the Analysis of Computer Experiments by Kriging-Based Metamodeling and
1225 Optimization, Journal of Statistical Software, 51(i01), 2012.

1226 Rowlands, D. J., Frame, D. J., Ackerley, D., Aina, T., Booth, B. B., Christensen, C., and
1227 Gryspeerdt, E.: Broad range of 2050 warming from an observationally constrained large
1228 climate model ensemble, Nature Geoscience, 5(4), 256, 2012.
1229 Rupp, D.E., Li, S., Mote, P.W., Massey, N., Sparrow, S.N., and Wallom, D.C.: Influence
1230 of the Ocean and Greenhouse Gases on Severe Drought Likelihood in the Central US in
1231 2012, Journal of Climate (30), 1789-1806, doi: 10.1175/JCLI-D-16-0294.1, 2017a.
1232 Rupp, D. E., Li, S., Mote, P. W., Shell, K.M., Massey, N., Sparrow, S. N., Wallom, D. C.
1233 H., and Allen, M. R.: Seasonal Spatial Patterns of Projected Anthropogenic Warming in
1234 Complex Terrain: A Modeling Study of the Western USA, Climate Dynamics (48), 2191-
1235 2213, doi: 10.1007/s00382-016-3200-x, 2017b.
1236 Rupp, D. E. and Li, S.: Less warming projected during heavy winter precipitation in the
1237 Cascades and Sierra Nevada, Int. J. Climatol., 37(10): 3984–3990. doi:10.1002/joc.4963,
1238 2017.
1239 Saha, S., Moorthi, S., Pan, H.L., Wu, X., Wang, J., Nadiga, S., Tripp, P., Kistler, R.,
1240 Woollen, J., Behringer, D. and Liu, H.: The NCEP climate forecast system reanalysis,
1241 Bulletin of the American Meteorological Society, 91(8), 1015-1058, 2010.
1242 Saltelli, A., Tarantola, S., and Chan, K. S.: A quantitative model-independent method for
1243 global sensitivity analysis of model output, Technometrics, 41(1), 39-56, 1999.
1244 Sanderson, B. M.: A multimodel study of parametric uncertainty in predictions of climate
1245 response to rising greenhouse gas concentrations, Journal of Climate, 24(5), 1362-1377,
1246 2011.
1247 Sanderson, B. M., Knutti, R., Aina, T., Christensen, C., Faull, N., Frame, D. J., Ingram,
1248 W.J., Piani, C., Stainforth, D.A., Stone, D.A., and Allen, M. R.: Constraints on model

response to greenhouse gas forcing and the role of subgrid-scale processes, Journal of Climate, 21(11), 2384-2400, 2008a--ANN.

Sanderson, B. M., Piani, C., Ingram, W. J., Stone, D. A., and Allen, M. R.: Towards constraining climate sensitivity by linear analysis of feedback patterns in thousands of perturbed-physics GCM simulations, Climate Dynamics, 30(2-3), 175-190, 2008b--entcoef.

Sanderson, B. M., Shell, K. M., and Ingram, W.: Climate feedbacks determined using radiative kernels in a multi-thousand member ensemble of AOGCMs, Climate dynamics, 35(7-8), 1219-1236, 2010.

Schaller, N., Kay, A.L., Lamb, R., Massey, N.R., van Oldenborgh, G.J., Otto, F.E.L., Sparrow, S.N., Vautard, R., Yiou, P., Ashpole, I., Bowery, A., Crooks, S.M., Haustein, K., Huntingford, C., Ingram, W.J., Jones, R.G., Legg, T., Miller, J., Skeggs, J., Wallom, D., Weisheimer, A., Wilson, S., Stott, P.A. and Allen, M.R. : Human Influence on Climate in the 2014 Southern England Winter Floods and Their Impacts, Nature Climate Change, 6: 627-634, 2016.

Schirber, S., Klocke, D., Pincus, R., Quaas, J., and Anderson, J. L.: Parameter estimation using data assimilation in an atmospheric general circulation model: From a perfect toward the real world, Journal of Advances in Modeling Earth Systems,5(1), 58–70, doi:10.1029/2012MS000167, 2013.

Schneider, U., Becker, A., Finger, P., Meyer-Christoffer, A., Rudolf, B., and Ziese, M.: GPCC Full Data Reanalysis Version 6.0 at 0.5°: Monthly Land-Surface Precipitation from Rain-Gauges built on GTS-based and Historic Data, doi:10.5676/DWD_GPCC/FD_M_V6_050, 2011.

1272 Seager, R., Neelin, D., Simpson, I., Liu, H., Henderson, N., Shaw, T., Kushnir, Y., Ting,
1273 M. and Cook, B.: Dynamical and thermodynamical causes of large-scale changes in the
1274 hydrological cycle over North America in response to global warming, Journal of Climate,
1275 27(20), 7921-7948, 2014.
1276 Seneviratne, S. I., Lüthi, D., Litschi, M., and Schär, C.: Land–atmosphere coupling and
1277 climate change in Europe, Nature, 443(7108), 205, 2006.
1278 Sexton, D. M., Murphy, J. M., Collins, M., and Webb, M. J.: Multivariate probabilistic
1279 projections using imperfect climate models part I: outline of methodology, Climate
1280 dynamics, 38(11-12), 2513-2542, 2012a.
1281 Sexton, D.M. and Murphy, J.M.: Multivariate probabilistic projections using imperfect
1282 climate models. Part II: robustness of methodological choices and consequences for climate
1283 sensitivity. Climate Dynamics, 38(11-12), pp.2543-2558, 2012b.
1284 Sexton, D.M.H., Karmalkar, A.V., Murphy, J.M., Williams, K.D., Boutle, I.A., Morcrette,
1285 C.J., Stirling, A.J. and Vosper, S.B.: Finding plausible and diverse variants of a climate
1286 model. Part 1: establishing the relationship between errors at weather and climate time
1287 scales. Climate Dynamics, pp.1-34, 2019.
1288 Sippel, S., Otto, F.E., Forkel, M., Allen, M.R., Guillod, B.P., Heimann, M., Reichstein, M.,
1289 Seneviratne, S.I., Thonicke, K. and Mahecha, M.D.: A novel bias correction methodology
1290 for climate impact simulations, Earth System Dynamics, 7(1), 71-88, 2016.
1291 Solomon, S., Qin, D., Manning, M., Chen, Z., Marquis, M., Averyt, K. B., Tignor, M., and
1292 Miller, H. L.: Climate change 2007: The physical science basis, in Contribution of Working
1293 Group I to the Fourth Assessment Report of the Intergovernmental Panel on Climate
1294 Change, 2007 Cambridge University Press, Cambridge, United Kingdom and

1295 New York, NY, USA, 2007.
1296 Sparrow, S., Wallom, D., Mulholland, D. P., and Haines, K.: Climate model forecast biases
1297 assessed with a perturbed physics ensemble, Climate Dynamics, 2016.
1298 Stainforth, D. A., Aina, T., Christensen, C., Collins, M., Faull, N., Frame, D. J.,
1299 Kettleborough, J. A., Knight, S., Martin, A., Murphy, J., Piani, C., Sexton, D., Smith, L.
1300 A., Spicer, R. A., Thorpe, A. J., and Allen, M. R.: Uncertainty in predictions of the climate
1301 response to rising levels of greenhouse gases, Nature, 433(7024), 403–406, 2005.
1302 Stephens, G.L.:Cloud feedbacks in the climate system: A critical review, Journal of
1303 climate, 18(2), 237-273, https://doi.org/10.1175/JCLI-3243.1, 2005.
1304 Stephens, G. L., Li, J., Wild, M., Clayson, C. A., Loeb, N., Kato, S., L'ecuyer, T.,
1305 Stackhouse Jr, P.W., Lebsock, M. and Andrews, T. : An update on Earth's energy balance
1306 in light of the latest global observations, Nature Geoscience, 5(10), 691, 2012.
1307 Stott, P. A., Stone, D. A., and Allen, M. R.: Human contribution to the European heatwave
1308 of 2003, Nature, 432(7017), 610, 2004.
1309 Tett, S. F., Mitchell, J. F., Parker, D. E., and Allen, M. R.: Human influence on the
1310 atmospheric vertical temperature structure: Detection and observations, Science,
1311 274(5290), 1170-1173, 1996.
1312 Tett, S. F., Yamazaki, K., Mineter, M. J., Cartis, C., and Eizenberg, N.: Calibrating climate
1313 models using inverse methods: case studies with HadAM3, HadAM3P and HadCM3,
1314 Geoscientific Model Development, 10(9), 3567-3589, 2017.
1315 Uhe, P., Philip, S., Kew, S., Shah, K., Kimutai, J., Mwangi, E., van Oldenborgh, G.J.,
1316 Singh, R., Arrighi, J., Jjemba, E., Cullen, H. and Otto, F.E.L.: Attributing Drivers of the
1317 2016 Kenyan Drought, International Journal of Climatology, 38, e554-e568, 2018.

van Oldenborgh, G.J., Otto, F.E.L., Haustein, K. and AchutaRao, K.: The Heavy Precipitation Rvent of December 2015 in Chennai, India, In Explaining Extremes of 2015 from a Climate Perspective. Bulletin of the American Meteorological Society, 97(12), S87-S91, 2016.

van Oldenborgh, G.J., van der Wiel, K., Sebastian, A., Singh, R., Arrighi, J., Otto, F. E.L., Haustein, K., Li, S., Vecchi, G. and Cullen, H. : Attribution of Extreme Rainfall from Hurricane Harvey, August 2017, Environmental Research Letters,12(12),124009, 2017.

Van Weverberg, K., Morcrette, C.J., Petch, J., Klein, S.A., Ma, H.Y., Zhang, C., Xie, S., Tang, Q., Gustafson Jr, W.I., Qian, Y. and Berg, L.K., : CAUSES: Attribution of surface radiation biases in NWP and climate models near the U.S. Southern Great Plains, Journal of Geophysical Research: Atmospheres, 123, 3612–3644. https://doi.org/10.1002/2017JD027188, 2018.

Williams, J. H. T., Smith, R. S., Valdes, P. J., Booth, B. B. B., and Osprey, A.: Optimising the FAMOUS climate model: inclusion of global carbon cycling, Geoscientific Model Development, 5, 3089-3129, 2013.

Williamson, D., Goldstein, M., Allison, L., Blaker, A., Challenor, P., Jackson, L. and Yamazaki, K.: History matching for exploring and reducing climate model parameter space using observations and a large perturbed physics ensemble. Climate dynamics, 41(7-8), 1703-1729, 2013.

Williamson, D., Blaker, A. T., Hampton, C., and Salter, J.: Identifying and removing structural biases in climate models with history matching, Climate dynamics, 45(5-6), 1299-1324, 2015.

1340 Williamson, D. B., Blaker, A. T., and Sinha, B.: Tuning without over-tuning: parametric
1341 uncertainty quantification for the NEMO ocean model, Geoscientific Model Development,
1342 10(4), 1789-1816, doi:10.5194/gmd-10-1789-2017,2017.
1343 Wu, X. : Effects of ice mircrophysics on tropical radiative-convective- oceanic quasi-
1344 equilibrium states, J. Atmos. Sci., 59, 1885– 1897, 2002.
1345 Xie, P., and Arkin, P.A.: Global precipitation: a 17-year monthly analysis based on gauge
1346 observations, satellite estimates, and numerical model outputs. Bull. Amer. Meteor. Soc.,
1347 78, 2539-2558, 1996.
1348 Yamazaki, K., Rowlands, D. J., Aina, T., Blaker, A., Bowery, A., Massey, N., Miller, J.,
1349 Rye, C., Tett, S. F. B., Williamson, D., Yamazaki, Y. H., and Allen, M. R.: Obtaining
1350 diverse behaviors in a climate model without the use of flux adjustments, JGR-
1351 Atmospheres, 118, 2781–2793, doi:10.1002/jgrd.50304, 2013.
1352 Zelinka, M.D., Klein, S.A. and Hartmann, D.L.: Computing and partitioning cloud
1353 feedbacks using cloud property histograms. Part I: Cloud radiative kernels. Journal of
1354 Climate, 25(11), pp.3715-3735, 2012.
1355 Zhang, C., Xie, S., Klein, S.A., Ma, H.Y., Tang, S., Van Weverberg, K., Morcrette, C.J.
1356 and Petch, J.: CAUSES: Diagnosis of the summertime warm bias in CMIP5 climate models
1357 at the ARM Southern Great Plains site, Journal of Geophysical Research: Atmospheres,
1358 123, 2968–2992. https:// doi.org/10.1002/2017JD027200, 2018.
1359 Zhang, T., Li, L., Lin, Y., Xue, W., Xie, F., Xu, H., and Huang, X.: An automatic and
1360 effective parameter optimization method for model tuning, Geoscientific Model
1361 Development, 8, 3579–3591, doi:10.5194/gmd-8-3579-2015, http://www.geosci-model-
1362 dev.net/8/3579/2015/, 2015.

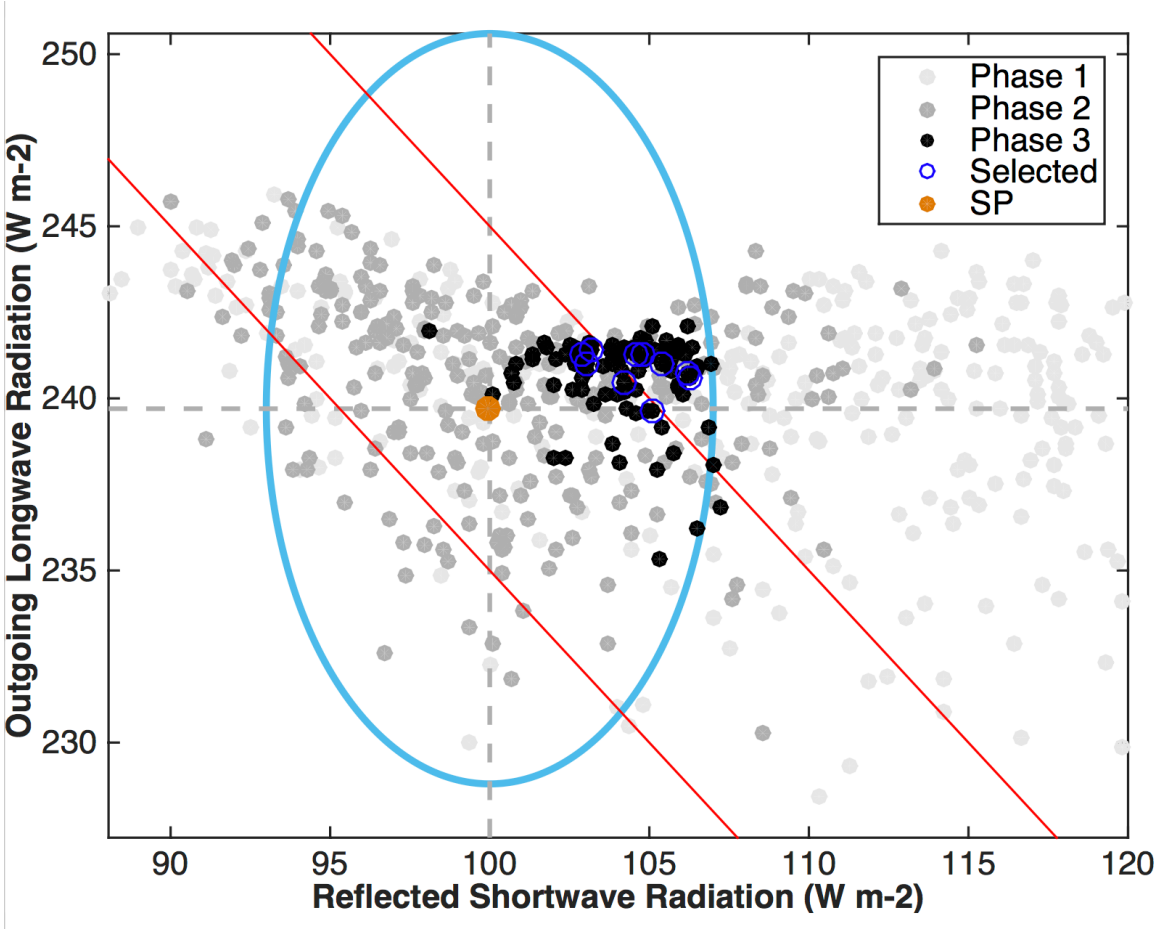

Figure 1. Global mean top-of-atmosphere (TOA) outgoing (reflected) shortwave radiation (SW) and outgoing longwave radiation (LW) from the four ensembles run through weather@home2. Horizontal and vertical dashed lines denote the reference values for SW and LW taken from Stephens et al. (2012). The filled brown circle denotes our SP. The ellipse indicates the uncertainty ranges we are willing to accept for SW and LW respectively, which includes the observational uncertainty range taken from Stephens et al. (2012), but tripled, plus the uncertainty range due to initial condition perturbations estimated from our SP reference ensemble. The red solid lines highlight net TOA energy flux of +/- 5 Wm^{-2}.

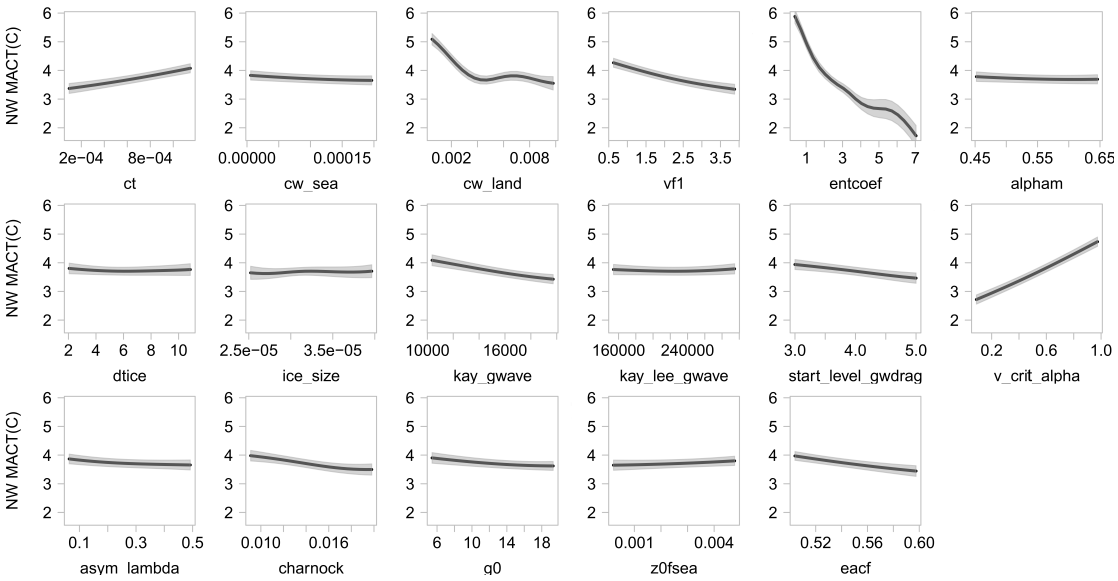

Figure 2. One-at-a-time sensitivity analysis of magnitude of annual cycle of temperature (MAC-T) over Northwest to each input parameter in turn, with all other parameters held at mean value of all the designed points. Heavy lines represent the emulator mean, and shaded areas represent the estimate of emulator uncertainty, at the ±1 SD level.

1390

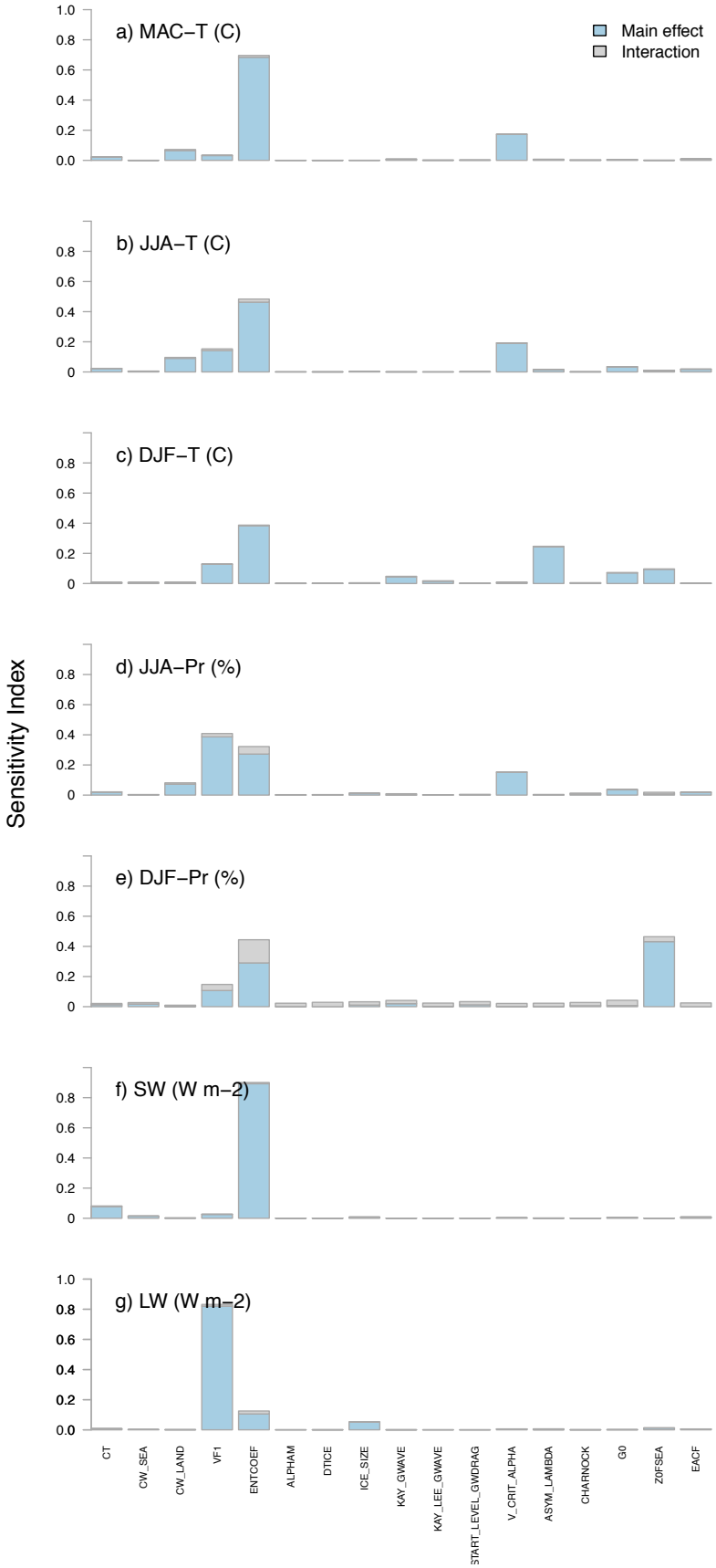
a) MAC–T (C)
b) JJA–T (C)
c) DJF–T (C)
d) JJA–Pr (%)
e) DJF–Pr (%)
f) SW (W m–2)
g) LW (W m–2)
Main effect
Interaction
Sensitivity Index
CT
CW_SEA
CW_LAND
VF1
ENTCOEF
ALPHAM
DTICE
ICE_SIZE
KAY_GWAVE
KAY_LEE_GWAVE
START_LEVEL_GWDRAG
V_CRIT_ALPHA
ASYM_LAMBDA
CHARNOCK
G0
Z0FSEA
EACF

1391

Figure 3. Sensitivity analysis of model output metrics in Phase 2 via the FAST algorithm of Saltelli et el. (1999).

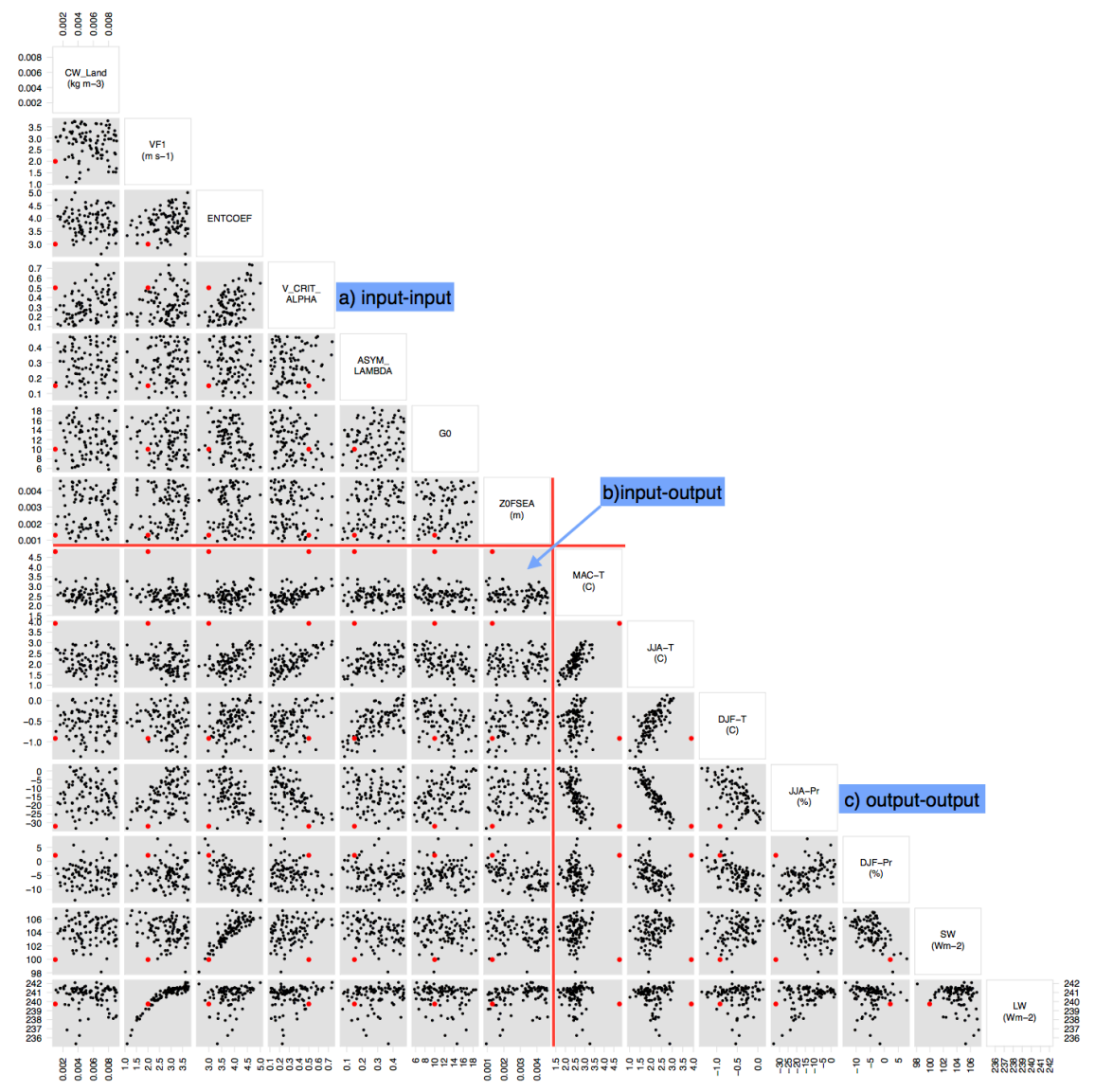

Figure 4. Phase 3 PPE parameter inputs and summary model output metrics evaluated. 95 parameter sets are shown. The parameter values and model outputs under SP are marked in red. The horizontal and vertical red lines mark the transition from parameter inputs and model output metrics.

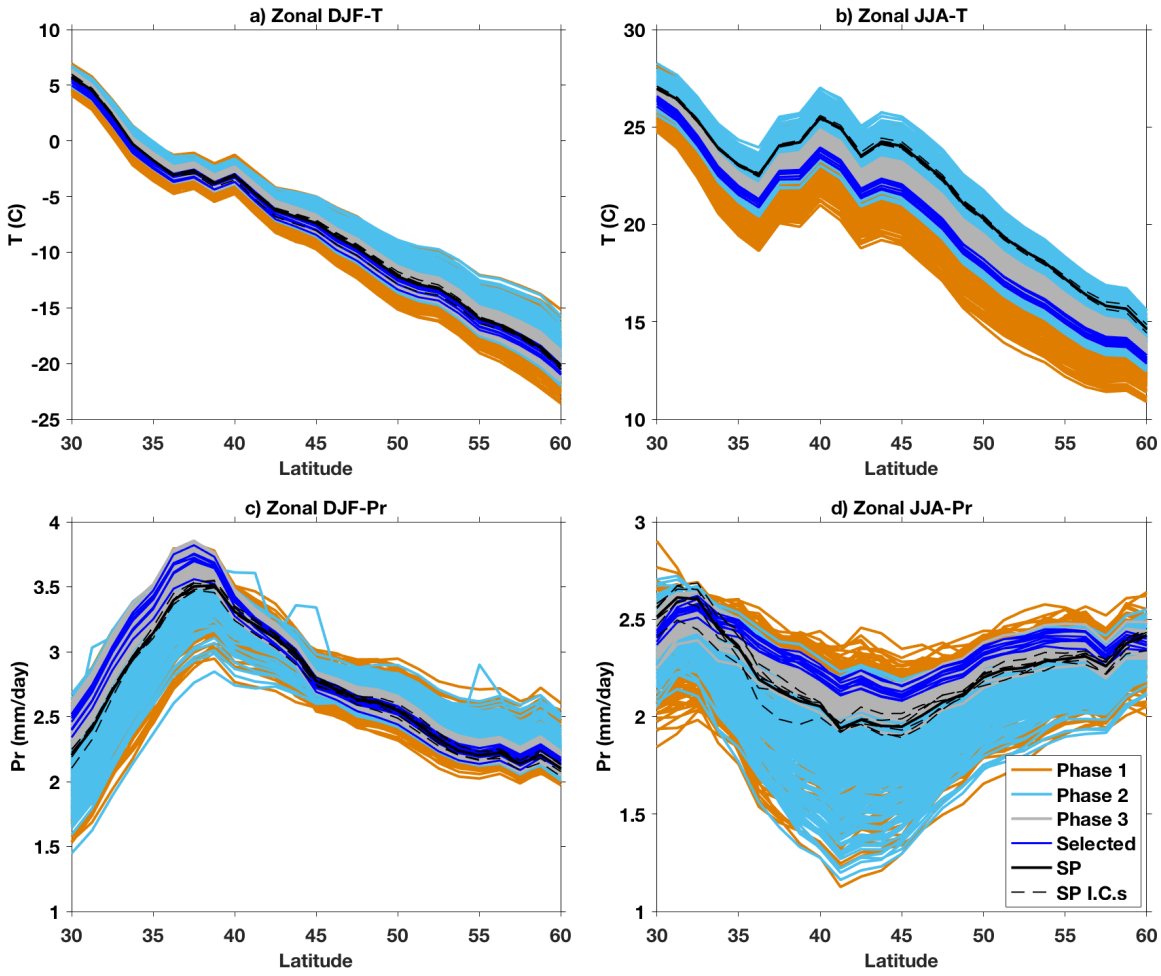

Figure 5. Comparison between three PPEs and SP zonal mean HadAM3P simulated North Hemisphere mid-latitude (30°N-60°N) a) DJF mean temperature over land, b) JJA mean temperature over land, c) DJF mean precipitation, and d) JJA mean precipitation. Output from the selected 10 parameter sets selected, based on NWUS MAC-T, are shown in blue. Note that the plotting order is the same as the legend, so most Phase 1 curves are obscured by subsequent phases. The results from different initial conditions (I.C.s) under SP are shown as black dashed lines.

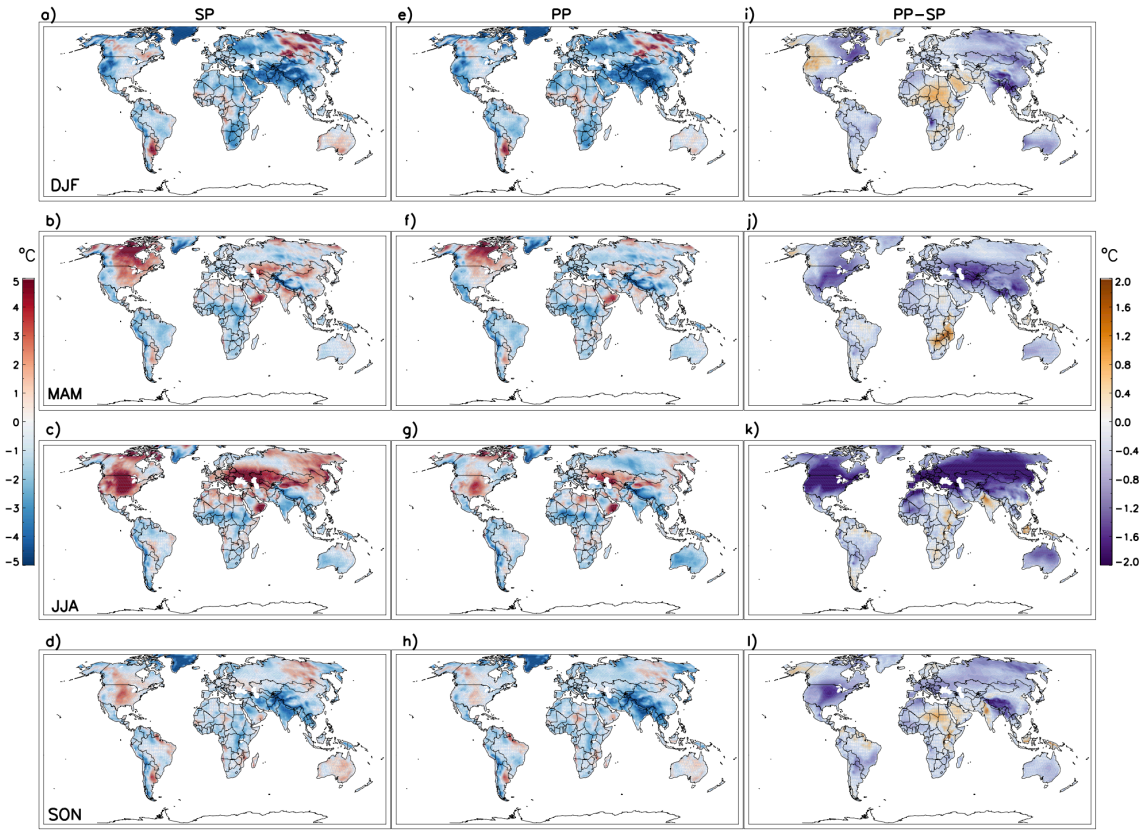

Figure 6. Biases of SP temperature over land in a) DJF, b) MAM, c) JJA, and d) SON, compared with CRU over December 1996 through November 2007. Biases of selected PP compared with CRU are shown in e)-h), while the differences between selected PP and SP, i.e. the absolute increase or decrease of biases in PP with respect to the SP values, are shown in i) - l). The PP results are the composites of the 10 selected sets, 6 IC per set.

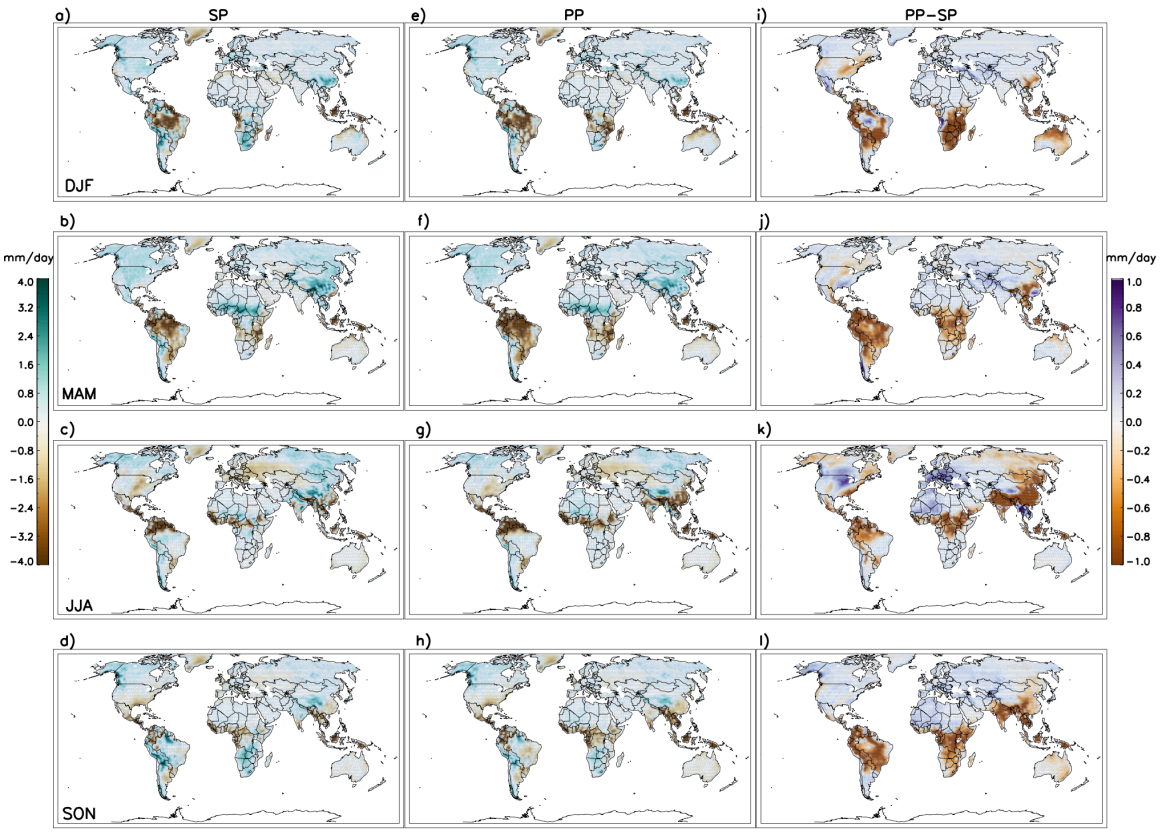

1418

1419 **Figure 7.** Same as Fig. 6, but for precipitation.

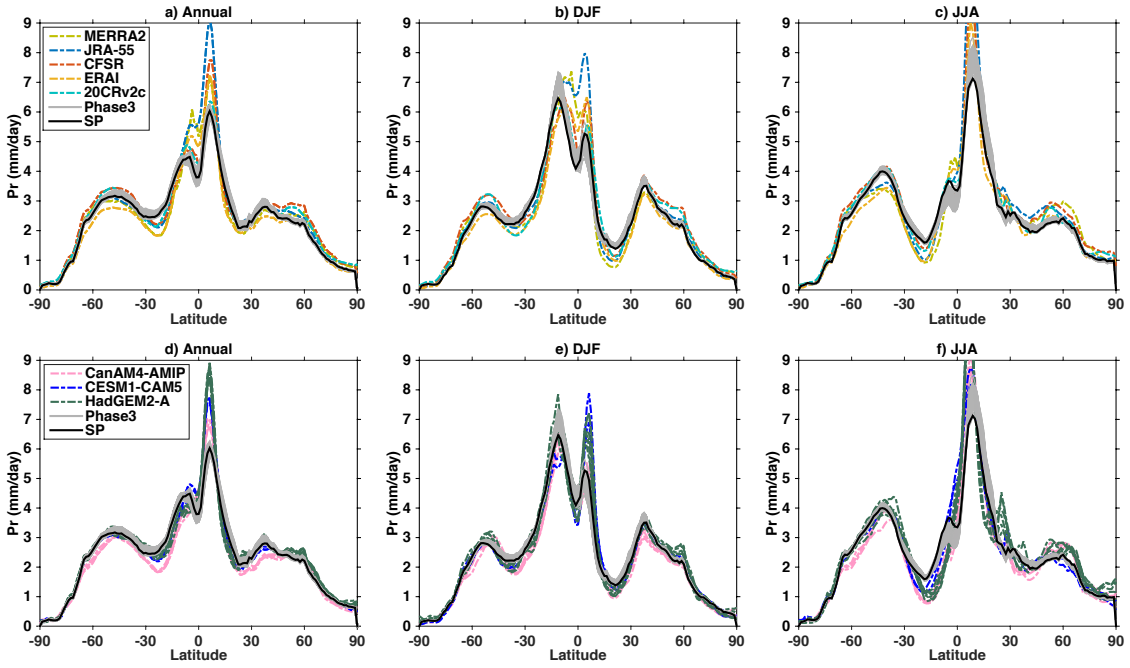

1420

1421 **Figure 8.** Annual (a,d), DJF (b,e) and JJA (c,f) meridional distributions of precipitation

1422 from Phase 3 and SP (all panels), reanalysis datasets MERRA2, JRA-55, CFSR, ERAI and

1423 20CRv2c shown (a - c) and GCMs CanAM4-AMIP, CESM1-CAM5, and HadGEM2-A,

1424 shown in (d - f).

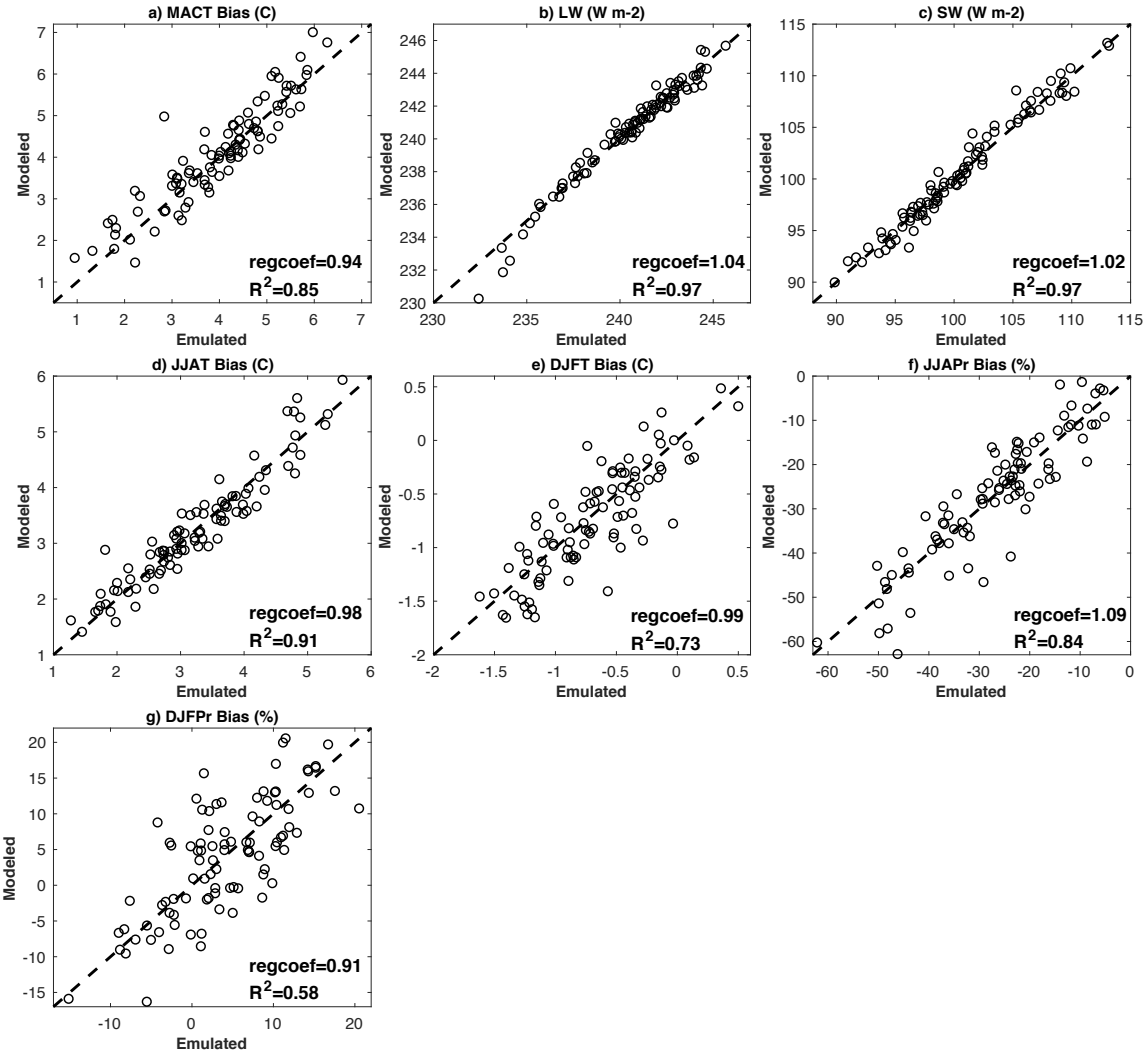

1425

1426 **Figure B1.** Emulator predicted results vs. model simulated results in Phase 2 for different
1427 model output metrics based on 94 parameter sets not used to train the emulator (the 94 sets
1428 that finished after starting Phase3). The regression coefficient (regcoef) and coefficient of
1429 determination (R^2) by emulated results are shown in each panel. The dashed line in each
1430 panel denotes the 1:1 line.

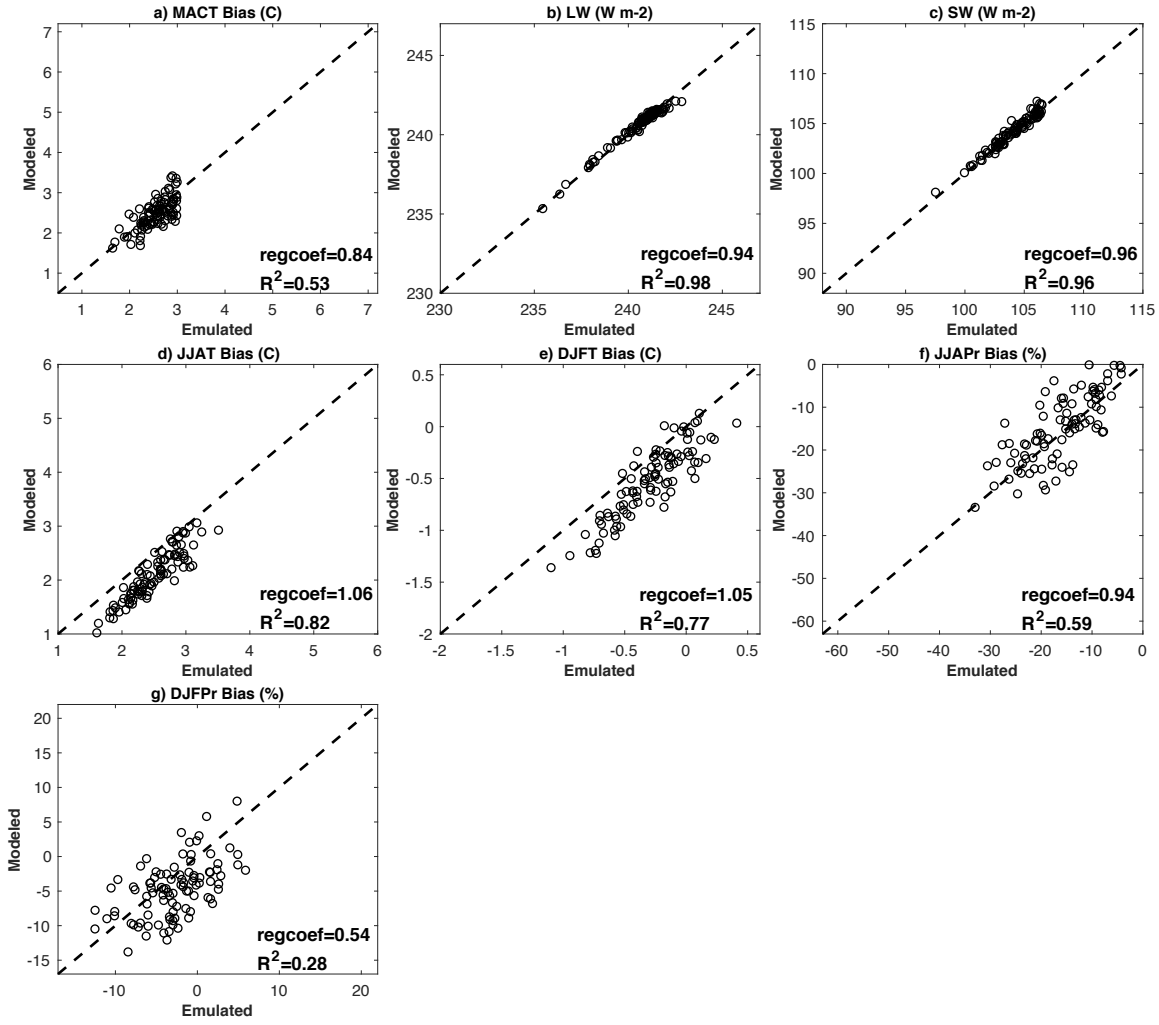

1431

1432 **Figure B2.** Same as Fig. B1, but for the 95 parameter sets in Phase 3. Note the ranges of

1433 x- and y-axis are set to be the same as in Fig. B1.

1434

1435

1436

1437

1438

1439

Table 1. Parameters perturbed in our tuning exercise with the post-culling parameters highlighted in bold.

Parameter	Default	Low	High	Description	Model component
CT (s^{-1})	6×10^{-4}	0.5×10^{-4}	1.2×10^{-3}	Rate at which cloud liquid water is converted to precipitation	Cloud
CW_SEA (kg m^{-3})	2.0×10^{-5}	0.5×10^{-5}	2.0×10^{-4}	Threshold cloud liquid water content over sea	Cloud
CW_LAND (kg m^{-3})	1.0×10^{-3}	0.5×10^{-3}	1.0×10^{-2}	Threshold cloud liquid water content over land	Cloud
EACF	0.5	0.5	0.6	Empirically adjusted cloud fraction	Cloud
VF1 (m s^{-1})	2	0.5	4	Ice fall speed	Cloud
ENTCOEF	3	0.3	9.5	Entrainment rate coefficient	Convection
ALPHAM	0.5	0.45	0.65	Albedo at melting point of sea ice	Radiation
DTICE (°C)	10	2	11	Temperature range over which ice albedo varies	Radiation
ICE_SIZE (m)	3.0×10^{-5}	2.5×10^{-5}	4.0×10^{-5}	Ice particle size	Radiation
KAY_GWAVE (m)	1.8×10^{4}	1.0×10^{4}	2.0×10^{4}	Surface gravity wave drag: typical wavelength	Dynamics
KAY_LEE_GWAVE ($m^{-3/2}$)	2.7×10^{5}	1.5×10^{5}	3.0×10^{5}	Surface gravity wave trapped lee wave constant	Dynamics
START_LEVEL_GWDRAG	3	3	5	Lowest model level for gravity wave drag	Dynamics
V_CRIT_ALPHA	0.5	0.01	0.99	Control of photosynthesis with soil moisture	Land surface
ASYM_LAMBDA	0.15	0.05	0.5	Vertical distance over which air parcels travel before mixing with their surroundings	Boundary layer

CHARNOCK	0.012	0.009	0.020	Constant in Charnock formula for calculating roughness length for momentum transport over sea	Boundary layer
G0	10	5	20	Used in calculation of stability function for heat, moisture, and momentum transport	Boundary layer
Z0FSEA (m)	1.3×10^{-3}	2.0×10^{-4}	5×10^{-3}	Roughness length for free heat and moisture transport over the sea	Boundary layer

Table 2. The specifics of four ensembles used in this study.

Experiment	Start dates	Number of parameters	Number of parameter sets in PPE	IC per parameter set per year used in the analysis
SP	1 Dec 1995, 1996, …, 2005	1	1	6
PPE Phase 1	1 Dec 1995	17	220	3
PPE Phase 2	1 Dec 1995, 1996, …, 2005	17	264	3
PPE Phase 3	1 Dec 1995, 1996, …, 2005	7	95	6

Supplementary Information

Subsequent to the model tuning in this study, a large ensemble of climatology simulations (from October1988 to September2015) were run with PP set2 from the final selected 10 sets, with more than 100 simulations per year. Some initial analysis of the surface energy budget and surface radiative fluxes from this PP climatology were compared with a large ensemble of climatology simulations under SP to better understand the reduction in near surface temperature biases, shown in Fig. S16.

Table S1. Information of models used in Fig. 8, including the modelling institutions, model standard names, pertinent references, and ensemble members shown for each model.

Modeling institution	Model name	References	Ensemble member
Canadian Centre for Climate Modeling and Analysis	CanAM4	Chylek et al. (2011)	4
National Center for Atmospheric Research Community Earth System Model	CESM-CAM5	Neale et al. (2010)	2
Met Office Hadley Centre	HadGEM2-A	Martin et al. (2006) Collins et al. (2011)	6

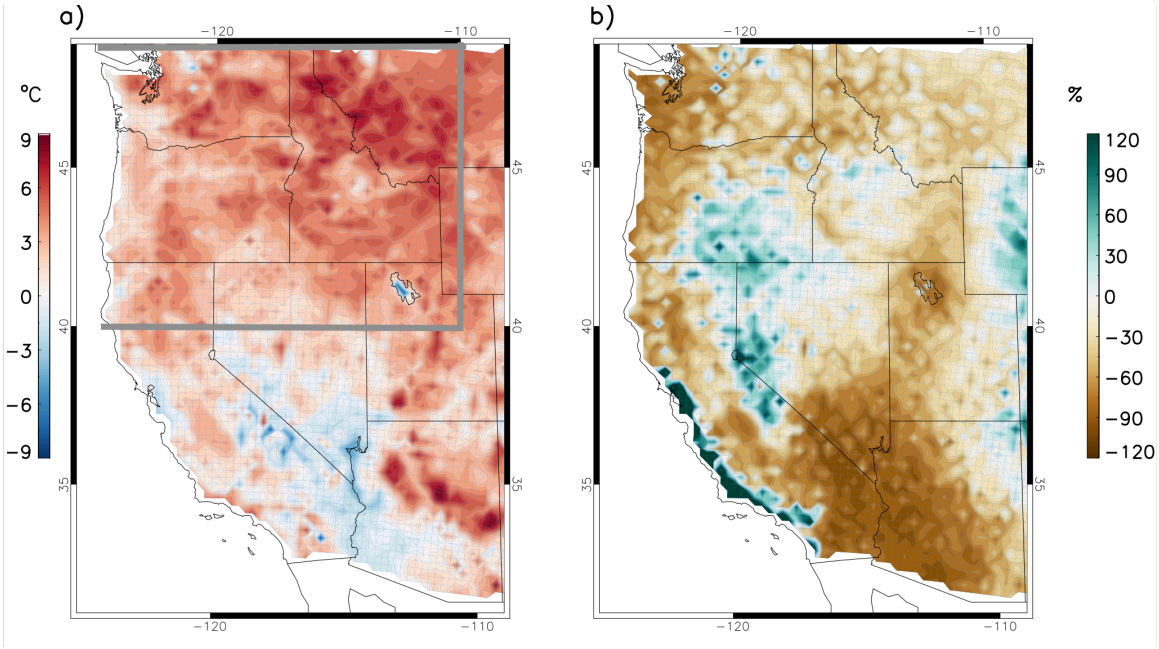

Figure S1. Biases in a) June-July-August (JJA) mean temperature (°C) , and b) precipitation (%) simulated by HadRM3P compared with PRISM over dec1996-nov 2007 under standard physics (SP) setting. The NWUS is defined as the land region bounded by the heavy grey line.

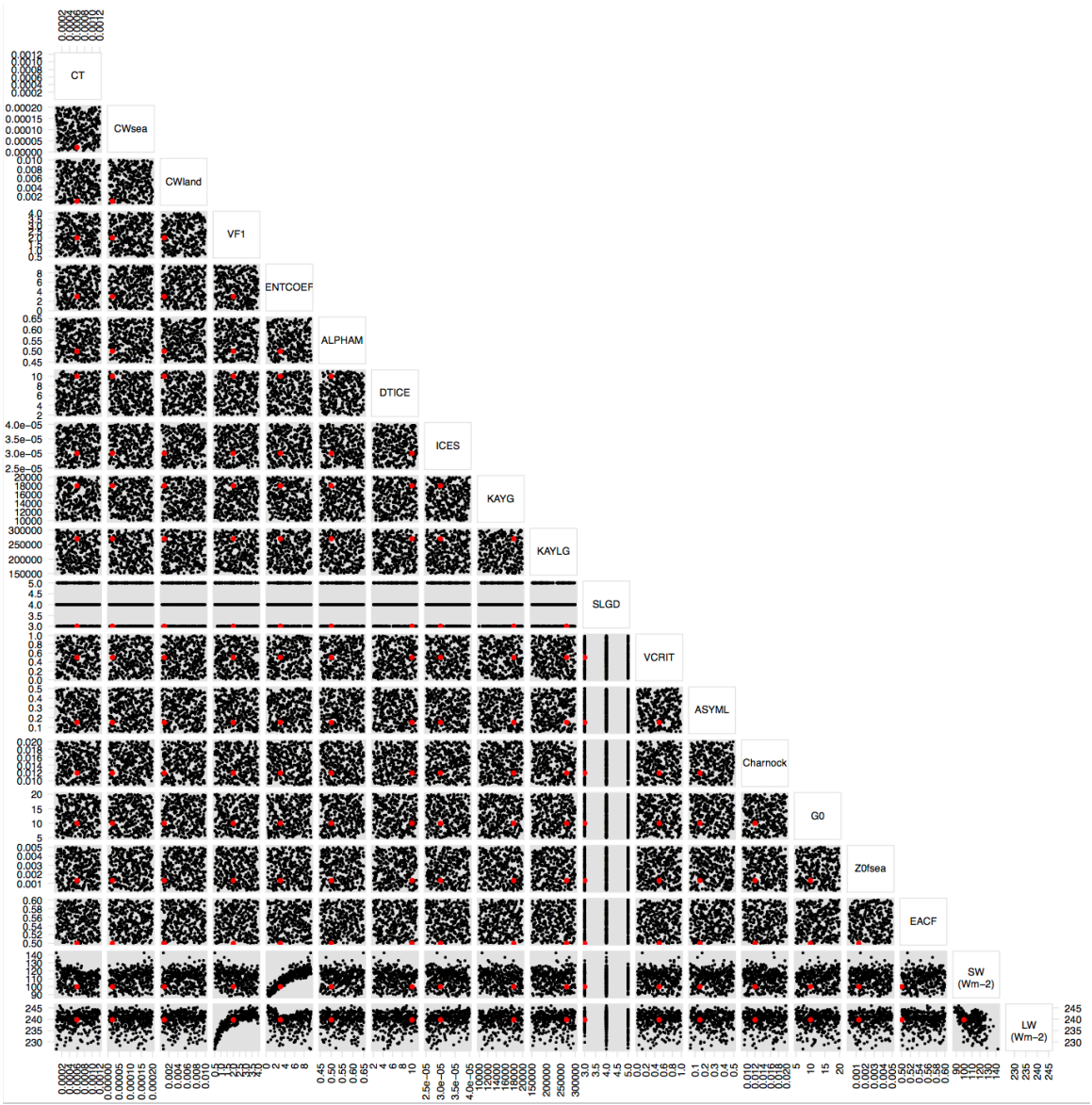

Figure S2. Phase 1 PPE parameter inputs and TOA outgoing SW and LW fluxes. 328 parameter sets are shown. The parameter values and model outputs under SP setting are marked in red.

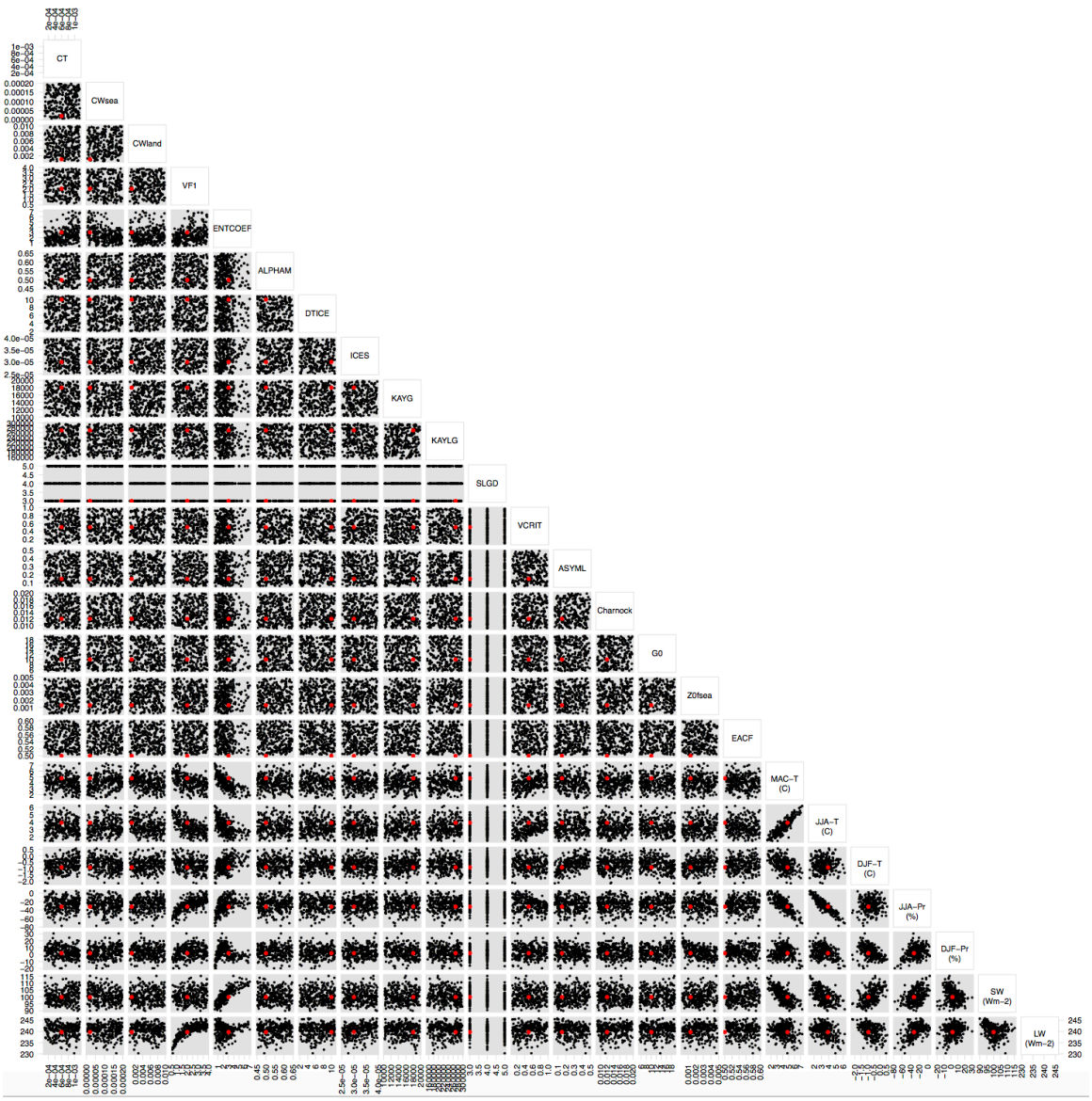

Figure S3. Same as Fig. S3, but for Phase 2 parameter inputs and summary model output metrics considered in this phase. 264 parameter sets are shown.

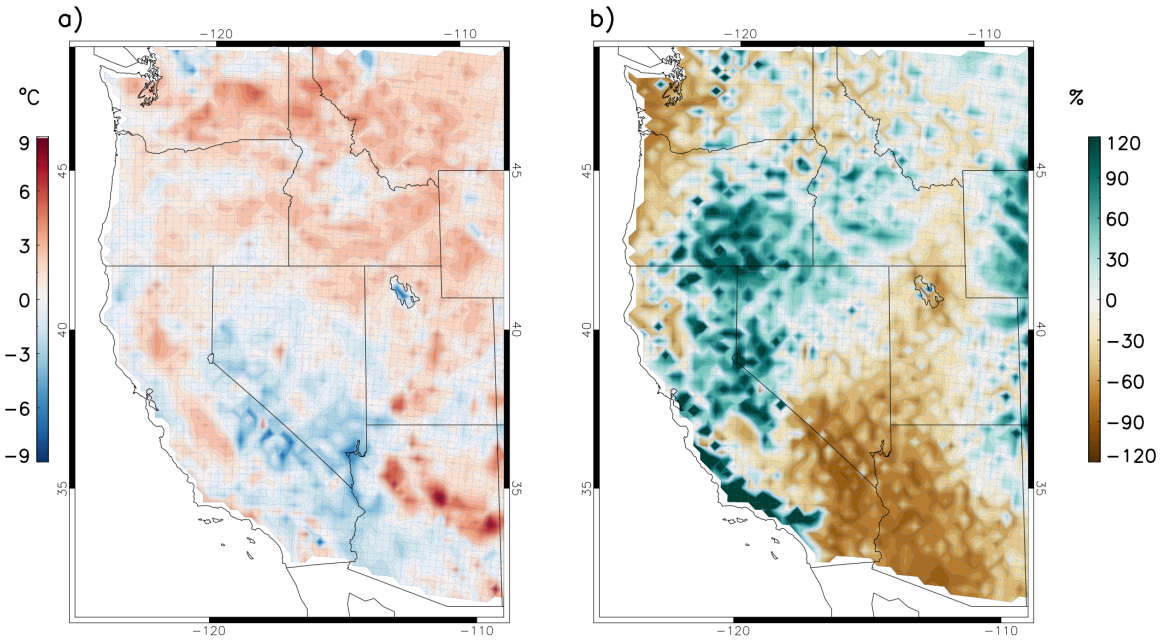

Figure S4. Biases in a) June-July-August (JJA) mean temperature (°C) , and b) precipitation (%) simulated by HadRM3P compared with PRISM over dec1996-nov 2007 under the selected PP settings, where the composite of the final 10 are taken.

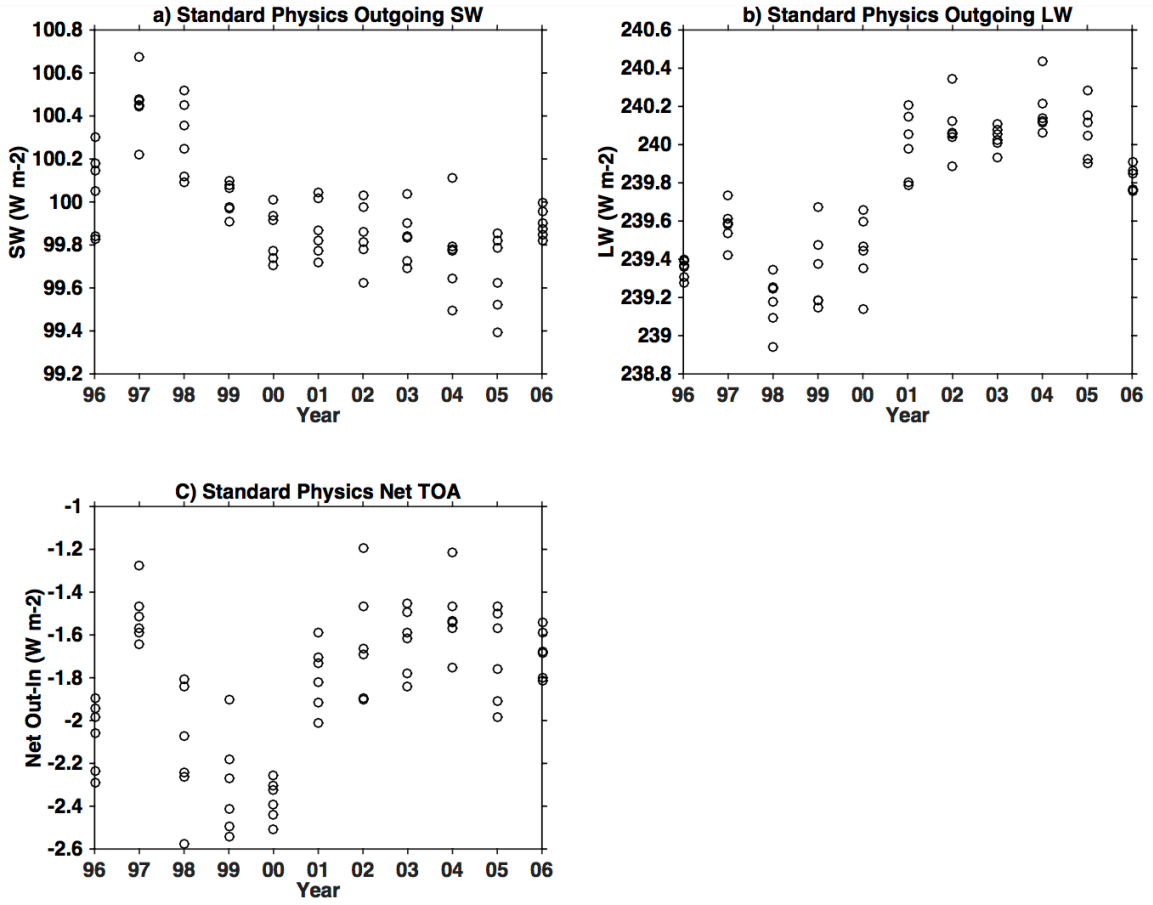

1471

1472 **Figure S5.** The range of internal variability for top-of-atmosphere a) outgoing shortwave
1473 radiation, b) outgoing longwave radiation, and c) net (outgoing minus incoming) under SP
1474 setting for each year. We rounded to the nearest Wm^{-2} (±1) to account for internal
1475 variability.

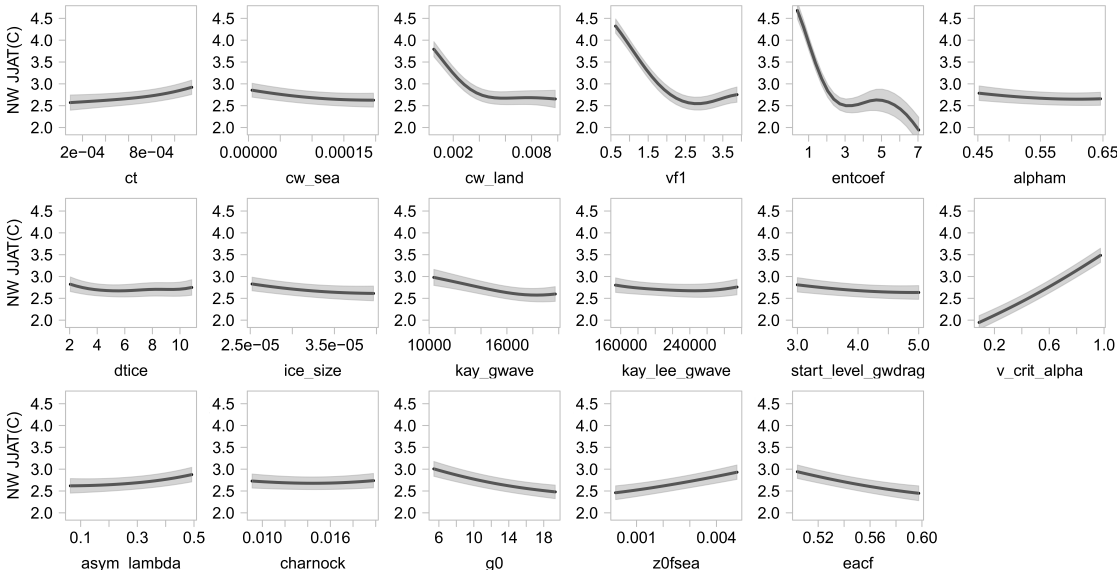

1476

1477 **Figure S6.** One-at-a-time sensitivity analysis of JJA temperature bias (compared with
1478 PRISM) over Northwest to each input parameter in turn, with all other parameters held at
1479 mean value of all the designed points. Central lines represent the emulator mean, and
1480 shaded areas represent the estimate of emulator uncertainty, at the ±1 SD level.

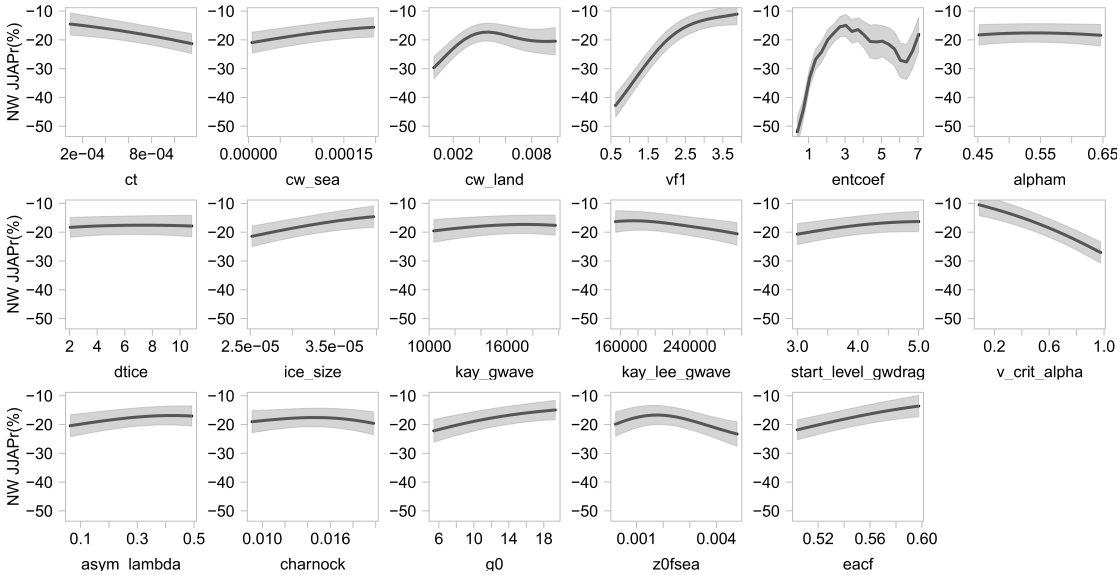

1481

1482 **Figure S7.** Same as Fig. S6, but for DJF temperature bias.

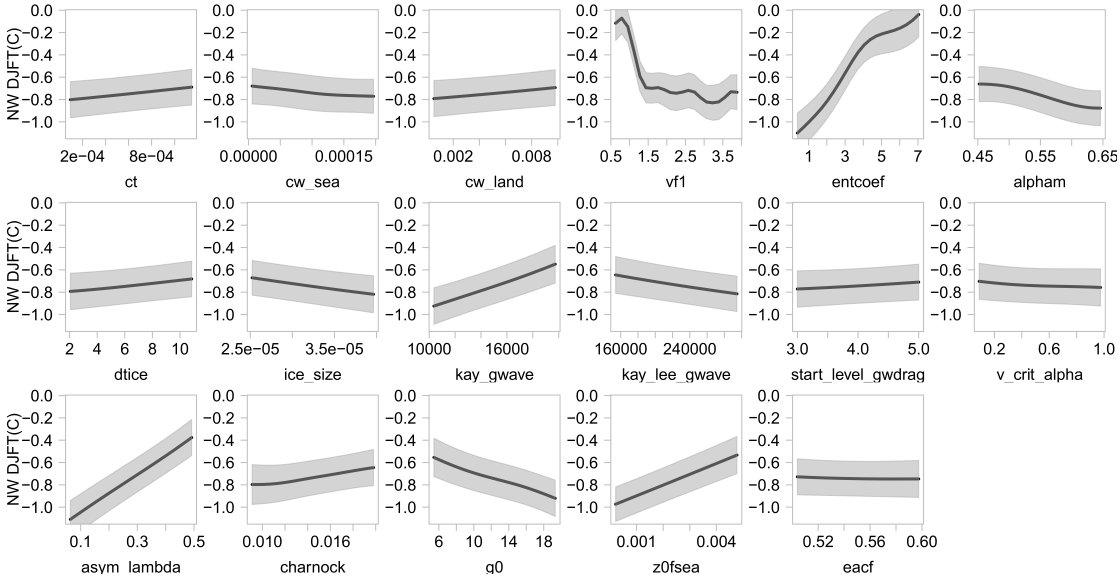

Figure S8. Same as Fig. S6, but for JJA precipitation bias.

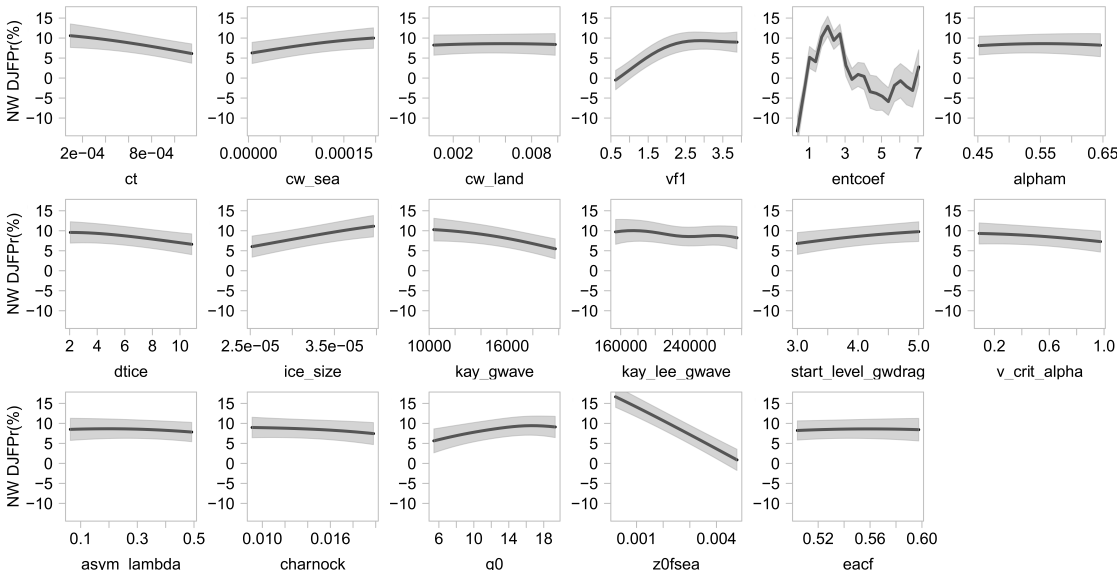

Figure S9. Same as Fig. S6, but for DJF precipitation bias.

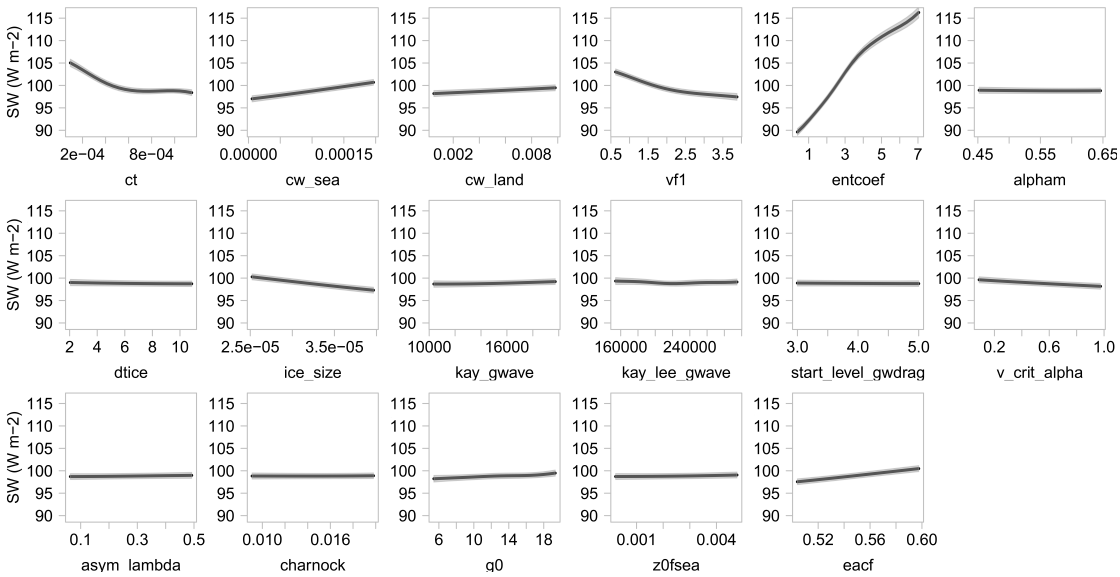

Figure S10. Same as Fig. S6, but for TOA SW fluxes.

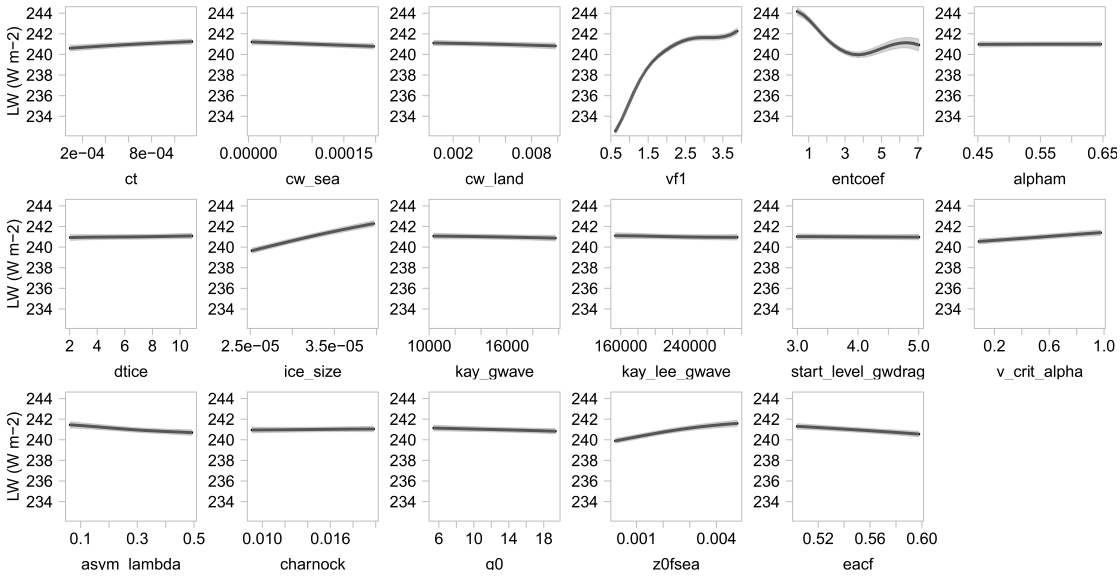

Figure S11. Same as Fig. S6, but for TOA LW fluxes.

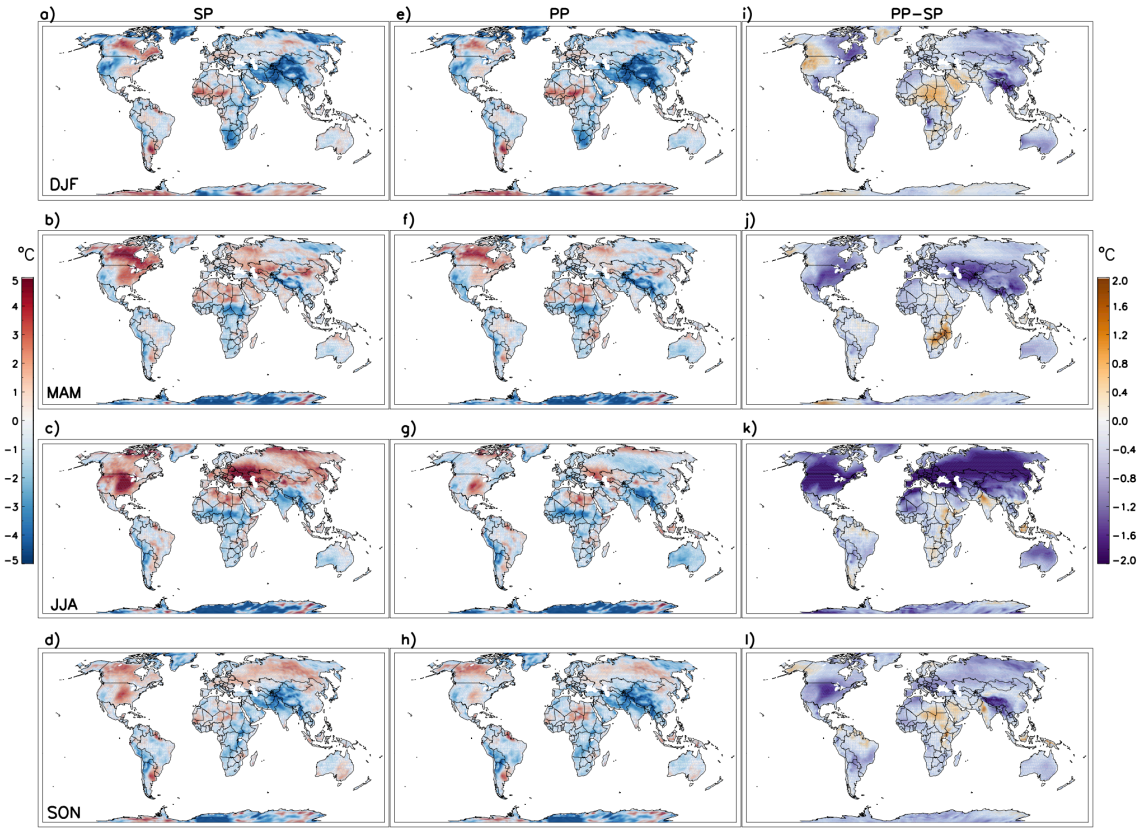

Figure S12. Biases of SP temperature over land in a) DJF, b) MAM, c) JJA, and d) SON, compared with MERRA over December 1996 through November 2007. Biases of selected PP compared with MERRA are shown in e)-h), while the differences between selected PP and SP, i.e. the absolute increase or decrease of biases in PP with respect to the SP values, are shown in i) - l). The PP results are the composites of the 10 selected sets, 6 IC per set.

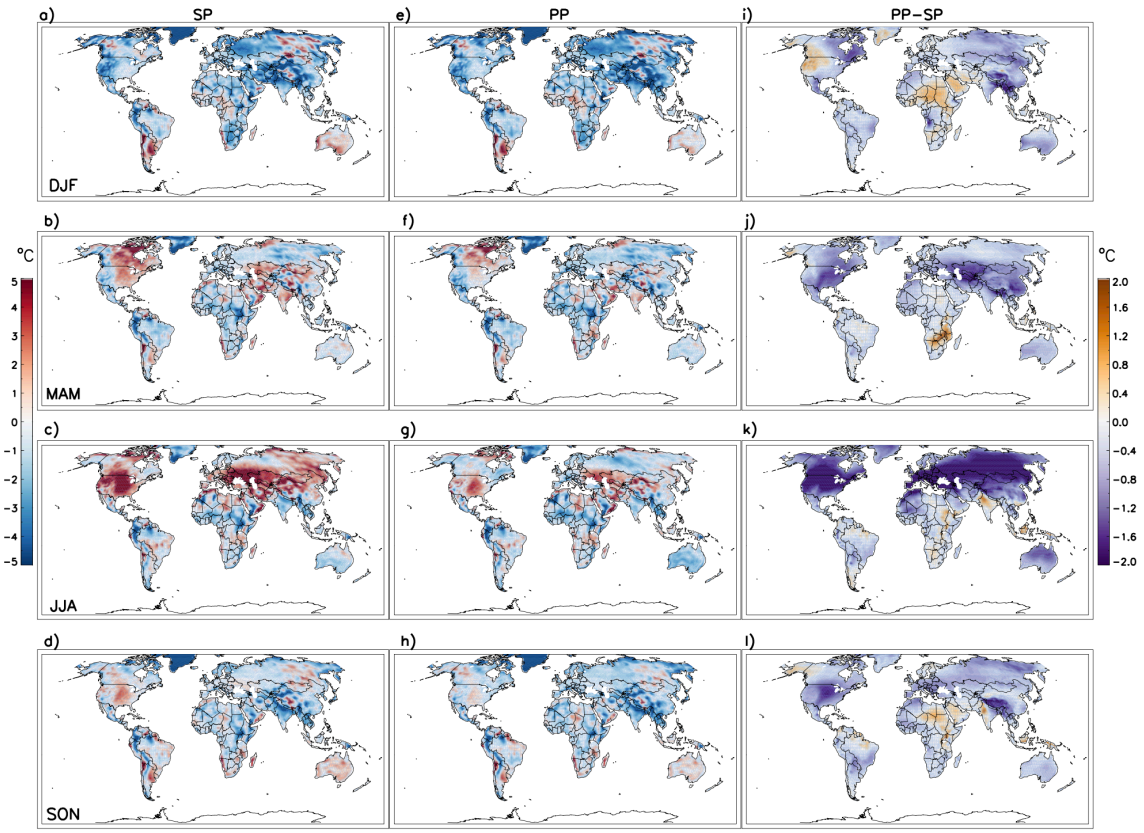

Figure S13. Same as Fig. S12, but for comparison with GHCN-CAMS.

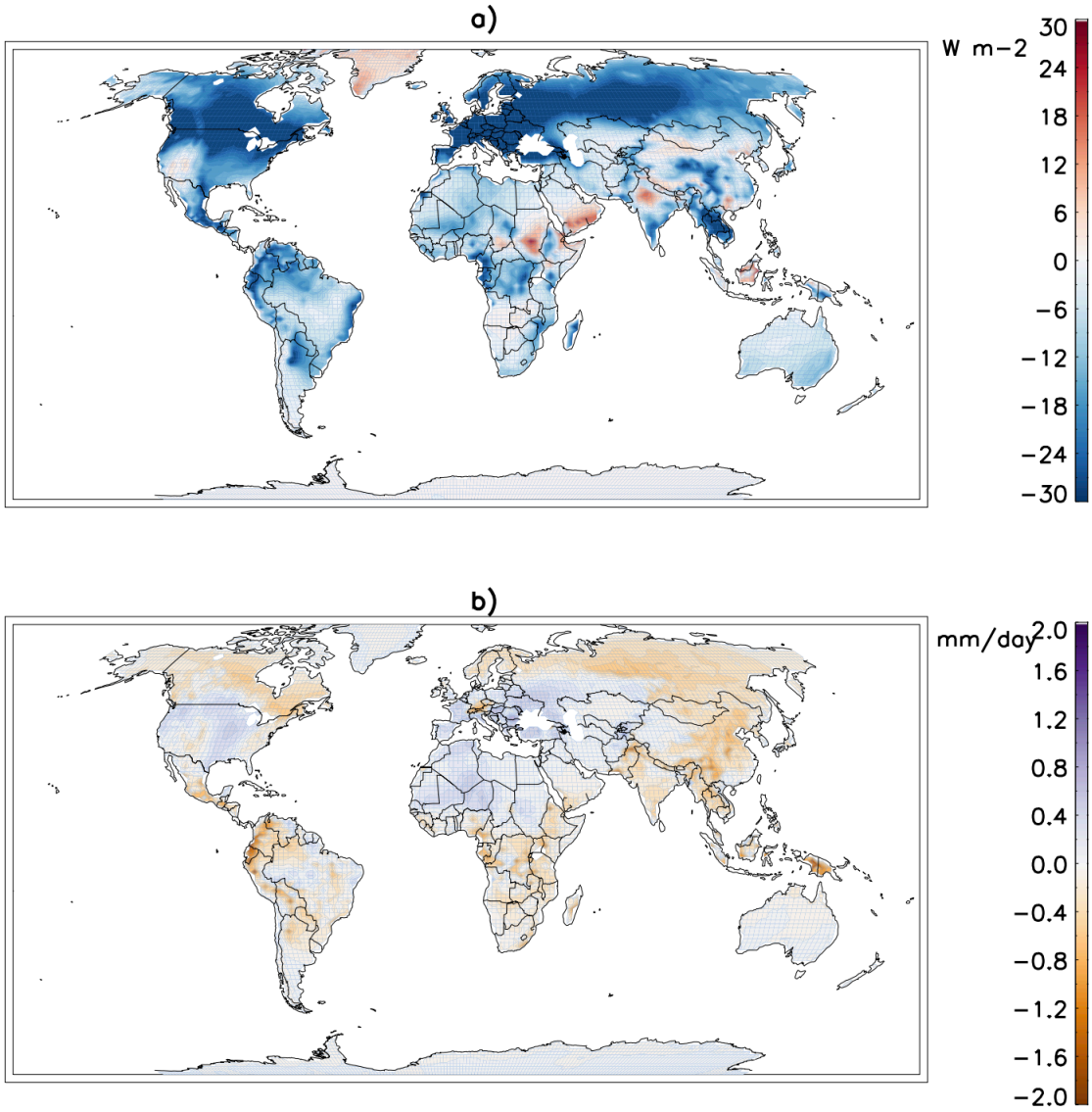

1499

1500 **Figure S14.** MEAN summer (JJA) differences between SP and PPset2 for a) total

1501 downward shortwave radiation, and b) latent heat fluxes for the period Oct1988 – Sep2015.

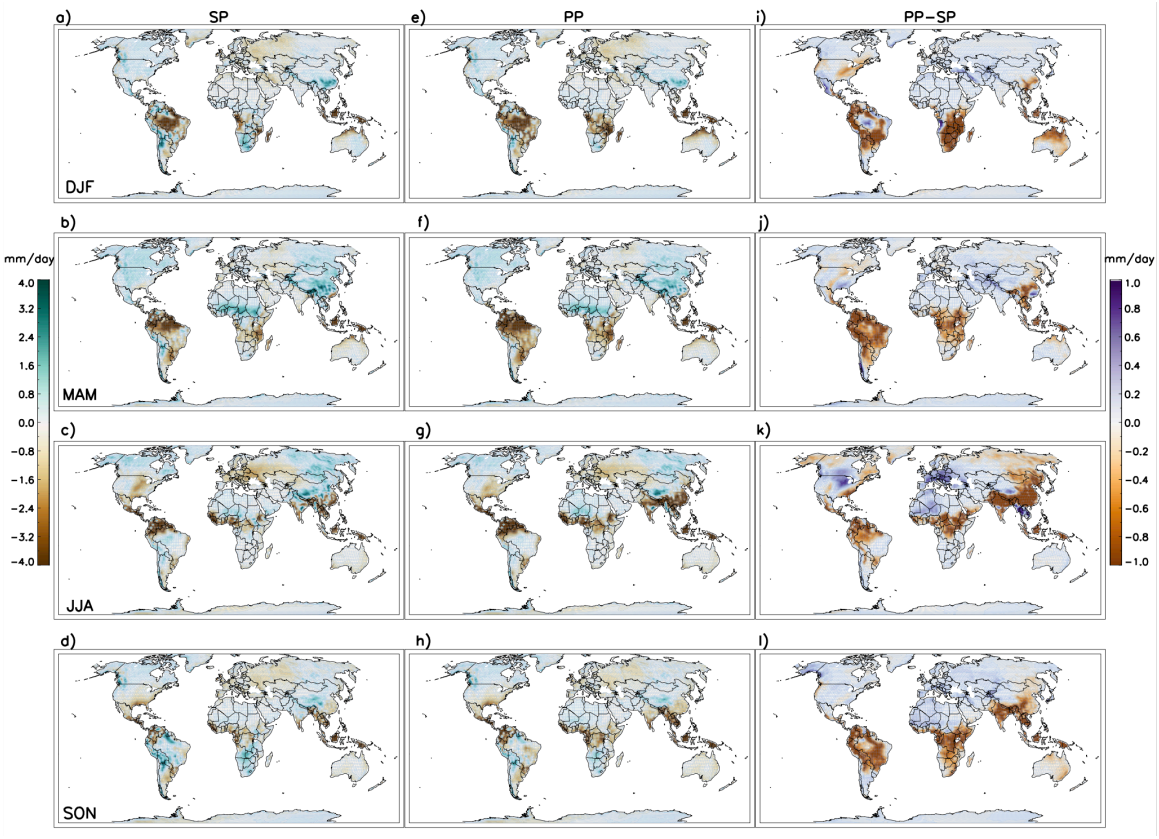

Figure S15. Biases of SP precipitation over land in a) DJF, b) MAM, c) JJA, and d) SON, compared with GPCP over December 1996 through November 2007. Biases of selected PP compared with GPCP are shown in e)-h), while the differences between selected PP and SP, i.e. the absolute increase or decrease of biases in PP with respect to the SP values, are shown in i) - l). The PP results are the composites of the 10 selected sets, 6 IC per set.

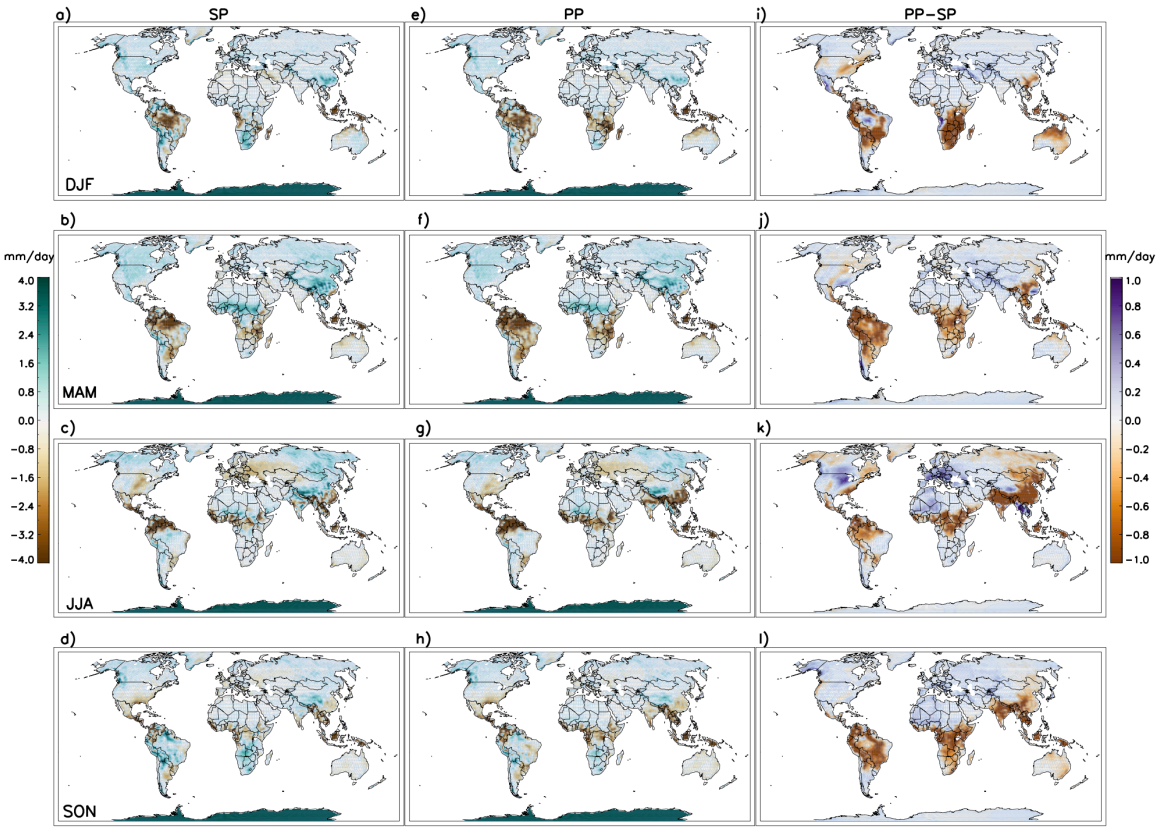

1508

1509 **Figure S16.** Same as Fig. S15, but for comparison with GPCC.

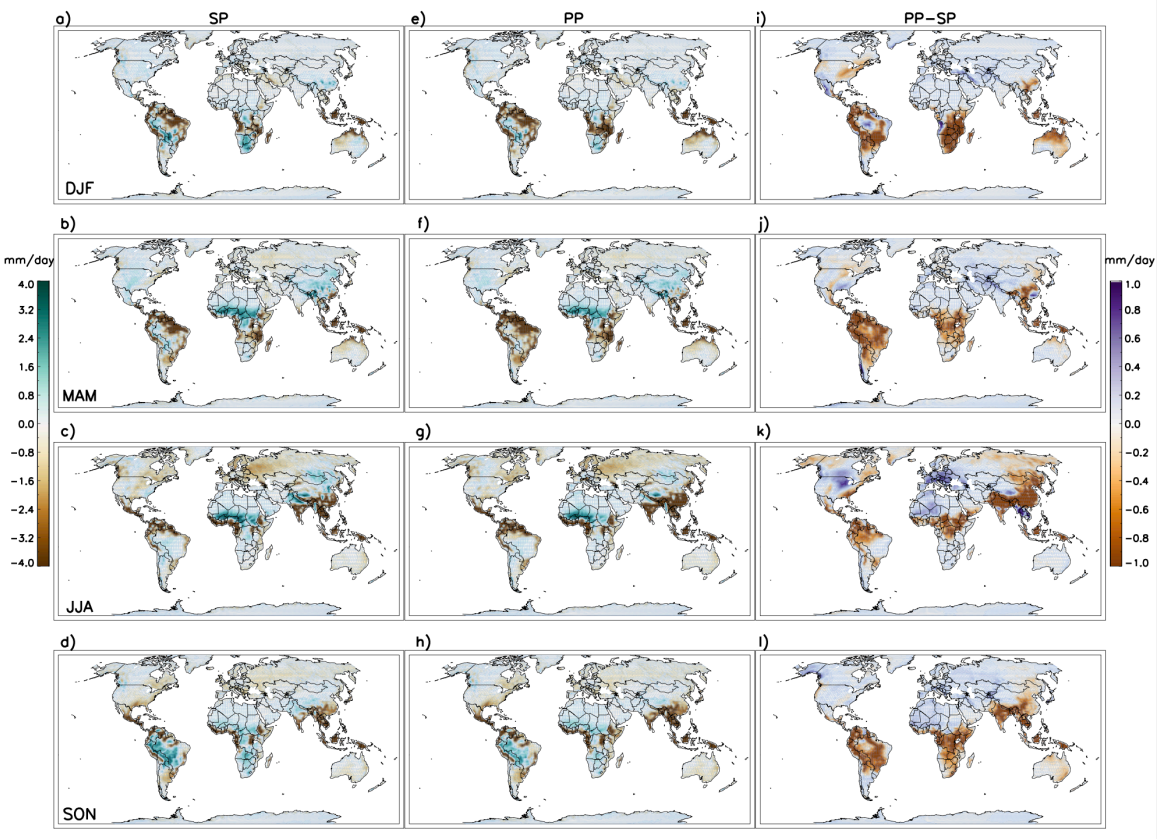

1510

1511 **Figure S17.** Same as Fig. S15, but for comparison with MERRA.

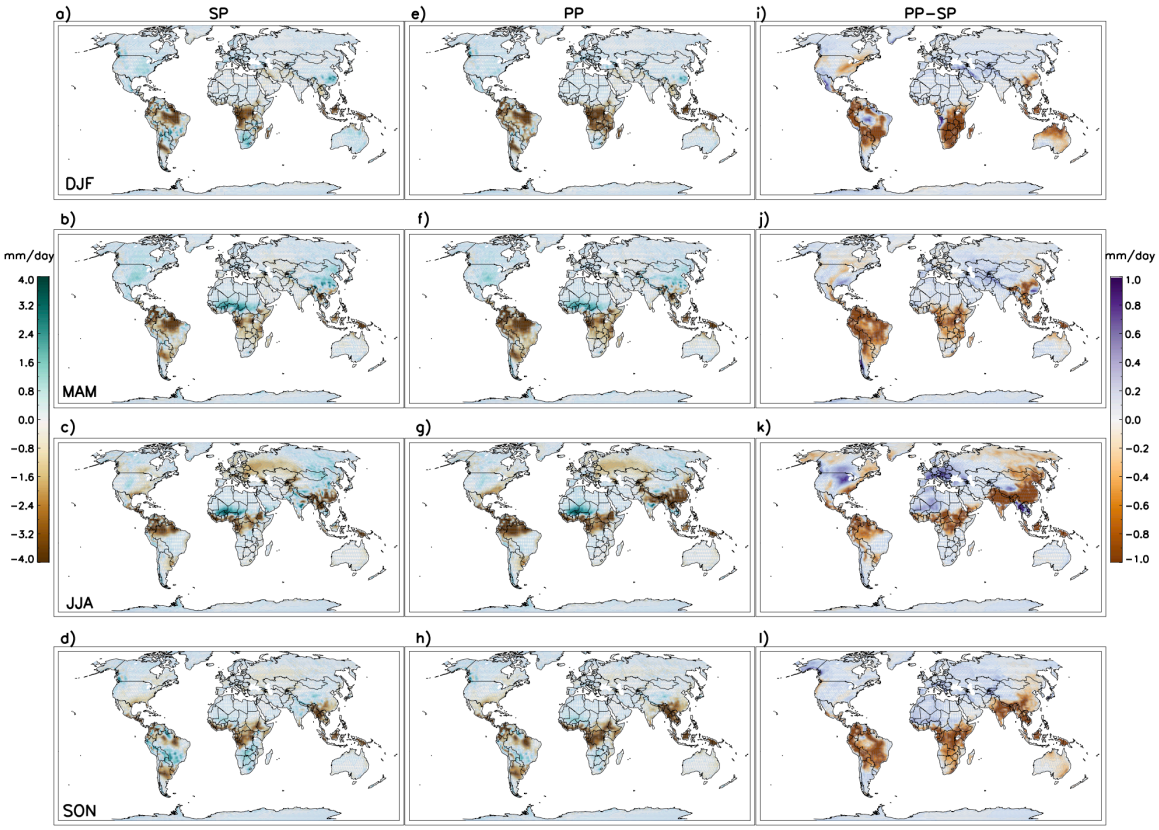

1512

1513 **Figure S18.** Same as Fig. S15, but for comparison with ERAI.

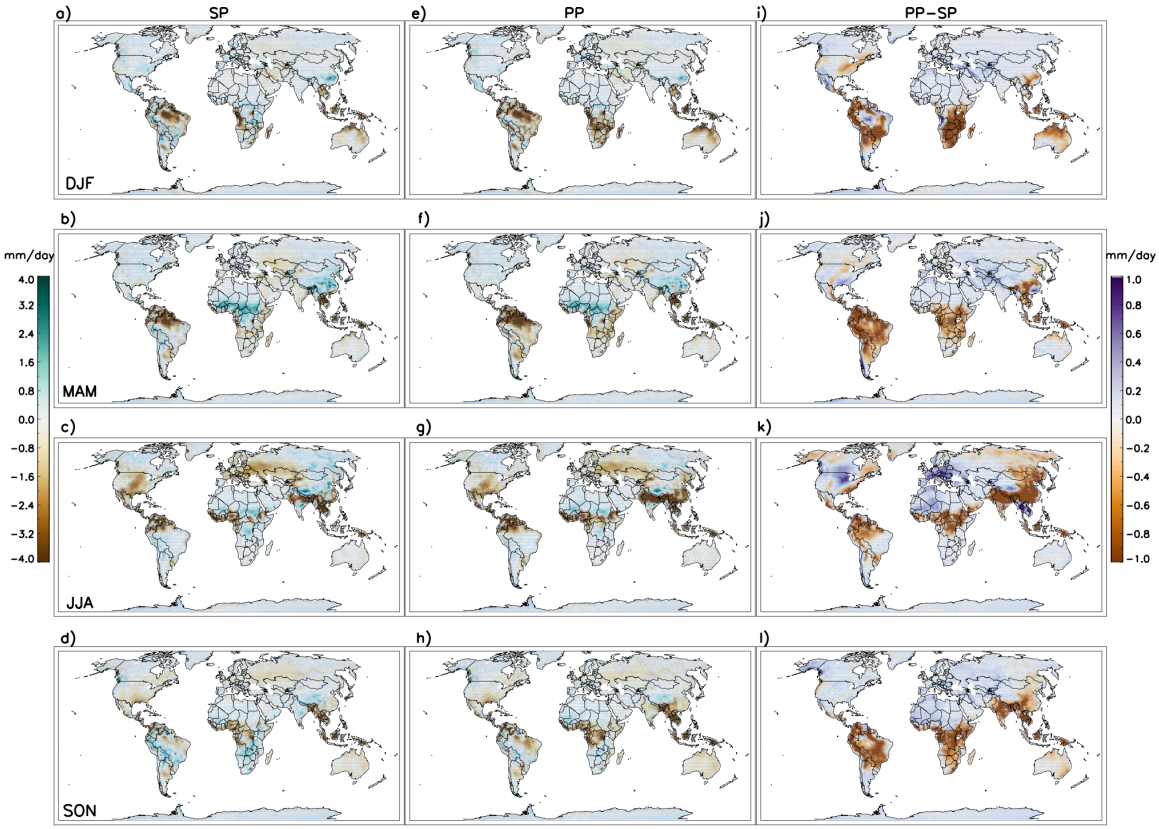

1514

1515 **Figure S19.** Same as Fig. S15, but for comparison with JRA-55.

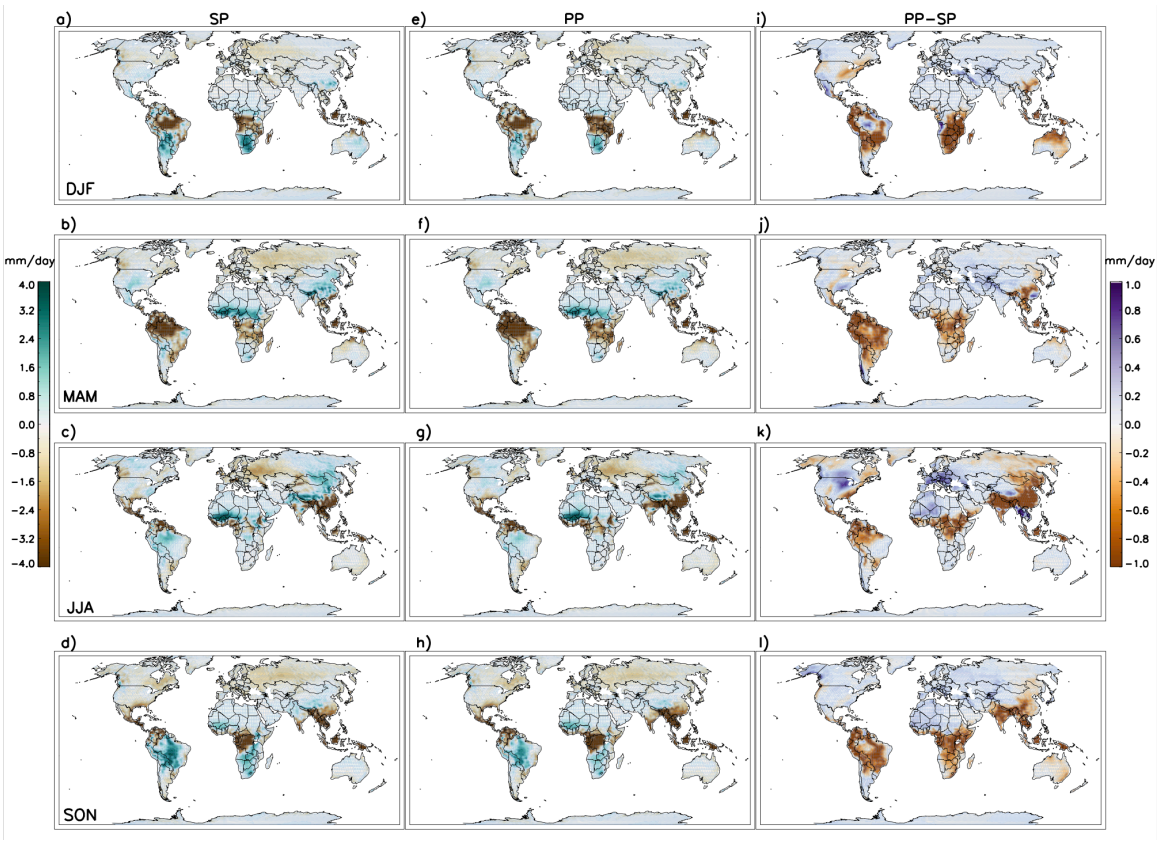

1516

1517 **Figure S20.** Same as Fig. S15, but for comparison with CFSR.

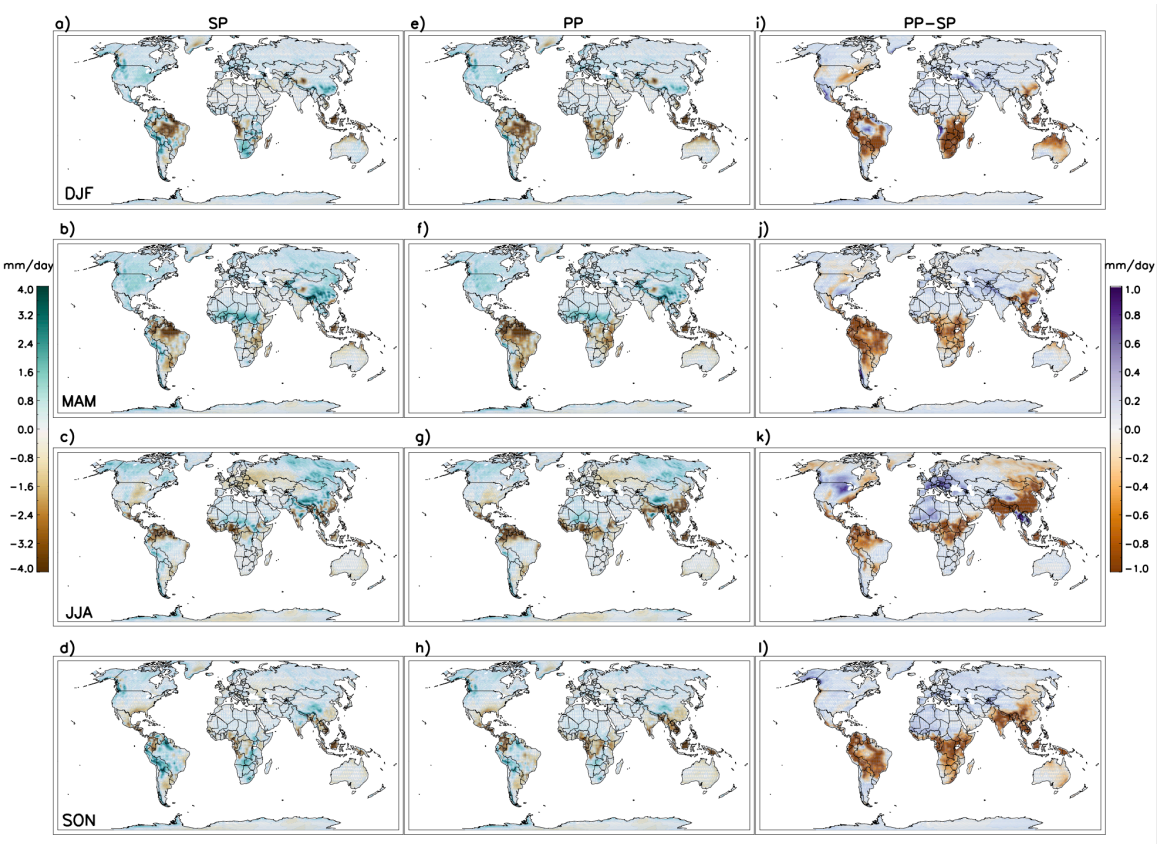

1518

1519 **Figure S21**. Same as Fig. S15, but for comparison with CMAP.

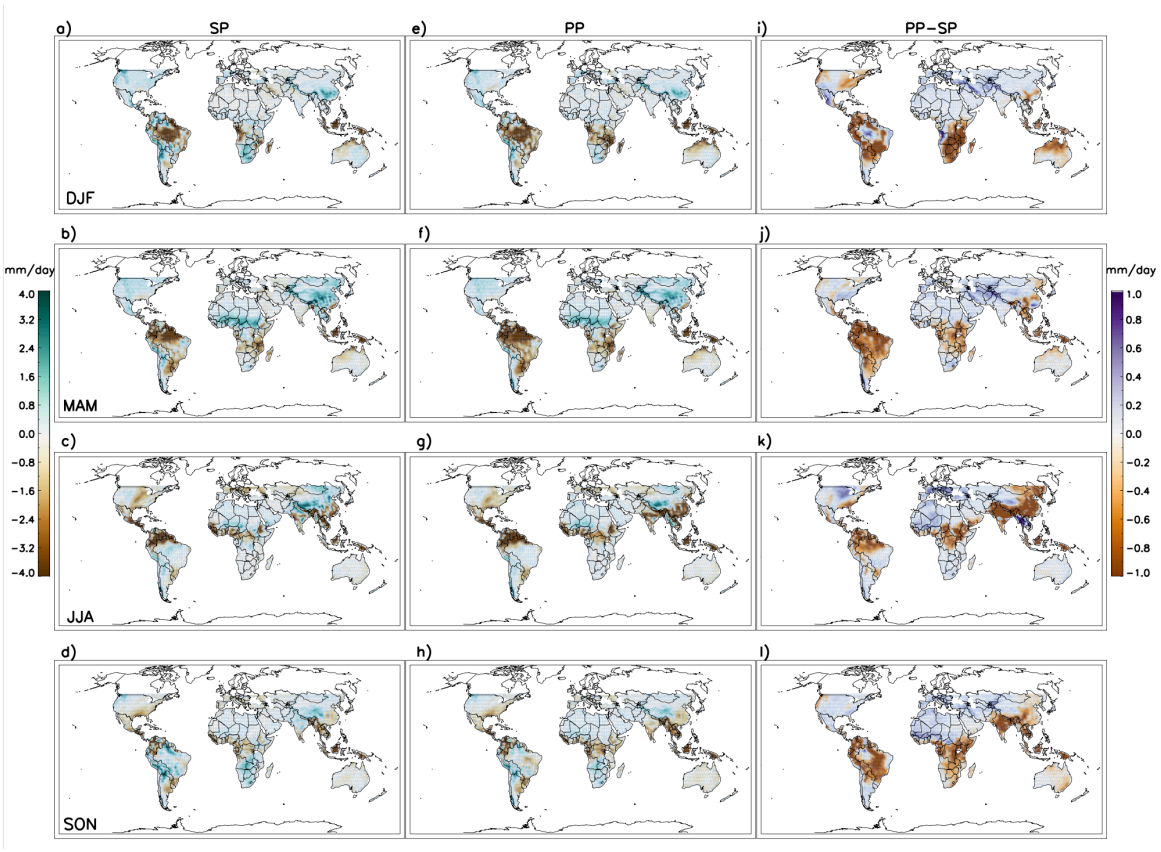

Figure S22. Same as Fig. S15, but for comparison with TRMM.

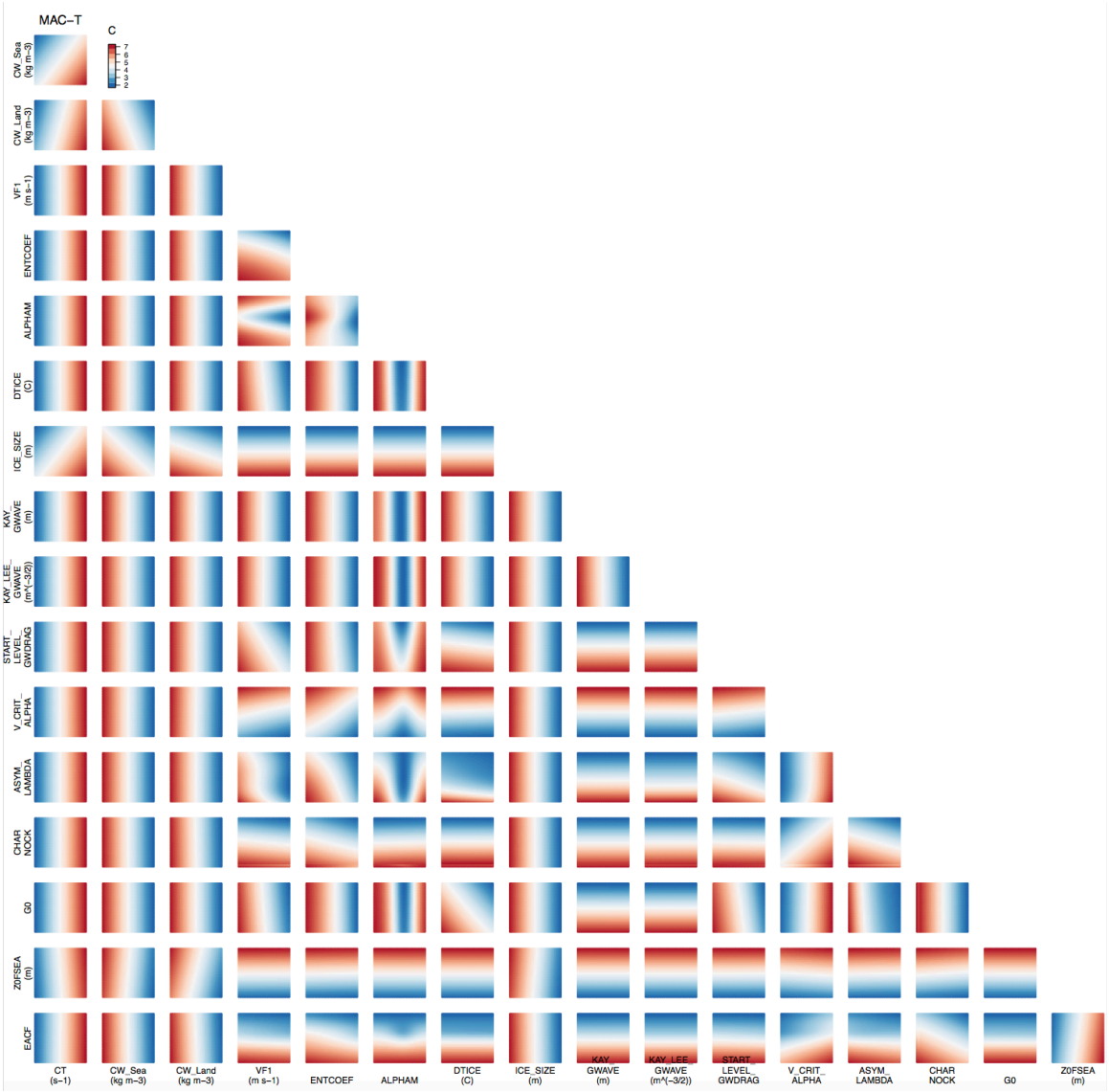

Figure S23. MAC-T biases projected into the two-dimensional spaces of each pair of input parameters using the emulator.

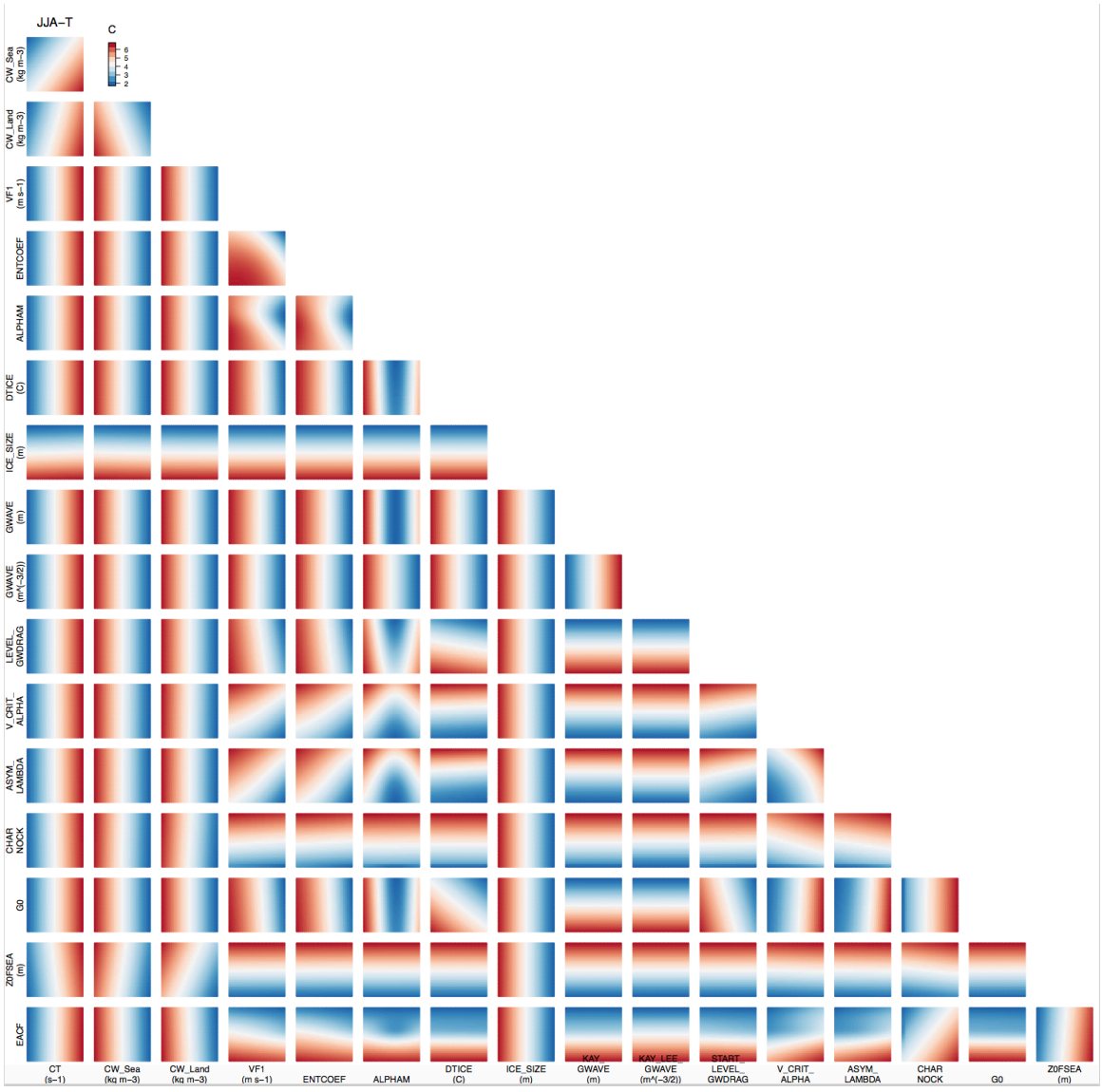

Figure S24. JJA-T biases projected into the two-dimensional spaces of each pair of input parameters using the emulator.

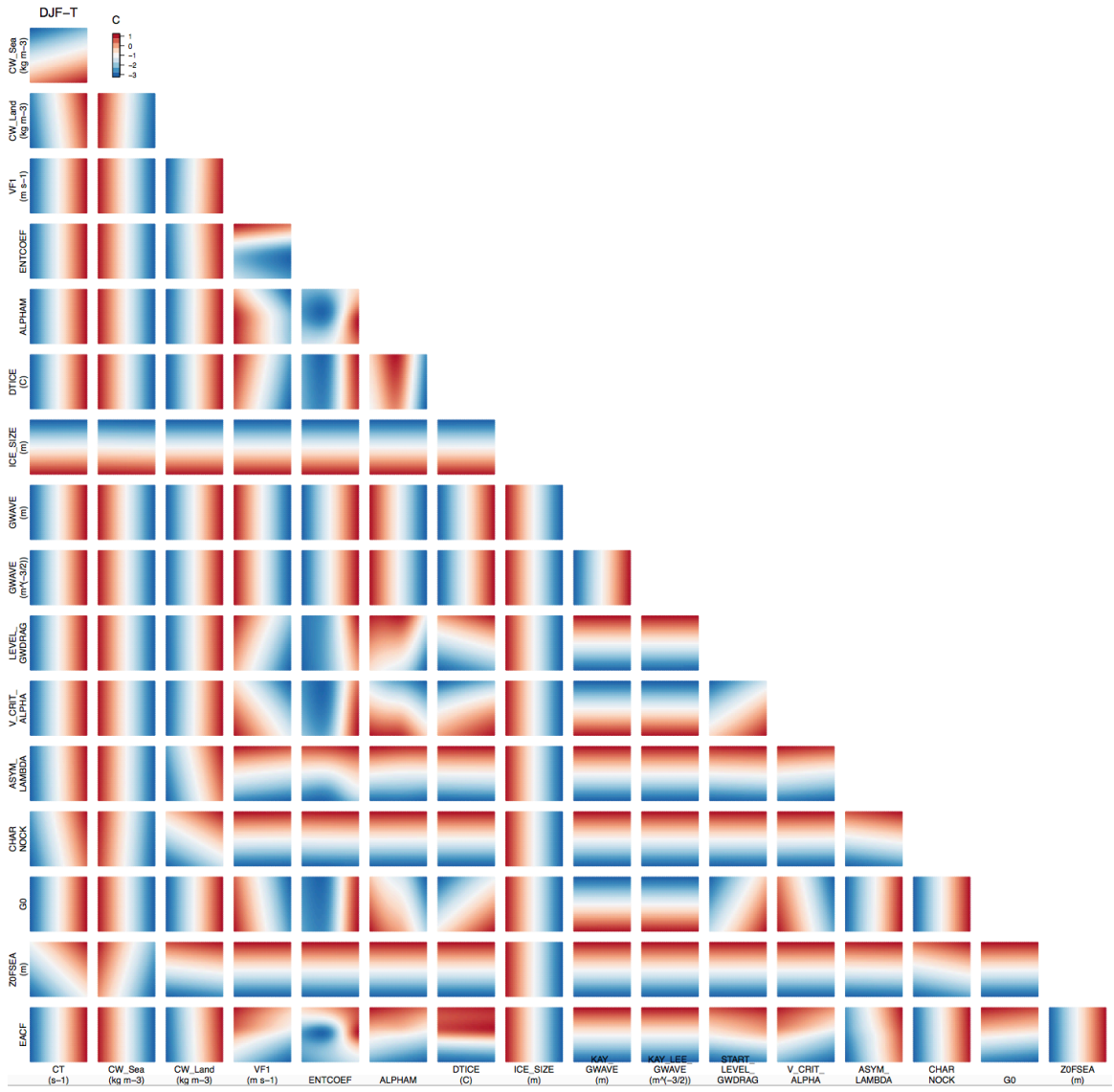

Figure S25. DJF-T biases projected into the two-dimensional spaces of each pair of input parameters using the emulator.

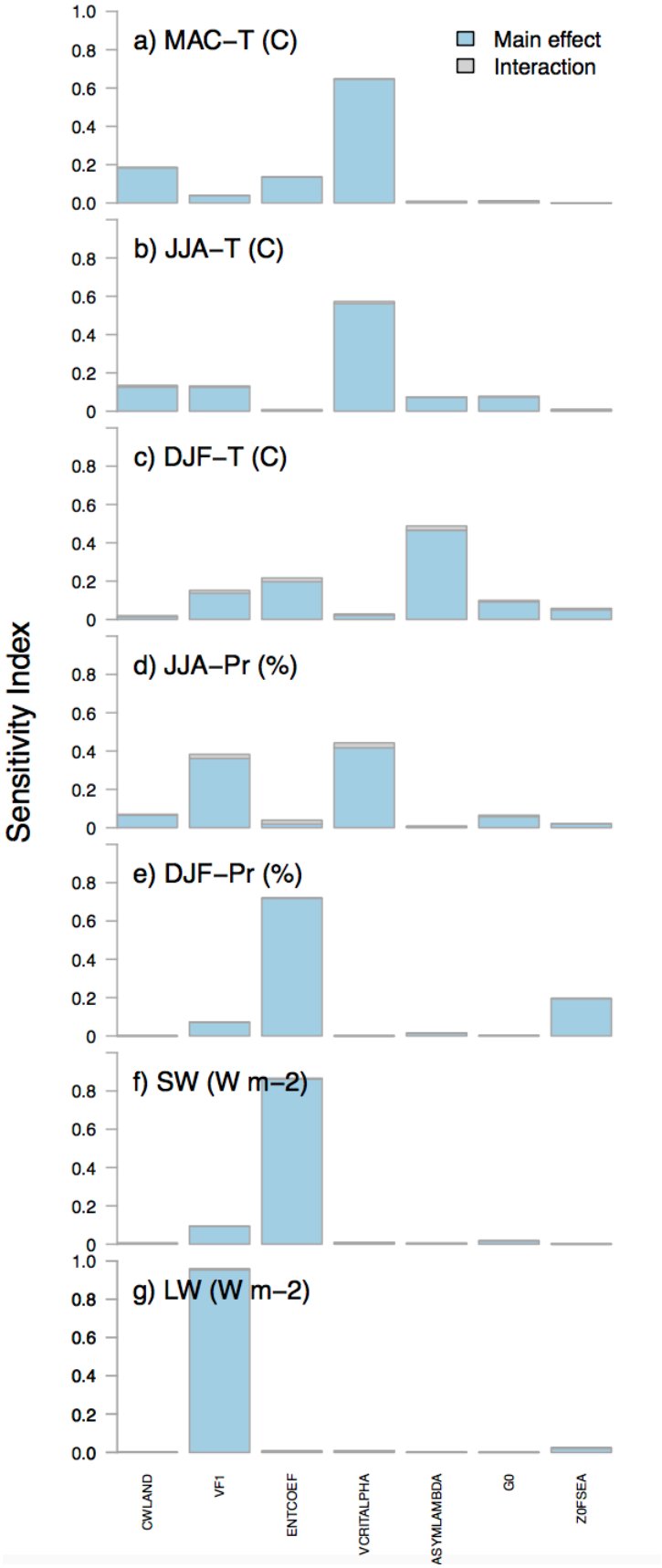
a) MAC–T (C)
Main effect
Interaction
b) JJA–T (C)
c) DJF–T (C)
d) JJA–Pr (%)
e) DJF–Pr (%)
f) SW (W m–2)
g) LW (W m–2)
Sensitivity Index
CWLAND
VF1
ENTCOEF
VCRITALPHA
ASYMLAMBDA
G0
Z0FSEA

1531

Figure S26. The sensitivity indices for the refined parameter space in Phase 3.

References:

Chylek, P., Li, J., Dubey, M. K., Wang, M., and Lesins, G.: Observed and model simulated 20th century Arctic temperature variability: Canadian Earth System Model CanESM2, Atmospheric Chemistry and Physics Discussions, 11(8), 22,893–22,907. https://doi.org/10.5194/ acpd-11-22893-2011, 2011.

Collins, W. J., Bellouin, N., Doutriaux-Boucher, M., Gedney, N., Halloran, P., Hinton, T., Hughes, J., Jones, C.D., Joshi, M., Liddicoat, S. and Martin, G.: Development and evaluation of an Earth- System model— HadGEM2, Geoscientific Model Development, 4(4), 1051–1075. https://doi.org/10.5194/gmd-4-1051-2011, 2011.

Martin, G. M., Ringer, M. A., Pope, V. D., Jones, A., Dearden, C., and Hinton, T. J.: The physical properties of the atmosphere in the new Hadley Centre Global Environmental Model (HadGEM1). Part I: Model description and global climatology, Journal of Climate, 19(7), 1274–1301. https://doi.org/10.1175/JCLI3636.1, 2006.

Neale, R.B., Chen, C.C., Gettelman, A., Lauritzen, P.H., Park, S., Williamson, D.L., Conley, A.J., Garcia, R., Kinnison, D., Lamarque, J.F. and Marsh, D.: . Description of the NCAR Community Atmosphere Model (CAM 5.0). Tech. Rep. NCAR/TN-486+ STR, 1(1), pp.1-12., 2010.